Advances in High Field Asymmetric Ion Mobility Spectrometry (FAIMS) Analyzers and FAIMS-Mass Spectrometry Interfaces

Mark E. Ridgeway Jr.

A dissertation submitted to the faculty of the University of North Carolina at Chapel Hill in partial fulfillment of the requirements for the degree of Doctor of Philosophy in the Department of Chemistry

Chapel Hill

2010

Approved by:

Advisor: Professor Gary L. Glish

Reader: Professor James Jorgenson

Reader: Professor R. Mark Wightman

Reader: Professor John Papanikolas

Reader: Professor Chris Fecko

ABSTRACT

Mark E. Ridgeway Jr.

Advances in High Field Asymmetric Ion Mobility Spectrometry (FAIMS) Analyzers and FAIMS-Mass Spectrometry Interfaces

(Under the direction of Dr. Gary L. Glish)

High field asymmetric ion mobility spectrometry (FAIMS) is a gas phase separation technique that separates ions by the ratio of high to low electric field mobility, which is a characteristic of the three dimensional structure of ions. FAIMS separation in front of mass spectrometric analysis has the ability to reduce chemical noise thereby increasing signal-to-noise ratios and limits of detection; it can also be used to separate isobaric and isomeric compounds. FAIMS analyzers are simple to construct and are easily integrated into the atmospheric pressure ion source of current mass spectrometers without major modifications. The motivation of developing FAIMS analyzers in the Glish lab has been for the study of three dimensional gas phase ion structure of biological molecules, as well as to improve separation of compounds which are irresolvable using low resolution mass spectrometry and liquid chromatography. This dissertation does not focus on the application of FAIMS for structural elucidation, but instead on the development of a FAIMS device that combines excellent speed, resolution, and sensitivity in a simple to use small package. Described in the following chapters are the background for selection of gas phase ions by shape-to-charge, the development of a high amplitude asymmetric waveform power supply, modifications made the planar FAIMS

device designed by the Pacific Northwest National Lab and the development of four generations of planar FAIMS devices. For each device limitations and flaws in the design are discussed along with proposed solutions and data demonstrating the results of modifications to analyzer design, and the successful construction of a planar FAIMS device with high speed, high sensitivity, and resolving power equal to much larger and more expensive devices.

ACKNOWLEDGEMENTS

I would like to thank my grandmother “Mama”, a lifetime teacher who never let summer vacations get in the way of her grandson’s learning.

I would like to thank my parents and sisters for everything they have done for me, which includes forgiving me when I disassembled your things but didn’t know how to put them together, and using your personal living space for parts storage. I would not have learned half of what I know now if it hadn’t been for your kind support.

I would like to thank Dr. Gary L. Glish for allowing so much diversity and freedom in the research of his group members, who are encouraged to try their own ideas, and follow their own interests.

Thanks to all the Glish lab members who are always helpful, even when I’m being a diva.

TABLE OF CONTENTS

LIST OF TABLES

Table

LIST OF FIGURES

Figure

LIST OF ABBREVIATIONS AND SYMBOLS

3D	three dimensional
A	Ampere
a	acceleration
Å	Angstrom; (10^{-10} meters).
Ar	Argon
AWG	American wire gauge; a measure of wire thickness
BNC	Bayonet Neill-Concelman; a bayonet style electrical connection
BSA	bovine serum albumin
C	capacitance
CID	collision induced dissociation
cm	centimeter
CO_2	carbon dioxide
CV	compensation voltage
CV_{peak}	value of compensation voltage at center of analyte peak
ΔCV_{FWHM}	width of peak in compensation voltage scan at full width half maximum
D	diffusion coefficient
D_{II}	diffusion coefficient parallel to the analytic gap in FAIMS
d_h	distance traveled by an ion during the E_h
d_l	distance traveled by an ion during E_l
Da	Dalton; unit of mass equal to 1 atomic mass unit
dc	direct current
DV	dispersion voltage

D_z	potential well depth for ions stored in an ion trap
E	electric field strength
e	fundamental charge constant; equal to $1.602e^{-19}$ coulombs/mole
E_h	electric field during high field portion of an asymmetric waveform
E_l	electric field during low field portion of an asymmetric waveform
E/N	electric field divided by gas number density
$E/N_{critical}$	E/N at which ions begin to deviate from low field conditions
ECD	electron capture dissociation
E_{com}	center of mass collision energy
E_{lab}	laboratory frame collision energy
ESI	electrospray ionization
eV	electron volt; unit of energy equal to $1.602e^{-19}$ joules
F	force
f	high frequency sinusoidal wave used to construct asymmetric waveform
FET	field effect transistor
G1	first generation FAIMS developed in UNC-Bruker collaboration
G2	second generation FAIMS developed in UNC-Bruker collaboration
G3	third generation FAIMS developed in UNC-Bruker collaboration
G4	forth generation FAIMS developed in UNC-Bruker collaboration
g	the distance between two parallel FAIMS electrodes
g_{opt}	optimum FAIMS analytical gap width for a ratio of K_h/K_l
g_e	effective gap width for specific mobility ion
F	force

F_3	form factor coefficient for a FAIMS waveform
f	frequency
FAIMS	high field asymmetric waveform ion mobility spectrometry
FT-ICR	Fourier transform ion cyclotron resonance mass spectrometer
FWHM	full width at half maximum
GC	gas chromatography
GC/MS	gas chromatography coupled with mass spectrometry
H/D exchange	hydrogen deuterium exchange mass spectrometry
He	helium
Hz	Hertz; unit of frequency equal to 1 cycle per second
i	current
ICC	ion current control
IMS	ion mobility spectrometry
IMS-MS	ion mobility spectrometry coupled with mass spectrometry
IR	infrared
IRMPD	infrared multiphoton dissociation
K	mobility
K_0	reduced mobility; corrected for temperature and pressure
K	Kelvin; unit of temperature
k_b	Boltzmann's constant $1.38e^{-23}$ J/K
kDa	kiloDalton; $1e^3$ Da
kHz	kiloHertz; $1e^3$ Hz
K_h	mobility during the high electric field portion of FAIMS waveform

K_l	mobility during the low electric field portion of FAIMS waveform
kV	kilovolt
L	inductance
L	drift tube length
LC	liquid chromatography
LC/MS	liquid chromatography coupled with mass spectrometry
m	meter
m	mass
m/z	mass-to-charge ration
m_1	mass of ion
m_2	mass of neutral molecule
MHz	MegaHertz; $1e^6$ Hz
mm	millimeter
mTorr	unit of pressure; $1e^{-3}$ Torr
MOSFET	metal-oxide-semiconductor field effect transistor
MS	mass spectrometry
ms	millisecond
MS/MS	tandem mass spectrometry
MΩ	megaOhms
N	number density
N_2	nitrogen
NMR	nuclear magnetic resonance
ns	nano seconds; $1e^{-9}$ seconds

P	pressure in Torr
pA	pico Ampere = $1e^{-12}$ Amperes
PCB	printed circuit board
PEEK	polyetherertherketone
pf	pico Farad; unit of capacitance
p-FAIMS	planar FAIMS
PNNL	Pacific Northwest National Labs
q	charge
q_z	Mathieu stability parameter for an ion in the z dimension
Q-TOF	hybrid mass spectrometer coupling a linear quadrupole and time of flight
R	resolving power
r_0	radial dimension of an rf ion trap
rf	radio frequency
RLC	resonant circuit using inductance and capacitance
RSD	relative standard deviation
s	seconds
SF_6	sulfur-hexafluoride
S/N	signal to noise ratio
T	temperature
t	time
"T" connection	an electric connector with three equal potential fittings.
ΔT	difference in temperature between two points
t_d	drift time

t_{DV}	duration of the dispersion voltage
t_h	duration of the high field portion of FAIMS waveform
t_l	duration of the low field portion of FAIMS waveform
TOF	time of flight (a type of mass analyzer)
Torr	unit of pressure (760 Torr = 1 atm)
TTL	transistor transistor logic; high/low logic consisting of 0 or 5 V amplitude
t_{res}	time an ion spends in the analytical gap of a FAIMS analyzer
U	a standard height of rack mounted electronics enclosure
UNC	University of North Carolina
V	Voltage
$V_{0\text{-peak}}$	Voltage of waveform measured from 0 V to maximum amplitude
V_{cc}	voltage between ground and the collector of a bipolar junction transistor
v_d	ion drift velocity
$V_{peak\text{-}to\text{-}peak}$	Voltage amplitude measured from peak to peak of an AC signal
W	Watt; unit of power; 1 Joule per second
z	charge
z_0	dimensions of an ion trap in the z direction
ΔF	correctional form factor used to correct for no idea FAIMS waveforms
μF	micro Farad; unit of capacitance
π	3.14
Ω	drive frequency for rf ion traps
Ω_{avg}	orientationally averaged collision cross section
Φ	phase shift between two sinusoidal waveforms

ω	frequency of sinusoidal waveform in radians/second
°C	temperature on the Celsius scale

Chapter 1
Introduction to shape-to-charge analysis of gas phase ions

1.1 What mass analyzers can tell you

Modern mass analyzers are capable of analyzing molecules from a single dalton (Da) to millions of Da[1, 2] over a range of concentrations from attomolar[3] to millimolar. Currently available high resolution instruments can baseline resolve two peaks from ions with mass-to-charge ratios of 906.49100 and 906.49145, a resolving power of over 2000000[4]. Analysis times range from seconds for high resolution trapping instruments down to microseconds for a single time-of-flight spectrum[5]. With such a wide dynamic range and the high analysis speed of current mass analyzers, there would seem to be no problem too difficult, no sample too complex, and no question unanswerable with the right mass spectrometer at your disposal.

Of course, mass spectrometry cannot analyze every sample nor can it provide every piece of information one might desire to know about a compound. As interest in analytical chemistry shifts away from the traditional small molecular analysis, for which mass spectrometry first proved so valuable, to analysis of larger biological samples, mass spectrometers have undergone a change in role. Although the samples may have changed, the desired information remains the same. Mass analyzers are used to provide insight into the molecular structure of the ion, which has traditionally meant the connectivity of atoms in organic molecules[6]. However, structure is a broad term and can be interpreted to mean many different levels. Critical to the study of biological samples, most often proteins, is not only

the primary structure, but also the higher order secondary, tertiary, and quaternary structure which are closely related to biological function[7].

Determination of ion structure through mass analysis alone is a challenging task due to the possibility of multiple structures existing in a sample prior to analysis[8, 9], interconversion between structures[10], and rearrangements of ions following energy deposition[11-13]. Methods used in mass analyzers to determine structure, such as tandem mass spectrometry (MS/MS)[14], hydrogen deuterium (H/D) exchange[15], and gas phase ion spectroscopy[16-18] are valuable but limited tools. Each of these techniques provides unique structural information, and by using multiple tools, limitations inherent to any single technique may be reduced or eliminated. This chapter is intended to serve as introduction to the tools available to those interested in studying biological structure through mass analysis and provide some insight into the advantages and limitations each technique.

1.1.1 Primary structure via dissociation

The elucidation of primary structure is most often accomplished by first isolating a single mass-to-charge ratio, referred to as the precursor ion, and depositing sufficient energy into the selected ion to induce dissociation. The fragments of the precursor ion, referred to as product ions, provide information about the connectivity of the molecule through both the mass of the product ion and the difference in mass between product and precursor ions. At a minimum, this method, referred to as MS/MS, requires the use of two stages of mass analysis to select the precursor and analyze the products[14].

Determination of primary structure through fragmentation can be inhibited by the presence of multiple isomeric structures in a single sample[19] and rearrangements of fragments that lead to scrambling of primary sequence[11, 12, 20]. In the case of smaller polypeptides, rearrangements can be eliminated through the use of sodiation of the peptide[13],

but this method has not be applied to larger biological molecules. For primary sequencing of larger more complex biomolecules, a digestion step may be used to prior to mass analysis to produce smaller polypeptides which are more easily sequenced[21]. The use of a digestion step prior to mass analysis significantly increases the number of peaks in a spectrum leading to increased spectral complexity.

1.1.1.1 Collisions with neutral gasses or surfaces

Dissociation of selected precursor ions can be achieved through the use of collisions with a neutral gas or surface to convert the kinetic energy of the ion into internal energy. The internal energy deposited in the ion is then statistically redistributed throughout the molecule and induces fragmentation at the weakest bonds first[22]. This collision induced dissociation (CID) has limited usefulness for the study of higher order structure, since the weak intramolecular bonds are broken prior to the fragmentation of covalent bonds resulting in observable mass losses.

In CID, a neutral gas is used as the collision target. The maximum kinetic energy which can be converted into internal energy from an ion and neutral collision is on the order of 1 eV. Energy from collisions is distributed throughout the entire ion, resulting in the per bond energy transferred through a collision with a neutral gas of much less than 1 eV. Considering the average peptide bond strength is on the order of 2 eV[23], CID requires multiple collisions, or a higher energy transfer per collision through the use of heavy bath gases, to achieve high product ion yields. For multiple collisions to occur in the path length of a rf collision cell or three dimensional ion tap, gas pressures on the order of mTorr are used.

Surface induced dissociation (SID) offers an alternative to CID which requires no collision gas and can induced fragmentation from a single collision. SID is achieved by colliding ions with a solid surface held at approximately at a 45° angle of incidence. Interaction efficiency is 100% for SID, and large amounts of energy (7-100 eV) can be converted to internal energy per single collision. While more energy is transferred in a single collision resulting in a shorter fragmentation time than CID, SID fragmentation still occurs on a time scale in which vibrational distribution of internal energy occurs and higher order structural information is lost prior to backbone cleavage and product ion formation[24, 25].

1.1.1.2 Fragmentation by irradiation with photons

An alternative to collisions with a neutral gas or surface, ions can have energy deposited in them through irradiation with photons. Most commonly, the laser is of fixed wavelength in the far infrared spectrum. 10.6 μm wavelength CO_2 lasers are often used because they are plentiful and low cost. Each photon of 10.6 μm absorbed by the ion deposits 0.1 eV of energy into the ion which is then redistributed as vibrational energy. Again assuming a peptide bond strength of 2 eV, the energy per photon is well below the fragmentation threshold of most bonds and multiple photons must be absorbed for the ion to fragment. Hence the term often applied to this method of ion activation is infrared multi photon dissociation (IRMPD). Due to the slow nature of IRMPD, the vibrational redistribution of energy may causes changes in structure prior to fragmentation and is not well suited to the study of higher order structure[26].

1.1.2 Higher order structure

As highlighted by the discussion above, CID, SID, and IRMPD techniques are limited in providing information about the higher order structure of ions. Information regarding higher order structure (secondary, tertiary, and quaternary) may be lost when using these

"slow" fragmentation techniques due to the statistical redistribution of collision energy throughout the bonds of the molecule resulting in fragmentation of the weakest bonds first[27]. These weakest bonds in biological molecules are those which determine the higher order structure of the molecule, such as non-covalent intramolecular hydrogen bonds[28]. Higher order structure may be probed through the use of electron induced fragmentation[29], or using methods which do not use the mass-to-charge ratio of fragment ions such as H/D exchange[28] or laser spectroscopy[30].

No single technique yields sufficient information to provide a complete picture of higher order structure[31]. Just as x-ray crystallography, the technique which has dominated protein structural study to date, must measure diffraction from many different angles to produce a crystal structure, mass spectrometry must gain information from many different experimental angles to piece back together the three dimensional ion structures. Information from cross section measurements[32], H/D exchange[15], or laser spectroscopy[17], can be combined with high levels of theoretical calculations[33] to gain the full picture of structure.

At this point, one may question whether the increasing complexity of the experiments required to determine gas phase ion structure via mass spectrometry has any real advantage over more mature techniques, such as x-ray crystallography or nuclear magnetic resonance (NMR) used to determine protein structure. At the very least, mass spectrometry based structural elucidation has the advantage of reduced sample requirements compared to the need for samples to form crystalline structures as for x-ray crystallography, and for samples to be high purity (>95%) as for NMR. Further, both x-ray crystallography and NMR require milligrams of sample, while mass spectrometry requires only micrograms[34]. Currently, the time required to determine a protein structure from any of these techniques is on the same

order of magnitude. The bottleneck for mass spectrometry lies at the calculations and data interpretation, not at the collection of data, which literally can be accomplished in minutes. If software and computers continue to evolve at the current rate, the time needed for structural calculations will decrease eventually making mass spectrometry substantially faster than other current alternatives.

1.1.2.1 Studied by irradiation with electrons and hydrogen/deuterium exchange

The capture of a low energy electron by an ion results in a rapid transfer of energy to the ion with dissociation occurring faster than electron emission ($<10^{-14}$ s). The electron capture and subsequent bond cleavage occur faster than the time required for vibration redistribution of energy within the ion. Because of the short time frame for fragmentation, the lowest energy bonds in the molecule often remain intact, including those non-covalent interactions which are largely responsible for structure. Also because electrons may cause bond cleavage wherever they are captured, primary structure information for large molecules maybe increased through more extensive fragmentation and a reduced number of rearrangements comparative to CID[29, 35-37].

An alternative approach to fragmentation through irradiation with electrons is probing of higher order structure through exchange of labile hydrogen atoms with deuterium atoms in either the solution phase or gas phase. Two types of information can be extracted from H/D exchange experiment, the extent of exchange and the rate of exchange. The extent of H/D exchange provides largely qualitative information about the folding of the entire protein, the accessibility of the specific exchange sites, or insight into how ordered the structure is in a specific region[15]. The rate of H/D exchange can be combined with theoretical calculations to provide validation of theoretical structures[38]. Current computational methods may produce many proposed structures of equal probability. Exchange rates for each exchange site in the

proposed structures can also be calculated and compared with direct measurements to support or disprove computationally derived theoretical structures. Using computational tools in conjunction with H/D exchange can provide insight into the secondary, tertiary, and quaternary structure of proteins. However, a disadvantage of the H/D technique is the time required to acquire enough data points to produce accurate rate curves, with total experimental times lasting hours[8, 28].

1.1.2.2 Gas phase laser spectroscopy

Quantum theory states that atoms and molecules only exist in discrete energy states. To transition between states an amount of energy exactly equal to the difference between states must be input or emitted[39]. Because the amount of energy needed to transition between states is a property specific not only to the molecule but is also affected by the molecule's surroundings, measurements of the energy between states provide higher order structural information. Similar to computer modeling used in conjunction with H/D exchange, proposed structures can be used to calculate theoretical infrared (IR) spectra. IR radiation is chosen as the energy range of choice for structural studies because IR provides information about the vibrational motion of molecular bonds, which can be directly related to bond strength, and has extensive theory existing to support experiments[40].

The conceptually simplest method to measure the amount of energy needed to transition between states uses direct absorption measurements, in which the intensity of radiation of a specific wavelength is measured before and after interacting with the ions of interest. By scanning through a wavelength one at a time and plotting the change in intensity of light as it interacts with the ions an IR spectrum would be produced. However, ions in the gas phase are extremely diffuse, and the change in light intensity due to absorption is so low as to be immeasurable. Instead most IR spectroscopy experiments performed on ions in the

gas phase rely on the action spectroscopy method, where the absorption of a photon leads to a change in state which enables or precludes the absorption of a higher energy photon preventing/causing fragmentation of the ion[41]. Plots of ion signal abundance plotted against the IR photon wavelength have peaks at wavelengths where absorption occurs and can be compared to theoretical IR spectra for calculated structures.

IR spectroscopy requires high cost lasers ($100,000+ for a tunable IR laser system) as well as cooling of the ions in the ion trap in order to ensure all ions are near the ground state to simplify spectra. Ion density is low, and irradiation time for each wavelength maybe long resulting in complete spectra taking up to hours to complete. In addition, the presence of multiple conformations for a single ion will result in a complex IR spectrum which may lead to inconclusive comparisons to calculated spectra. For IR spectra to provide conclusive results, it may be necessary to couple IR spectroscopy with some form of ion mobility separation[42, 43].

1.2 What shape-to-charge instruments provide

To this point, the discussion of higher order structure elucidation has hinted that multiple conformations (protein structures) may be present in the mass spectrum for a single mass-to-charge ratio ion. Mass spectrometers have no means of separating ions other than by the momentum, kinetic energy, or mass-to-charge ratio of an ion. Under conditions typical for mass analysis, none of the characteristics by which mass analyzers select ions is affected by the shape of the ion. ECD, H/D exchange, and IR spectroscopy may be able to detect the presence of multiple structures, but they cannot separate or eliminate ion structures, and often cannot differentiate the contribution each structure makes to the experimental results. Some other form of ion filtering must be employed to filter a single structure prior to further investigation by mass spectrometry. A method of shape-to-charge selection is needed to

provide a handle by which different conformations of the same mass-to-charge ratio ion can be selected. Shape-to-charge selection provides additional information and many benefits to the study of structure which are discussed in the following sections.

1.2.1 How many conformations are present

In the absence of the ability to filter single conformations, it would be advantageous to know the number of conformations present. ECD and IR spectroscopy provide very limited information about the number of structures present, and data interpretation becomes difficult due to the convolution of multiple conformations. H/D exchange can, in some cases, provide information about the number of different conformations based on the distribution of the deuterated species[8], however in the case of very similar structures the resolution of H/D exchange may prove too low to differentiate species[31].

For a shape-to-charge analysis technique to be successful, it should be able to provide insight into the number of conformations present. Not all charge states for a protein may have multiple conformations present, and information about the number of conformations per charge state allows those studying ion structures to pick charge states accordingly. In addition, knowledge of the number of conformations within a charge state provides information which may allow deconvolution of data acquired using the techniques discussed in **section 1.1.2**[19]. Finally, the number of conformations present for a given ion provides some insight into the stability of the structure for that ion[44]. If only a single conformation is observed it can be inferred that the structure is energetically favorable compared to all other possible conformations, while those ions with several conformations present have structures which are of similar energy and conversion between structures may be low energy transitions[44] which occur within the time scale of the shape to charge selection.

1.2.2 Cross section and energy minimized structures

Some shape-to-charge analyzers experimentally determine the orientationally averaged cross section of ions in addition to separating conformations. Orientationally averaged cross sections are the result of free rotation of the molecule during shape-to-charge based selection and provide a cross sectional measurement which is not unlike determining the shape of a spinning aircraft propeller[45]. If the propeller is not rotating, the fine structure, such as the number of blades, shape of the blades, and contours of the transition from the tip to center section, can be easily identified. However, with the propeller spinning at operational speed, nothing more than the diameter of the circle which encompasses the propellers rotation can be easily determined (figure 1.1). The collisional cross section measured for an ion is a 3D rotational average, rather than the 2D example of a spinning propeller, which also lacks fine structure and gives the most accurate measure of the largest dimensions in the molecule. The accuracy of these measurements can be quite impressive (error on the scale of 10 Å), and provides sufficient accuracy for comparison with energy minimized structures created through computational methods. Programs such as AMBER

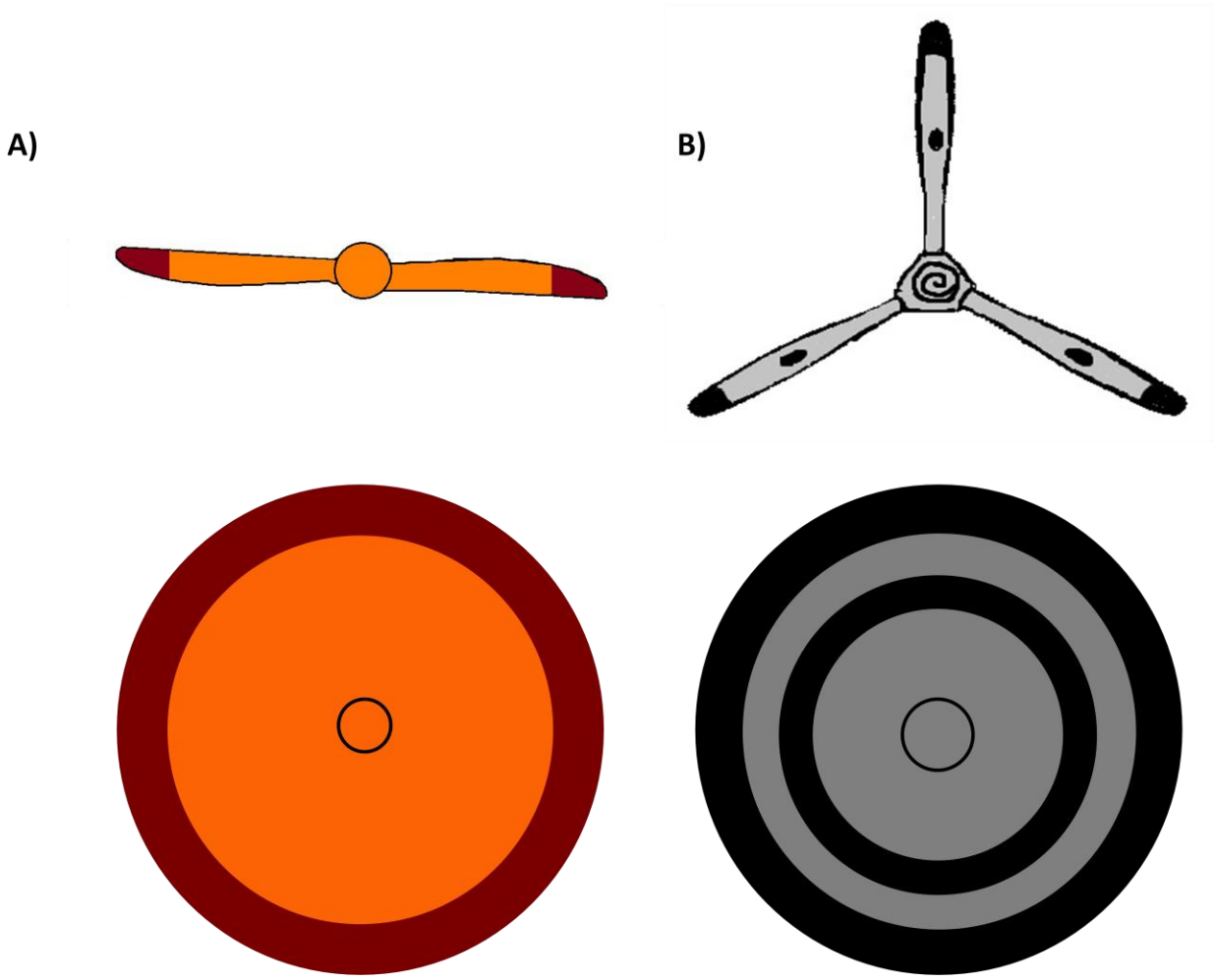

Figure 1.1 Rotation at high speed of a two bladed A) and three bladed B) propellers results in loss of fine structure due to 2 dimensional orientational averaging.

and GAUSSIAN provide computational tools to calculate minimum energy structures of user defined molecules. Several potential low energy structures may be calculated for a single ion. Each minimized structure can then undergo Monte Carlo type simulations of collisions between gas molecule and the proposed structure[46]. The error of these calculations is proportional to the square root of the number of trajectories and for 0.1% error $>10^6$ calculated gas ion collision trajectories are typically used[47]. These calculated cross sections may then be compared with experimentally determined collision cross section as a means of validating proposed structures.

1.2.3 High speed gas phase ion filtering

In addition to providing a tool to study conformation, shape-to-charge analyzers can be used to filter ions based on shape-to-charge ratio[48]. Because the shape-to-charge ratio of an ion is similar for ions of a similar class, entire families of ions may be selected to be transmitted simultaneously allowing identification of like ions in the mass spectrum, or single shape-to-charge ratio ions may be selected to perform an isolation step prior to mass analysis[49]. Shape-to-charge separations are carried out in the gas phase, making the time required to filter one structure from another short, on the order of milliseconds, and complex samples maybe rapidly separated[50]. Filtering ions by structure may be used to perform analysis of complex mixtures on single stage mass analyzers[51], improve limits of detection for low abundance analytes in complex matrices[52], or improve the selectivity of existing analytical methods such as liquid chromatography coupled to mass spectrometry by providing an additional dimension of separation[53]. Shape-to-charge separations are especially valuable for improvements in signal-to-noise ratio in trapping instruments, where a maximum ion capacity exists, by eliminating background ions and allowing more efficient use of ion storage capacity (discussed in **Chapter 6**).

1.3 Tools for selecting shape-to-charge

Shape-to-charge analyzers come in a number of sizes (lengths vary from 65 µm to 2 m)[54, 55], operate over a range of ion residence time (µs to .2 seconds)[54, 56], have very different figures of merit in terms of resolving power (from <10 to over 200), and provide separations based on different structural characteristics. In some cases, two shape-to-charge analyzers maybe coupled to form a hybrid analyzer which has improved capabilities due to an additional dimension of separation[9]. The following sections are intended to provide the

background, advantages, and disadvantages of the two most common type of shape to charge analyzer. While stand alone versions of these analyzers exist, only designs intended to couple to mass spectrometry will be discussed.

1.3.1 Ion mobility spectrometry

The most mature of shape-to-charge analyzer, ion mobility spectrometry (IMS), has been used in conjunction with mass spectrometry for over 40 years[48]. Ions are separated in IMS based on the velocity of the ion through a buffer gas under the influence of an electric

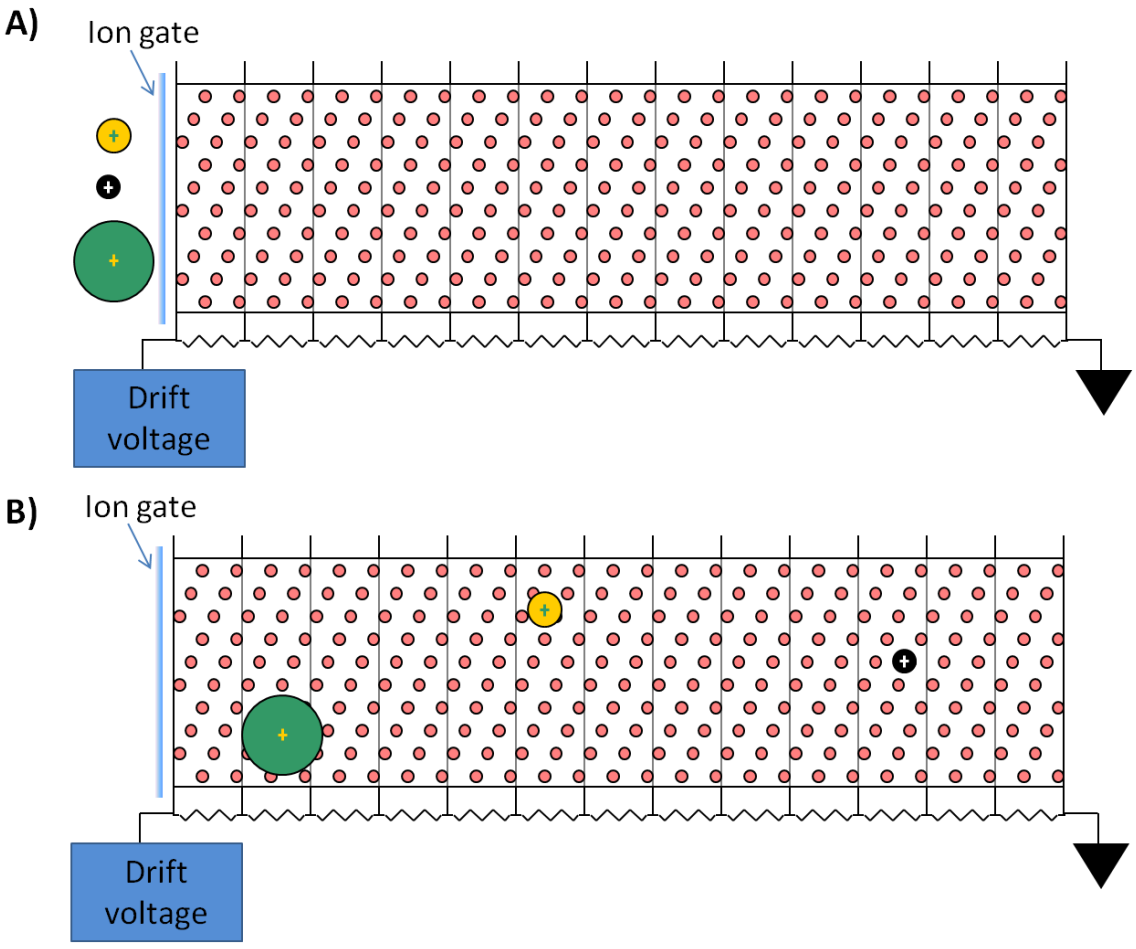

Figure 1.2 Diagram of IMS drift tube. The drift tube consists of multiple segments resistively connected to produce a linear voltage gradient through the tube. A collision gas (red dots) provides a friction against ion motion. Small packets of ions are gated into the drift tube A) and are separated in time based on their collision cross section B).

field generated along the length of a drift tube (figure 1.2). At the pressures (2-20 Torr) and

electric fields (10-300 V/cm) used in IMS, the acceleration due to the force of the electric field is counteracted by collisions with the buffer gas, resulting in ions moving through the drift tube at a constant velocity[57]. The velocity of the ion (v_d) as a function of the electric field (E) is referred to as the mobility of the ion (K) (equation 1.1).

$$K = \frac{v_d}{E} \qquad \text{Equation 1.1}$$

K for an ion is experimentally determined by injecting a small pulse of ions into the drift tube and measuring the time it takes for the ion to traverse the drift tube and reach a detector. The time for an ion to traverse the drift tube (t_d) is a function of the mobility of the ion, and the E applied along the length of the drift tube (L) (equation 1.2). To make K independent of the

$$t_d = \frac{L}{KE} \qquad \text{Equation 1.2}$$

experimental conditions, the reduced mobility can be calculated by standardizing the mobility to 273.2 K and 760 Torr. The reduced mobility, K_0, can then be calculated using equation 1.3, if the temperature (T) and pressure (P) used in the drift tube are known. The K of an ion can also be used to calculate the average collisional cross section (Ω_{avg}) for an ion of mass m_1, and charge z,

$$K_0 = K\frac{273.2}{T}\frac{P}{760} \qquad \text{Equation 1.3}$$

when a gas of mass m_2 and number density N acts as the buffer gas (equation 1.4).

$$K = \frac{\sqrt{18\pi}}{16}\sqrt{\left[\frac{1}{m_1}+\frac{1}{m_2}\right]}\frac{ze}{\sqrt{k_bT}}\frac{1}{N\Omega_{avg}} \qquad \text{Equation 1.4}$$

IMS provides the advantage of a fast (<100 ms) and accurate measurement of cross section which can be used in conjunction with theoretical calculations. Resolving power for

IMS, which is defined as peak width at half max (Δt) divided by t_d, frequently exceeds 100 for small multiply charged peptide ions. However, high resolution comes at the cost of size with drift cells measuring 1-2 m typically[55]. IMS systems also operate at reduced pressures, so they must be integrated into the vacuum system of the mass analyzer, between the source and analyzer, which significantly increases the difficulty of designing such systems. Finally, the pulsed nature of IMS reduces duty cycle, and the separation of mobilities in time make coupling IMS to many mass spectrometers difficult with most IMS-MS systems using time-of-flight mass analyzers.

1.3.2 High field asymmetric ion mobility spectrometry

High field asymmetric ion mobility spectrometry (FAIMS) is a relatively new analytical technique that separates gas phase ions at atmospheric pressure based on the difference in the mobility of an ion in high ($>10^4$ V/cm) and low ($<10^3$ V/cm) electric fields[58, 59]. The separation achieved in FAIMS is complementary to both conventional chromatographic techniques and mass spectrometry, allowing the selection of gas phase conformations or removing unwanted ions which would otherwise complicate mass spectra[53]. FAIMS does not provide a direct measurement of collision cross section as it measures neither the high (K_h) nor low field (K_l) mobilities, but instead separates based on the difference of K_h and K_l. The residence time of ions in FAIMS is on the order of milliseconds, thus enabling gas phase separations of ions in FAIMS to occur rapidly[60]. FAIMS can be used to differentiate isomers[61-63], resolve isobaric compounds[49, 64], and to improve the signal-to-noise ratio (S/N) when coupled to mass spectrometry[49, 65-67].

The FAIMS device (discussed in detail in **Chapter 3**) consists of two parallel electrodes. Ions are introduced into the FAIMS device from an atmospheric pressure source

and transported between the parallel electrodes by a carrier gas (figure 1.3). Separation is achieved by applying an asymmetric waveform to the electrodes described in detail in **Chapter 2**. This asymmetric waveform generates alternating high (E_h) and low electric fields (E_l). The displacement of an ion during the high (d_h) and low (d_l) portion of the waveform with duration of (t_h) for the E_h and t_l for E_l are described by equations 1.5 and 1.6

$$d_h = K_h E_h t_h \qquad \text{(Equation 1.5)}$$

$$d_l = K_l E_l t_l \qquad \text{(Equation 1.6)}$$

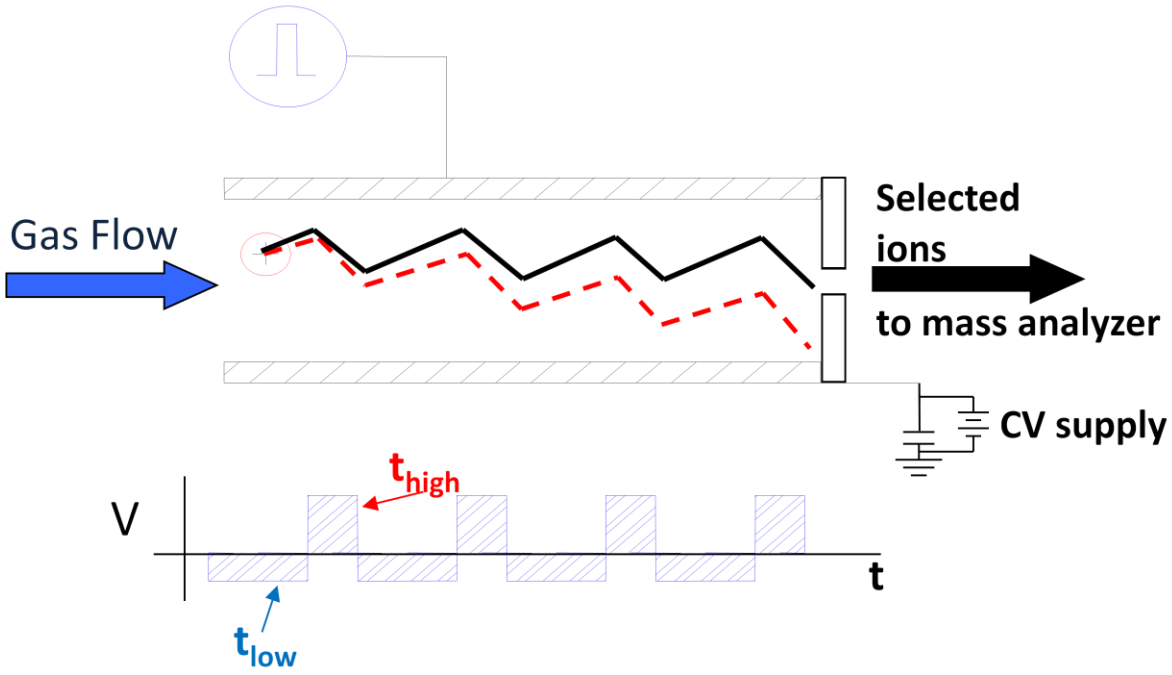

Figure 1.3 Schematic for FAIMS analyzer demonstrating ion motion within the FAIMS without compensation voltage applied (red dotted line) and with compensation voltage adjusted to transmit the selected ion to the mass analyzer. The ideal waveform for FAIMS is a square wave of equal area for the high and low field potions, which requires the duration of the high field to be shorter than the low field potion.

Ions are separated spatially by differing net displacements away from the central plane of the device due to a difference in mobility between the high and low electric field strength ($K_h \neq K_l$) which is due to the shape and charge of the ion. Ions are selected by application of a dc

potential, referred to as the compensation voltage (CV), to compensate for the off axis displacement of selected ions.

FAIMS is an atmospheric pressure ion filtering technique which produces a continuous beam of ions of a specific $K_h - K_l$ making it easily coupled to the source of any mass analyzer. Resolving power in FAIMS, defined as $\frac{CV_{peak}}{\Delta CV_{FWHM}}$, is typically lower than IMS normally in the range of 10-30 for peptides and proteins, however through use of gas blends resolving powers similar to IMS (over 100) have been achieved[55]. Residence times for ions are variable depending on device geometry but range between 20 μs and 0.2 seconds making FAIMS amenable to coupling to liquid chromatography or capillary electrophoresis. Due to the lack of FAIMS ability to experimentally derive collision cross sections, FAIMS is sometimes coupled to IMS which leads to improved peak capacity.

1.4 Interfacing shape-to-charge analyzers with mass spectrometers

The difficulty associated with constructing a shape-to-charge-mass spectrometry analyzer should be a consideration for those contemplating development of such systems. IMS and FAIMS have vastly different footprints, require different electronics, typically operate in different pressure regimes and couple to mass analyzers with varying degrees of difficulty. The following two sections attempt to highlight the design considerations and provide information about the potential problems associated with each design. Commercially available versions of FAIMS analyzers have now been in production for some time and provide an efficient, albeit costly relative to the cost of in house fabrication, solution to those in need of shape to charge separation. An ion mobility like analyzer is also currently in production, although the T-wave mobility analyzer operates off of a time dependent electric field[68] and cross sections must be acquired from calibration curves produced by the manufacturer[69]. The commercial success of the T-wave has prompted development of other

ion mobility based analyzers[70, 71], but no dates for availability have been made public at this time. These systems promise to be costly (~$750,000 for a complete IMS-MS instrument) and may limit user control to a degree which will continue to make in-house construction of an IMS-mass spectrometry systems an attractive alternative.

1.4.1 Coupling IMS drift cells with mass analyzers

IMS drift cells typically operate at reduced pressure, requiring their installation within the vacuum housing of the mass analyzer. The collision gas pressure in the drift cell (2-20 Torr) is similar to the first pumping region of many atmospheric pressure sampling sources used with mass analyzers. The pulsed nature of IMS drift cells result in poor coupling to continuous ion sources such as electrospray ionization (ESI) unless an ion accumulation device is used prior to the IMS gate lens[70, 72, 73]. Many ion sources today include an ion funnel which can be modified to accumulate ions prior to IMS injection. For these reasons IMS drift tubes are most often installed between the ion source region and the second pumping region, which operates at lower pressure ($<10^{-4}$ Torr) and may include ion guides or mass analyzing quadrupoles. Installing the drift tube in this region requires increasing the length of the first vacuum region to accommodate the IMS drift tube which maybe meters long.

IMS systems may employ a number of gases, but for those using IMS to determine collision cross sections to compare with theoretical structures, helium is preferred because it simplifies calculation of collision cross sections, provides high resolution, and high ion transmission[74, 75]. Helium has a low electric discharge barrier limiting the maximum electric fields which can be applied at a given pressure[55], and has a high diffusion rate making helium a difficult gas to pump using standard turbomolecular pumps[76]. When coupling IMS to a

mass analyzer which operates at high vacuum (<10^{-6} Torr), careful thought must be put into the vacuum system, and multiple stages of differential pumping may be necessary to maintain optimal pressure for each analyzer region.

IMS systems require high voltage power supplies, excellent electrical isolation between floating voltages and ground, and mass spectrometer signal acquisition hardware which is capable of handling large amounts of data. IMS drift tubes use dc gradients along the length of the drift tube of up to 300 V/cm[57]. When combined with 2 m long drift tubes, IMS systems may require dc power supplies capable of outputting up to 60 kV of drift voltage. Any ion focusing or storage device prior to the flight tube must be floated above the drift voltage resulting in the need for ion funnels and ion funnel rf and dc power supplies to be floated at 60 kV above ground potential. A final problem to consider is that of data handling. IMS is a pulsed technique with the time between IMS peaks measure in milliseconds. Coupling of IMS to beam type analyzers or slow acquisition trapping instruments require either loss of IMS resolution or multiple IMS scans per mass spectrum[77]. IMS is most often coupled to time-of-flight mass analyzers due to the high speed of analysis, and the ability to determine mass-to-charge ratios of all ions in a spectrum in parallel. While a typical mass spectrum yields mass-to-charge ratio and intensity, IMS-MS systems produce mass-to-charge ratio, intensity, and drift time information. Spectral acquisition must be of a high enough rate to provide accurate IMS peak shapes, and the IMS spectrum must be reconstructed from hundreds of mass spectra, requiring the processing of large amounts of data.

1.4.2 FAIMS analyzers

In comparison to IMS, FAIMS devices are simple to couple to mass analyzers. FAIMS devices are much smaller than the average IMS drift cell and operate at atmospheric

pressure. Coupling FAIMS to the mass analyzer is done external to the vacuum system and requires only a gas tight seal between the FAIMS and inlet capillary of the mass analyzer. Asymmetric waveform generators for FAIMS are more difficult to acquire than the dc power supplies needed for IMS, but some low cost designs exist which can be built in house (**Chapter 2**)[78]. Data acquisition is also simplified relative to IMS since FAIMS devices produce a constant beam of selected ions. CV voltages can be linked to the instrument control software to scan the CV in tandem with spectrum acquisition and adequate resolution for CV scan plots is achieved using less than 100 mass spectra for full range CV scans. Further, the constant ion beam produced by FAIMS makes coupling to any mass analyzer feasible, although the scan speed of FAIMS will be a function of mass spectra acquisition speed in the case of slow scanning analyzers.

1.5 Summary

The goal of this introduction chapter has been to outline the tools available for the study of ion structure with a particular focus towards protein structure. While mass spectrometry provides a means of studying higher order structure, it lacks the ability to isolate individual conformations prior to conducting experiments on structure, thus complicating data interpretation. Shape-to-charge analyzers provide a means to separate ions based on three dimensional structure prior to mass analysis thus simplifying the study of ion structure. Shape-to-charge analyzers provide offer other benefits such as improved signal to noise ratio for analytes, reduced spectra complexity, and improvement in limits of detection. FAIMS analyzers are a type of shape to charge analyzers which is relatively simple, can be coupled to any mass analyzer type, and provides high speed gas phase separations.

Chapter 2 is intended to provide background information on the production of high amplitude asymmetric waveforms for FAIMS analyzers. Discussion of the types of

waveform supplies attempts to highlight the advantages and disadvantages of each design. The remainder of the chapter is dedicated to the development of a dual harmonic waveform supply in house at UNC and evaluation of the waveform supplies performance.

Chapter 3 discusses results of protein conformation selection using the waveform supply developed in **Chapter 2** and a FAIMS analyzer designed by the Pacific Northwest National Labs (PNNL). Limitations of the PNNL design found during use to select protein structures are addressed through modification to the PNNL design. The results for modifications performed at UNC to develop a collinear electrospray ion source and reduce carrier gas temperature in the PNNL FAIMS are discussed. The reasons for the need of a FAIMS device which can operate in a "passive mode" are presented as well as some lessons learned about FAIMS design from work with the PNNL FAIMS.

Chapter 4 begins with the reasons for the development of in-capillary FAIMS device in collaboration between UNC and Bruker Daltonics. The design flaws of failed in-capillary FAIMS devices are discussed with an emphasis on the minimum requirements for a working FAIMS design. The lessons learned from the PNNL device, combined with the experience of two failed in-capillary FAIMS devices leads to the development of the third generation (G3) FAIMS device which is successful. The chapter closes with some examples of G3 applications.

Chapter 5 continues use of the G3 working to develop gas blends which can improve ion transmission and/or resolving power in FAIMS. Blends of argon and nitrogen lead to no significant improvements in ion transmission or resolution. The addition of small amounts of carbon dioxide with nitrogen leads to slight increases in the compensation voltage, and resolving power, but blends of made up of greater than 20% carbon dioxide are shown to

cause a decrease in resolving power. A mixture of helium and nitrogen is also evaluated which shows increases in resolving power for all blends testing of to 60% helium by composition, although signal intensity for low mass-to-charge ration ions is significantly decreased. To reduce the loss of low mass-to-charge ratio ions while taking advantage of the increased resolving power using high percentage mixtures of helium a method of linking helium content to compensation voltage is discussed.

Chapter 6 focuses on the development of a FAIMS device which is integrated into the electrospray ionization source of a commercial Bruker mass spectrometer. The design considerations for the fourth generation (G4) are discuss as well as early results from modified G3 systems to mimic G4 designs. The G4 is tested and shows the ability to provide high scan speed (12 second complete spectrum scans) at moderate resolving power (~15). Applications using the G4 to eliminate chemical noise, separate isobaric compounds, and filter protein conformations are discussed and the future directions for the device are briefly highlighted. Finally, **Chapter 7** summarizes the results and implications of each chapter and discusses the future development of FAIMS instrumentation.

1.6 References

1. Smith, R. D.; Cheng, X.; Bruce, J. E.; Hofstadler, S. A.; Anderson, G. A., Trapping, Detection, and Reaction of Very Large Single Molecular Ions by Mass Spectrometry. *Nature* **1994,** 369, 137-139.

2. Chen, R.; Cheng, X.; Mitchell, D. W.; Hofstadler, S. A.; Wu, Q.; Rockwood, A. L.; Sherman, M. G.; Smith, R. D., rapping, Detection, and Mass Determination of Coliphage T4 DNA Ions by Electrospray Ionization Fourier Transform Ion Cyclotron Resonance Mass Spectrometry. *Analytical Chemistry* **1995,** 67, 1159-1163.

3. Valaskovic, G. A.; Kelleher, N. L.; Little, D. P.; Aaserud, D. J.; McLafferty, F. W., Attomole-Senstivity Electrospray Source for Large-Molecule Mass Spectrometry. *Analytical Chemistry* **1995,** 67, 3802-3805.

4. He, F.; Hendrickson, C. L.; Marshall, A. G., Baseline mass resolution of peptide isobars: A record for molecular mass resolution. *Analytical Chemistry* **2001,** 73, (3), 647-650.

5. Hoffmann, E. D.; Charette, J.; Stroobant, V., *Mass Spectrometry: Principles and Applications*. John Wiley & Sons: New York, 2007; p 340.

6. Kaltashov, I. A.; Eyles, S. J., Studies of Biomolecular Conformations and Conformational Dynamics by Mass Spectrometry. *Mass Spectrometry Reviews* **2002,** 21, 37-71.

7. Loo, J. A.; He, J. X.; Cody, W. L., Higher Order Structure in the Gas Phase Reflects Solution Structure. *Journal of the American Chemical Society* **1998,** 120, (18), 4542-4543.

8. Freitas, M. A.; Hendrickson, C. L.; Emmett, M. R.; Marshall, A. G., Gas-phase bovine ubiquitin cation conformations resolved by gas-phase hydrogen/deuterium exchange rate and extent. *International Journal of Mass Spectrometry* **1999,** 185/186/187, 565-575.

9. Shvartsburg, A. A.; Li, F. M.; Tang, K. Q.; Smith, R. D., Characterizing the Structures and Folding of Free Proteins Using 2-D Gas-Phase Separations: Observation of Multiple Unfolded Conformers. *Analytical Chemistry* **2006,** 78, (10), 3304-3315.

10. Hart, K. J.; McLuckey, S. A.; Glish, G. L., Evidence of Isomerization During Ion Isolation in the Quadrupole Ion Trap. *Journal of the American Society for Mass Spectrometry* **1992,** 3, (6), 680-682.

11. Vachet, R. W.; Bishop, B. M.; Erickson, B. W.; Glish, G. L., Novel Peptide Dissociation: Gas-Phase Intramolecular Rearrangement of Internal Amino Acid Residues. *Journal of the American Chemical Society* **1997,** 119, (24), 5481-5488.

12. Yague, J.; Paradela, A.; Ramos, M.; Ogueta, S.; Marina, A.; Barahona, F.; de Castro, J. A. L.; Vazquez, J., Peptide rearrangement during quadrupole ion trap fragmentation: Added complexity to MS/MS spectra. *Analytical Chemistry* **2003,** 75, (6), 1524-1535.

13. Lin, T.; Glish, G. L., C-Terminal Peptide Sequencing via Multistage Mass Spectrometry. *Analytical Chemistry* **1998,** 70, (24), 5162-5165.

14. Futrell, J. H.; Miller, C. D., Tandem Mass Spectrometer for Study of Ion-Molecule Reactions. *Review of Scientific Instruments* **1966,** 37, (11), 1521-1526.

15. Campbell, S.; Rogers, M. T.; Marzluff, E. M.; Beauchamp, J. L., Deuterium Exchange Reactions as a Probe of Biomolecule Structure. Fundamental Studies of Gas Phase H/D Exchange Reactions of Protonated Glycine Oligomers with D2O, CD3OD, CD3CO2D, and ND3. *Journal of the American Chemical Society* **1995,** 117, (51), 12840-12854.

16. Nauta, K.; Moore, D. T.; Stiles, P. L.; Miller, R. E., Probing the structure of metal cluster-adsorbate systems with high-resolution infrared spectroscopy. *Science (Washington, DC, United States)* **2001,** 292, (5516), 481-484.

17. Bakker, J. M.; Mac Aleese, L.; Meijer, G.; von Helden, G., Fingerprint IR Spectroscopy to Probe Amino Acid Conformations in the Gas Phase. *Physical Review Letters* **2003,** 91, (20), 203003/1-203003/4.

18. Oomens, J.; Young, S.; Molesworth, S.; van Stipdonk, M., Spectroscopic Evidence for an Oxazolone Structure of the b(2) Fragment Ion from Protonated Tri-Alanine. *Journal of the American Society for Mass Spectrometry* **2009,** 20, (2), 334-339.

19. Badman, E. R.; Hoaglund-Hyzer, C. S.; Clemmer, D. E., Dissociation of Different Conformations of Ubiquitin Ions. *J Am Soc Mass Spectrom* **2002,** 13, (6), 719 - 723.

20. Harrison, A. G.; Young, A. B.; Bleiholder, C.; Suhai, S.; Paizs, B., Scrambling of Sequence Information in Collision-Induced Dissociation of Peptides. *J. Am. Chem. Soc.* **2006,** 128, (32), 10364-10365.

21. Kelleher, N. L.; Lin, H. Y.; Valaskovic, G. A.; Aaserud, D. J.; Fridriksson, E. K.; McLafferty, F. W., Top Down versus Bottom Up Protein Characterization by Tandem High-Resolution Mass Spectrometry. *Journal of the American Chemical Society* **1999,** 121, 806-812.

22. Alexander, A. J.; Thibault, P.; Boyd, R. K.; Curtis, J. M.; Rinehart, K. L., Collision Induced Dissociation of Peptide Ions. Part 3. Comparison of Results Obtained Using Sector-Quadrupole Hybrids with Those from Tandem Double-Focusing Instruments. *International Journal of Mass Spectrometry and Ion Processes* **1990,** 98, 107-134.

23. Polce, M. J.; Ren, D.; Wesdemiotis, C., Dissociation of the peptide bond in protonated peptides. *Journal of Mass Spectrometry* **2000,** 35, 1391-1398.

24. Cooks, R. G.; Ast, T.; Mabud, M. A., Collisions of Polyatomic Ions with Surfaces. *International Journal of Mass Spectrometry and Ion Processes* **1990,** 100, 209-265.

25. Despeyroux, D.; Wright, A. D.; Jennings, K. R.; Evans, S.; Riddoch, A., The Effect of Collision Energy and Nature of the Surface on the Surface-induced Dissociation Mass Spectra of Fluorobenzene Using a Four-Sector Mass Spectrometer. *International Journal of Mass Spectrometry and Ion Processes* **1992,** 122, 133-141.

26. Jockusch, R. A.; Paech, K.; Williams, E. R., Energetics from Slow Infrared Multiphoton Dissociation of Biomolecules. *Journal of Physical Chemistry A* **2000,** 104, 3188-3196.

27. McLuckey, S. A.; Goeringer, D. E., Slow heating methods in tandem mass spectrometry. *Journal of Mass Spectrometry* **1997,** 32, (5), 461-474.

28. Smith, D. L.; Deng, Y.; Zhang, Z., Probing the Non-covalent Structure of Proteins by Amide Hydrogen Exchange and Mass Spectrometry. *Journal of Mass Spectrometry* **1997,** 32, 135-146.

29. Zubarev, R. A.; Kelleher, N. L.; McLafferty, F. W., Electron Capture Dissociation of Multiply Charged Protein Cations. A Nonergodic Process. *Journal of the American Chemical Society* **1998,** 120, 3265-3266.

30. Stearns, J. A.; Boyarkin, O. V.; Rizzo, T. R., Spectroscopic signatures of gas-phase helices: Ac-Phe-(Ala)(5)-Lys-H+ and Ac-Phe-(Ala)(10)-Lys-H+. *Journal of the American Chemical Society* **2007,** 129, (45), 13820-+.

31. Robinson, E. W.; Williams, E. R., Multidimensional separations of ubiquitin conformers in the gas phase: Relating ion cross sections to H/D exchange measurements. *Journal of the American Society for Mass Spectrometry* **2005,** 16, (9), 1427-1437.

32. Clemmer, D. E.; Jarrold, M. F., Ion Mobility Measurements and Their Applications to Clusters and Biomolecules. *Journal of Mass Spectrometry* **1997,** 32, 577-592.

33. Balaj, O. P.; Kapota, C.; Lemaire, J.; Ohanessian, G., Vibrational signatures of sodiated oligopeptides (GG-Na+, GGG-Na+, AA-Na+ and AAA-Na+) in the gas phase. *International Journal of Mass Spectrometry* **2008,** 269, (3), 196-209.

34. Crews, P.; Rodriguez, J.; Jaspars, M., *Organic Structure Analysis*. Oxford University Press: New York, 1998.

35. Cerda, B. A.; Breuker, K.; Horn, D. M.; McLafferty, F. W., Charge/Radical Site Initiation versus Coulombic Repulsion for Cleavage of Multiply Charged Ions. Charge Solvation in Poly(alkene glycol) Ions. *Journal of the American Society for Mass Spectrometry* **2001,** 12, 565-570.

36. Olsen, J. V.; Haselmann, K.; L., N. M.; Budnik, B.; Nielsen, P.; Zubarev, R. A., Comparison of electron capture dissociation and collisionally activated dissociation of polycations of peptide nucleic acids. *Rapid Communications in Mass Spectrometry* **2001,** 15, 969-974.

37. Vekey, K.; Brenton, A. G.; Beynon, J. H., Electron Capture-Induced Decomposition (ECID): A New Method to Study Electron-Capture Collisions. *International Journal of Mass Spectrometry and Ion Processes* **1986,** 70, 277-300.

38. Engen, J. R.; Smith, D. L., Investigating Protein Structure and Dynamics by Hydrogen Exchange MS. *Analytical Chemistry* **2001,** 73, 256A-265A.

39. Skoog, D. A.; Leary, J. J., *Principles of Instrumental Analysis*. 4th ed.; Saunders College Publishing: Fort Worth, 1992.

40. Armentrout, P. B.; Rodgers, M. T.; Oomens, J.; Steill, J. D., Infrared Multiphoton Dissociation Spectroscopy of Cationized Serine: Effects of Alkali-Metal Cation Size on Gas-Phase Conformation. *The Journal of Physical Chemistry A* **2008,** 112, (11), 2248-2257.

41. Stearns, J. A.; Mercier, S.; Seaiby, C.; Guidi, M.; Boyarkin, O. V.; Rizzo, T. R., Conformation-specific Spectroscopy and photodissociation of cold, protonated tyrosine and phenylalanine. *Journal of the American Chemical Society* **2007,** 129, (38), 11814-11820.

42. DrayÎ², M. K.; Blunk, D.; Oomens, J.; Gao, B.; Wyttenbach, T.; Bowers, M. T.; SchaÌˆfer, M., Systematic Study of the Structures of Potassiated Tertiary Amino Acids: Salt Bridge Structures Dominate. *The Journal of Physical Chemistry A* **2009,** 113, (34), 9543-9550.

43. Drayss, M. K.; Blunk, D.; Oomens, J.; Polfer, N.; Schmuck, C.; Gao, B.; Wyttenbach, T.; Bowers, M. T.; Schafer, M., Gas-phase structures of solution-phase zwitterions: Charge solvation or salt bridge? *International Journal of Mass Spectrometry* **2009,** 281, (1-2), 97-100.

44. Li, J.; Taraszka, J. A.; Counterman, A. E.; Clemmer, D. E., Influence of solvent composition and capillary temperature on the conformations of electrosprayed ions: unfolding of compact ubiquitin conformers from pseudonative and denatured solutions. *International Journal of Mass Spectrometry* **1999,** 185/186/187, 37-47.

45. Shvartsburg, A. A., *Differential ion mobility spectrometry: nonlinear ion transport and fundamentals of FAIMS*. CRC Press: Boca Raton, 2009.

46. Wyttenbach, T.; Helden, G. v.; Bowers, M. T., Gas-Phase Conformation of Biological Molecules: Bradykinin. *Journal of the American Chemical Society* **1996,** 118, 8355-8364.

47. Shvartsburg, A. A.; Mashkevich, S. V.; Baker, E. S.; Smith, R. D., Optimization of algorithms for ion mobility calculations. *Journal of Physical Chemistry A* **2007,** 111, (10), 2002-2010.

48. Cohen, M. J.; Karasek, F. W., Plasma Chromatography(TM) - A New Dimension for Gas Chromatography and Mass Spectrometry. *Journal of Chromatographic Science* **1970,** 8, 330-337.

49. Robinson, E. W.; Garcia, D. E.; Leib, R. D.; Williams, E. R., Enhanced Mixture Analysis of Poly(ethylene glycol) Using High-Field Asymmetric Waveform Ion Mobility Spectrometry Combined with Fourier Transform Ion Cyclotron Resonance Mass Spectrometry
doi:10.1021/ac051709x. *Analytical Chemistry* **2006,** 78, (7), 2190-2198.

50. Eiceman, G. A., Ion-mobility spectrometry as a fast monitor of chemical composition. *Trac-Trends in Analytical Chemistry* **2002,** 21, (4), 259-275.

51. Nazarov, E. G.; Coy, S. L.; Krylov, E. V.; Miller, R. A.; Eiceman, G. A., Pressure effects in differential mobility spectrometry. *Analytical Chemistry* **2006,** 78, (22), 7697-7706.

52. Saba, J.; Bonneil, E.; Pomies, C.; Eng, K.; Thibault, P., Enhanced Sensitivity in Proteomics Experiments Using FAIMS Coupled with a Hybrid Linear Ion Trap/Orbitrap Mass Spectrometer. *Journal of Proteome Research* **2009,** 8, (7), 3355-3366.

53. Venne, K. B., Eric; Eng, Kevin; Thibault, P., Improvement in Peptide Detection for Proteomics Analyses Using Nano LC-MS and High-Field Asymmetry Waveform Ion Mobility Mass Spectrometry. *Analytical Chemistry* **2005,** 77, (7), 2176-2186.

54. Shvartsburg, A. A.; Tang, K. Q.; Smith, R. D.; Holden, M.; Rush, M.; Thompson, A.; Toutoungi, D., Ultrafast Differential Ion Mobility Spectrometry at Extreme Electric Fields Coupled to Mass Spectrometry. *Analytical Chemistry* **2009,** 81, (19), 8048-8053.

55. Kemper, P. R.; Dupuis, N. F.; Bowers, M. T., A new, higher resolution, ion mobility mass spectrometer. *International Journal of Mass Spectrometry* **2009,** 287, (1-3), 46-57.

56. Guevremont, R.; Ding, L. Y.; Ells, B.; Barnett, D. A.; Purves, R. W., Atmospheric pressure ion trapping in a tandem FAIMS-FAIMS coupled to a TOFMS: Studies with electrospray generated gramicidin S ions. *Journal of the American Society for Mass Spectrometry* **2001,** 12, (12), 1320-1330.

57. Eiceman, G. A.; Karpas, Z., *Ion Mobility Spectrometry*. Second ed.; CRC Press: 2005; Vol. 1, p 337.

58. Buryakov, I.; Krylov, E.; Nazarov, E.; Rasulev, U., A new method of separation of multi-atomic ions by mobility at atmospheric pressure using a high-frequency amplitude-

asymmetric strong electric field. *International Journal of Mass Spectrometry and Ion Processes* **1993,** 128, 143-148.

59. Purves, R. W.; Guevremont, R.; Day, S.; Pipich, C. W.; Matyjaszczyk, M. S., Mass Spectrometric Characterization of a High-Field Asymmetric Waveform Ion Mobility Spectrometer. *Review of Scientific Instruments* **1998,** 69, 4094-4105.

60. Shvartsburg, A. A.; Li, F. M.; Tang, K. Q.; Smith, R. D., High-resolution field asymmetric waveform ion mobility spectrometry using new planar geometry analyzers. *Analytical Chemistry* **2006,** 78, (11), 3706-3714.

61. Barnett, D. A.; Ells, B.; Guevremont, R.; Purves, R. W., Separation of leucine and isoleucine by electrospray ionization-high field asymmetric waveform ion mobility spectrometry-mass spectrometry. *Journal of the American Society for Mass Spectrometry* **1999,** 10, (12), 1279-1284.

62. Barnett, D. A.; Purves, R. W.; Ells, B.; Guevremont, R., Separation of o-, m- and p-phthalic acids by high-field asymmetric waveform ion mobility spectrometry (FAIMS) using mixed carrier gases. *Journal of Mass Spectrometry* **2000,** 35, (8), 976-980.

63. McCooeye, M.; Ding, L.; Gardner, G. J.; Fraser, C. A.; Lam, J.; Sturgeon, R. E.; Mester, Z., Separation and quantitation of the stereoisomers of ephedra alkaloids in natural health products using flow injection-electrospray ionization-high field asymmetric waveform ion mobility spectrometry-mass spectrometry. *Analytical Chemistry* **2003,** 75, (11), 2538-2542.

64. Guevremont, R.; Purves, R. W., High field asymmetric waveform ion mobility spectrometry-mass spectrometry: An investigation of leucine enkephalin ions produced by electrospray ionization. *Journal of the American Society for Mass Spectrometry* **1999,** 10, (6), 492-501.

65. Purves, R.; Guevremont, R., Electrospray Ionization High-Field Asymmetric Waveform Ion Mobility Spectrometry-Mass Spectrometry. *Analytical Chemistry* **1999,** 71, 2346-2357.

66. Cui, M.; Ding, L. Y.; Mester, Z., Separation of cisplatin and its hydrolysis products using electrospray ionization high-field asymmetric waveform ion mobility spectrometry coupled with ion trap mass spectrometry. *Analytical Chemistry* **2003,** 75, (21), 5847-5853.

67. Guevremont, R.; Makowski, B., Using FAIMS to increase selectivity for LC-MS analyses. *American Laboratory* **2005,** 37, (13), 11-+.

68. Pringle, S. D.; Giles, K.; Wildgoose, J. L.; Williams, J. P.; Slade, S. E.; Thalassinos, K.; Bateman, R. H.; Bowers, M. T.; Scrivens, J. H., An investigation of the mobility separation of some peptide and protein ions using a new hybrid quadrupole/travelling wave IMS/oa-ToF instrument. *International Journal of Mass Spectrometry* **2007,** 261, (1), 1-12.

69. Scarff, C. A.; Thalassinos, K.; Hilton, G. R.; Scrivens, J. H., Travelling wave ion mobility mass spectrometry studies of protein structure: biological significance and comparison with X-ray crystallography and nuclear magnetic resonance spectroscopy measurements. *Rapid Communications in Mass Spectrometry* **2008,** 22, (20), 3297-3304.

70. Baker, E. S.; Clowers, B. H.; Li, F. M.; Tang, K.; Tolmachev, A. V.; Prior, D. C.; Belov, M. E.; Smith, R. D., Ion mobility spectrometry-mass spectrometry performance using electrodynamic ion funnels and elevated drift gas pressures. *Journal of the American Society for Mass Spectrometry* **2007,** 18, (7), 1176-1187.

71. Clowers, B. H.; Ibrahim, Y. M.; Prior, D. C.; Danielson, W. F.; Belov, M. E.; Smith, R. D., Enhanced ion utilization efficiency using an electrodynamic ion funnel trap as an injection mechanism for ion mobility spectrometry. *Analytical Chemistry* **2008,** 80, (3), 612-623.

72. Hoaglund, C. S.; Valentine, S. J.; Clemmer, D. E., An Ion Trap Interface for ESI-Ion Mobility Experiments. *Analytical Chemistry* **1997,** 69, 4156-4161.

73. Tang, K.; Shvartsburg, A. A.; Lee, H. N.; Prior, D. C.; Buschbach, M. A.; Li, F. M.; Tolmachev, A. V.; Anderson, G. A.; Smith, R. D., High-sensitivity ion mobility spectrometry/mass spectrometry using electrodynamic ion funnel interfaces. *Analytical Chemistry* **2005,** 77, (10), 3330-3339.

74. Asbury, G. R.; Hill, H. H., Using different drift cases to change separation factors (alpha) in ion mobility spectrometry. *Analytical Chemistry* **2000,** 72, (3), 580-584.

75. Matz, L. M.; Hill, H. H.; Beegle, L. W.; Kanik, I., Investigation of drift gas selectivity in high resolution ion mobility spectrometry with mass spectrometry detection. *Journal of the American Society for Mass Spectrometry* **2002,** 13, (4), 300-307.

76. *Product and Vacuum Technology Reference Book*. Leybold Vacuum Products Inc. and Leybold Inficon Inc.: Export, PA, 1991.

77. Lennon, J. D.; Shinn, D.; Vachet, R. W.; Glish, G. L., Strategy for Pulsed Ionization Methods on a Sector Mass Spectrometer. *Analytical Chemistry* **1996,** 68, (5), 845-849.

78. Canterbury, J. D.; Gladden, J.; Buck, L.; Olund, R.; MacCoss, M. J., A High Voltage Asymmetric Waveform Generator for FAIMS. *Journal of the American Society for Mass Spectrometry* In Press, Accepted Manuscript.

Chapter 2
A Low Cost, High Amplitude, Asymmetric Waveform Generator

2.1 Introduction to asymmetric waveform generators

As stated in Chapter 1, FAIMS devices are easily fabricated since the device is little more than two parallel plates separated by al gap through which ions are introduced and separated based on the difference in K_h and K_l[1]. A more difficult to construct aspect of the device is a power supple capable of the production of the high amplitude asymmetric waveform. Ideally, the applied waveform would be an asymmetric square wave as shown in Figure 2.1 in which the area of the high and low field portions are of equal magnitude but opposite sign. In FAIMS, maximum sensitivity and selectivity requires the use of high amplitude waveforms with zero-to-peak voltages of 3 to 6 kV when using 1 to 2.5 mm analytical gaps[2, 3]. Production of these high amplitude waveforms can be achieved by four principle approaches. Linear, flyback, dual resonance, and differential sum type power supplies have all been used to produce waveforms for FAIMS analyzers. Though multiple high voltage waveform supply designs exist, the technology is by no means perfected and every supply currently available has shortcomings that make such designs limited in their analytical usefulness. This chapter describes the designs available for high amplitude asymmetric waveform supplies, and explains the work done at UNC in the development of a low cost, high amplitude supply. The chapter closes with characterization of the UNC supply.

2.1.1 The linear amplifier

Linear amplifiers are the simplest supply design but the least commonly used for the production of FAIMS waveforms. In the ideal case, they simply multiply the input

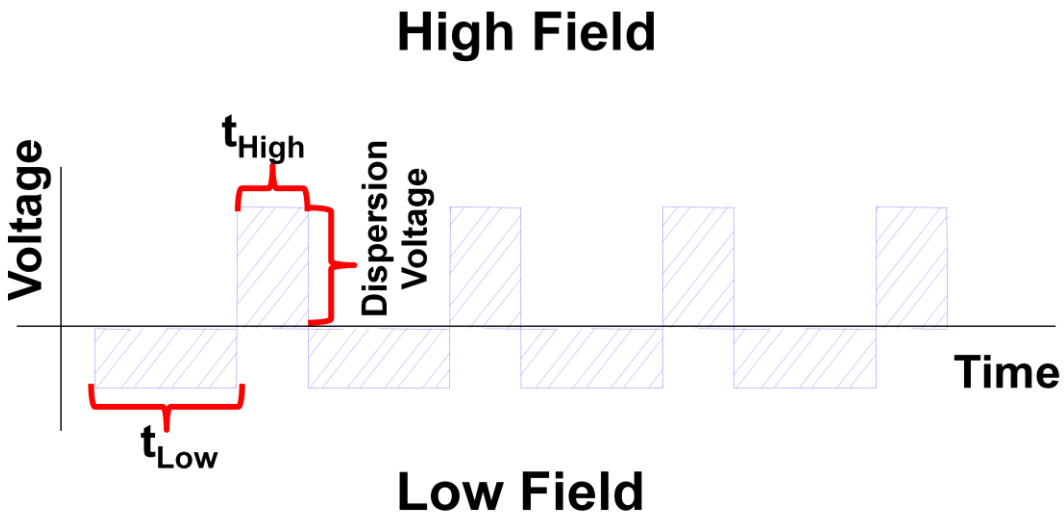

Figure 2.1 Ideal asymmetric square wave with high field portion twice the voltage but half the duration of the low field portion. The area of the high and low field portions of the waveform are exactly equal but of opposite sign. The peak amplitude during the high field segment of the waveform is referred to as the dispersion voltage (DV).

waveform by a fixed gain factor, producing a waveform with identical frequency and duty cycle as the input, but at much greater peak-to-peak amplitude. Figure 2.2 shows a simple schematic representation of the circuit used in linear amplifiers. In such designs, the desired waveform would be constructed using an arbitrary waveform generator and applied to the input. The waveform would then be amplified by some factor up to the rail voltage (+/- Vcc) applied to the power transistors. The rail voltage is limited by the maximum voltage difference between source and drain for the transistors, which rarely exceeds 1000 V with currently available high-power MOSFET transistors. The output of linear amplifiers can be a nearly ideal asymmetric square wave, or the shape and amplitude of the waveform can easily be changed through software control of the arbitrary waveform generator to produce

whatever waveform is desired. However, the peak amplitude of such designs are low compared with other circuit designs. Zero-to-peak voltage maximum for linear power amplifiers is ~1000 V, and would only provide sufficient waveform amplitude for devices with analytical gaps of reduced dimensions (see Chapter 4). Another problem is the amount of power linear amplifiers require. Even given the modest zero-to-peak voltage of 1000 V, the supply would need to be able to swing between -500 and positive 1000 V, if we assume the low field portion of the waveform is twice the time and half the amplitude of the high field portion (making the areas equal). The current required for a given change in voltage is calculated using equation 2.1.

$$i = \frac{V}{s} * C \qquad \text{(Equation 2.1)}$$

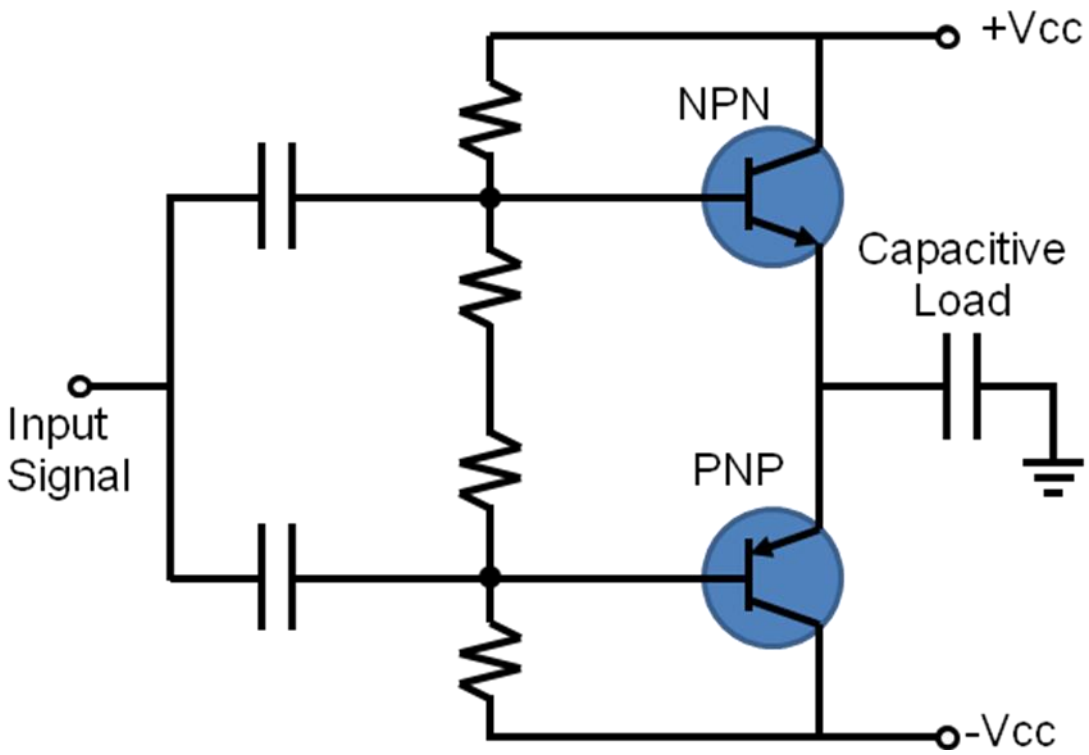

Figure 2.2 Schematic of linear power amplifier showing arrangements of transistors typical of a "B" class amplifier. When used to produce waveforms for FAIMS analyzers the capacitive load would be the FAIMS electrodes. + and – Vcc do not need to be equal; when using such a design for FAIMS waveforms –Vcc would be ½ or less of +Vcc.

Using this equation, given the capacitance (*C*) of the device, the voltage change (*V*), and the amount of time (*s*) to change the voltage, the required current (*i*) can be calculated. Assuming a rise time (13 ns) equal to 1% of the waveform period of a 750 kHz waveform and that the FAIMS device has 15 pF of capacitance, the current required for the rise is 1.7 A. The power that must be dissipated for a modest 1500 $V_{peak\text{-}to\text{-}peak}$ waveform is therefore 2600 W. The problem is further exasperated when we consider that in FAIMS devices with reduced analytical gap dimensions where 1500 $V_{peak\text{-}to\text{-}peak}$ amplitudes would produce acceptable performance, the waveform frequency required for optimal ion transmission increases (**Chapter 4**), further increasing the power needed to produce the waveform. While commercial power amplifiers do exist that could handle this power load they are larger and more expensive than resonant waveform type supplies which are discussed in the next sections. Furthermore, the large currents and voltages present potential safety hazards for individuals operating such amplifiers. Finally, linear amplifiers must be carefully protected against arcing or the amplifiers will be seriously damaged[4].

2.1.2 Flyback power oscillator

Flyback oscillators provide a waveform which is sinusoidal on the high voltage portion and clipped on the low field portion of the asymmetric waveform (Figure 2.3). The input waveform for triggering these devices is the ideal square wave discussed above. During the rising portion of the trigger input, the current is stored in the inductor. When the input drops to zero, voltage reverses through the inductor and builds up a high voltage across the FAIMS electrodes, which behave as a capacitor. The FAIMS electrodes discharge across the inductor in the same manner as a resonant LC circuit. The dispersion voltage DV and

duration (t_{DV})for the high voltage portion of the waveform maybe calculated by equations 2.2 and 2.3, respectively:

$$DV = \frac{Vt}{\sqrt{LC}} \qquad \text{Equation (2.2)}$$

$$t_{DV} = \pi\sqrt{\mathrm{LC}} \qquad \text{Equation (2.3)}$$

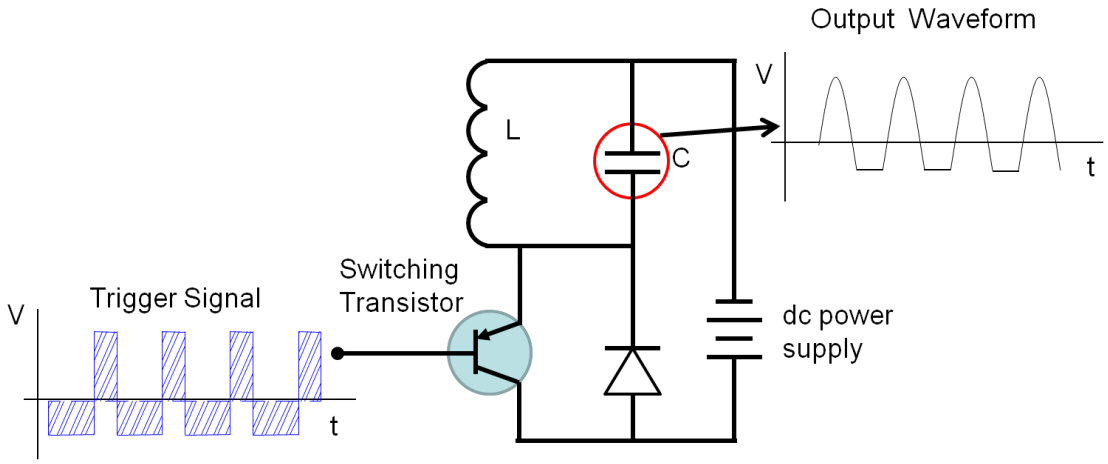

Figure 2.3 Schematic of flyback power oscillator. On the left is the ideal waveform being used as the trigger source, and on the right is the output waveform as measured across the FAIMS electrodes.

DV in Equation 2.2 a function of the voltage (V) output by the direct current (dc) power supply in Figure 2.3, the time (t) of the positive cycle of the trigger signal and the inductance (L) of the resonant coil and capacitance (C) of the load. The output is sinusoidal in shape until the voltage across the FAIMS electrodes goes negative, at which point the diode is properly biased to turn on (Figure 2.3). When the diode turns on, current is shunted away from the resonant LC circuit and returns to the power supply, clipping the low field waveform at a fixed voltage until the capacitor is again biased positive.

The output waveform is a compromise between the ideal asymmetric square wave and sinusoidal-derived asymmetric waveforms that are discussed in the sections below, and

results in instrument performance between the two (69 % of the resolution of an ideal waveform of the same amplitude [4]). Frequency and pulse duration are variable through the tuning of inductors or capacitors; however, the tuning range is relatively small due to the pulse duration being a function of $\sqrt{LC}$. Amplitude is a function of $\sqrt{LC}$ as well, which makes the stability of these supplies excellent. Published figures of merit are a maximum dispersion voltage of 1400 V at 2 MHz with variable duty cycle of up to 30%[5]. These supplies are far less sensitive to arcing than the previously discussed power amplifier, and generally can resume operation immediately after eliminating the cause of the arc[4].

2.1.3 Dual resonance waveform power supply

Due to the high power required to produce high amplitude square waves, most FAIMS rf supplies use the sum of sinusoidal waveforms to reduce the voltage rate of change across the capacitive load[6]. This waveform is described by the expression

$$V(t) = \left(2/3\right)D\sin(\omega t) + \left(1/3\right)D\sin(2\theta\omega t - \phi) \qquad \text{Equation (2.4)}$$

where D is the peak voltage on the high voltage portion of the waveform, also referred to as the dispersion voltage (DV), ω the waveform frequency in radian/s, and ϕ is a phase shift applied between the two waveforms (most often of $\pi/2$ radians)[7]. In dual resonance waveform power supplies, both sinusoidal waveforms are sent to a single input. The input waveform is not required to be a sinusoidal wave. For the purposes of the first amplifier stage, the input is similar to the ideal asymmetric square wave described in the previous section to provide optimal triggering for the linear amplifier. Regardless of the input waveform type, the low amplitude signal is generated by an arbitrary waveform generator and sent to the first stage amplifier input where it is then amplified to produce a high current, low voltage (tens of amps at 12 V) waveform that is applied to the primary of a doubly

resonant RLC circuit. A doubly resonant RLC circuit is created by two methods. One approach is to use two secondary coils in a single transformer with the output of transformer A wired in to the center tap of transformer B[8, 9]. Another approach is the use of a combination of series and parallel LC circuits combined[10]. Either approach creates a single output for the secondary of the transformer that has both sinusoids combined and applied to a single FAIMS electrode Figure (2.4).

Double resonant waveform power supplies are used in the majority of commercially available FAIMS systems and provide a reasonable compromise in terms of the power that must be dissipated by the initial amplification stage and the maximum voltage that can be produced (6000 $V_{0\text{-peak}}$), along with a waveform that is not ideal but offers similar performance (up to 56 % of maximum possible separation) to the ideal waveform[4, 6]. Because the output is produced by a resonant LC circuit, arcing poses little risk of damaging the supply, since the current stored in the LC circuit is small. In the case of a direct short circuit the resonance of the system is lost, eliminating power transfer and providing isolation between the sensitive power amplifier stage and the short.

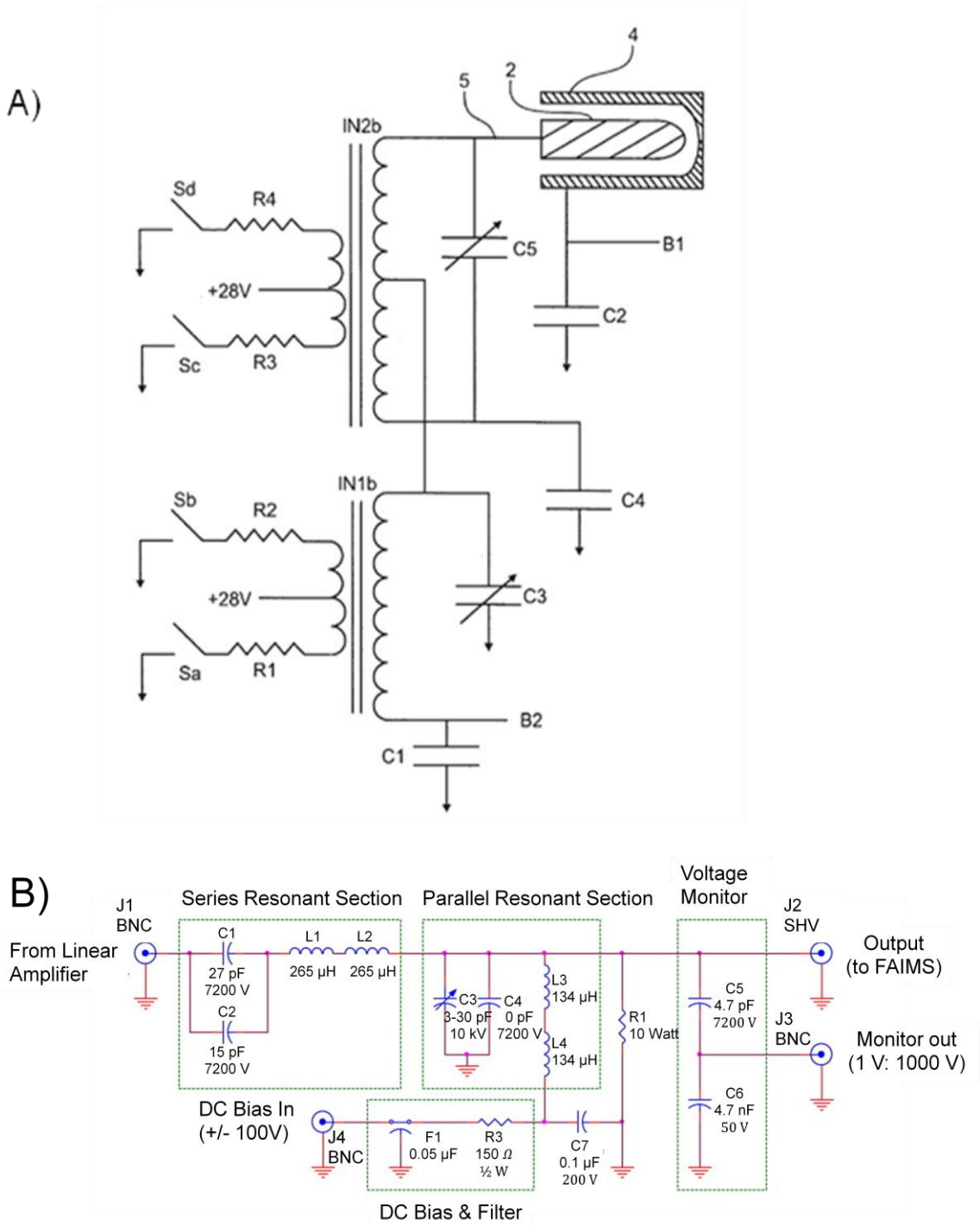

Figure 2.4 Schematics of dual resonant supplies show the two methods used to couple sinusoidal waves prior to the FAIMS device. In schematic A) the output of IN1b is sent to the center tap of IN2b and both waveforms are connected to the inner electrode of the cylindrical FAIMS device. In Schematic B) the output of the series LC section is combined with the parallel resonant section and sent to the single output J2.

Drawbacks for the design include a limited range of frequency and phase, and a maximum output voltage which is adequate for FAIMS geometries of 2.0 mm gaps and smaller but may limit resolution in the case of larger analytical gaps. Recently, designs for this type of supply have been published in the literature[10], but commercially available supplies are not sold separately from the FAIMS devices. For the university research lab working to build its own FAIMS system, purchasing such a supply will be difficult, and once acquired may not be flexible enough to work at different frequencies or high amplitudes.

2.1.4 Differential sum waveform generator

The differential sum asymmetric waveform supply differs from other asymmetric waveform supplies in that it utilizes two independent resonant LC circuits to produce two sinusoidal waves, which are then differentially summed across the analytical gap of the FAIMS device to generate the desired asymmetric waveform. This arrangement allows the user total control over the frequency, phase, and amplitude of each sinusoid while simplifying the electronics needed to produce the waveform. Each coil has a separate power amplifier stage and a separate input, eliminating the need for the waveform to be constructed by an arbitrary waveform card. Input signals consist of 50% duty cycle square waves of frequency *f* and *f/2*, which are independently amplified and sent to independent primaries on two separate coils. Each coil is a resonant circuit for a single frequency and is output to a single FAIMS electrode.

The power dissipated by the amplification stage is similar to that of a double resonant waveform generator as described previously. The output waveform shape is also similar to that of the double resonant waveform power supply. The design has the potential to be very low cost due to a simple, modular, low power amplifier stage; easy-to-create triggering

inputs; and low cost transformer design. Additionally, by using the differential sum, the high efficiency of resonant coils becomes additive when peaks are 180º out of phase, resulting in high voltages across the FAIMS gap (>8 kV_{0-p}). To date, these systems do not include feedback for amplitude or phase control, leading to the output waveform having some sensitivity to supply temperature. Once the supply temperature reaches equilibrium this type of supply exhibits very little drift in output amplitude or phase with time. While such designs have lower stability than other designs described previously the ability to produce very high amplitude waveforms at a fraction of the cost of other supplies lead the Glish lab to begin development of this type of supply for our own FAIMS waveform generator. The remainder of this chapter will discuss in detail the design and performance of a differential sum waveform generator build in collaboration between the Glish lab and the UNC electronics facility.

2.2 The UNC-built power supply

The development of FAIMS in the Glish lab required the design and development of a power supply which could produce the desired high amplitude asymmetric waveform needed for FAIMS devices with up to 2 mm analytical gaps. Commercially available power supplies, which all produce asymmetric waveforms through the summing of sinusoidal waves, proved to be too complex and expensive[8, 9, 11]. Less complex asymmetric waveform generators have been designed and constructed[6, 10, 12], but the maximum DV these supplies produce (<4 kV) limits their use to either miniature geometries or reduced sensitivity and selectivity in conventional geometry instruments[5, 6]. For this reason we began development of a FAIMS supply in collaboration with the UNC Electronics Facility.

The finished product (Figure 2.5) is a differential sum asymmetric waveform generator that can drive capacitive loads in excess of 15 pF at frequencies up to 5 MHz, and

produces output amplitudes in excess of 8 $kV_{0\text{-peak}}$. The operator has full control over frequency, phase, and amplitude. Perhaps the most impressive feature is that it can work so well, while being built for under $500.

2.2.1 Circuit design

Figure 2.5 is a simplified representation of the entire asymmetric waveform supply. The supply is made up of two identical FET modules, one for each sinusoid, and is driven by properly phased TTL square waves, of frequencies *f* and *f/2*. The *f* frequency square wave is generated by a synthesized function generator (DS335, Stanford Research Systems, Sunnyvale, CA). The output from the waveform generator is split at the output through a BNC "T" connection with one BNC providing the *f* frequency square wave to the *f* frequency FET module and the second BNC routed through a dual gate generator (Model 122, Molectron) which produces a variable delay time of 0-100 ms between the two waveforms. The phase shifted *f* frequency square wave is then applied to the gate input of a pulse generator (8013B, Hewlett Packard, Palo Alto, CA) which performs a divide by two function, outputting the *f/2* frequency square wave to the asymmetric waveform supply. Two low voltage, high current, regulated DC power supplies provide the switching current for the two FET modules. Each FET module drives the primary coil of a resonant ferrite core step-up transformer. The high voltage sinusoidal waveform produced by each coil is then applied to the FAIMS electrodes, with the *f* and *f/2* frequency waveforms being applied to opposite electrodes. Along with a dc bias voltage, the outputs of the transformers are differentially summed across the analytical gap of the FAIMS to produce the desired waveform (Figure 2.6).

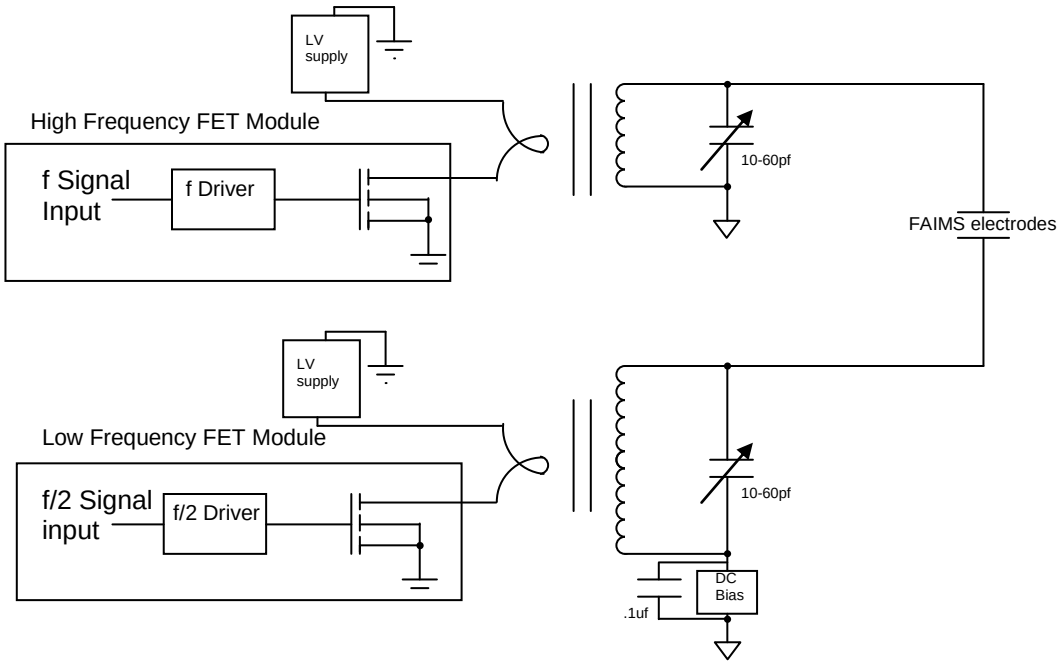

Figure 2.5 Simplified circuit of the asymmetric waveform generator functional elements, including the FET modules, two separate resonant coils and the output coupling of two sinusoidal waveforms.

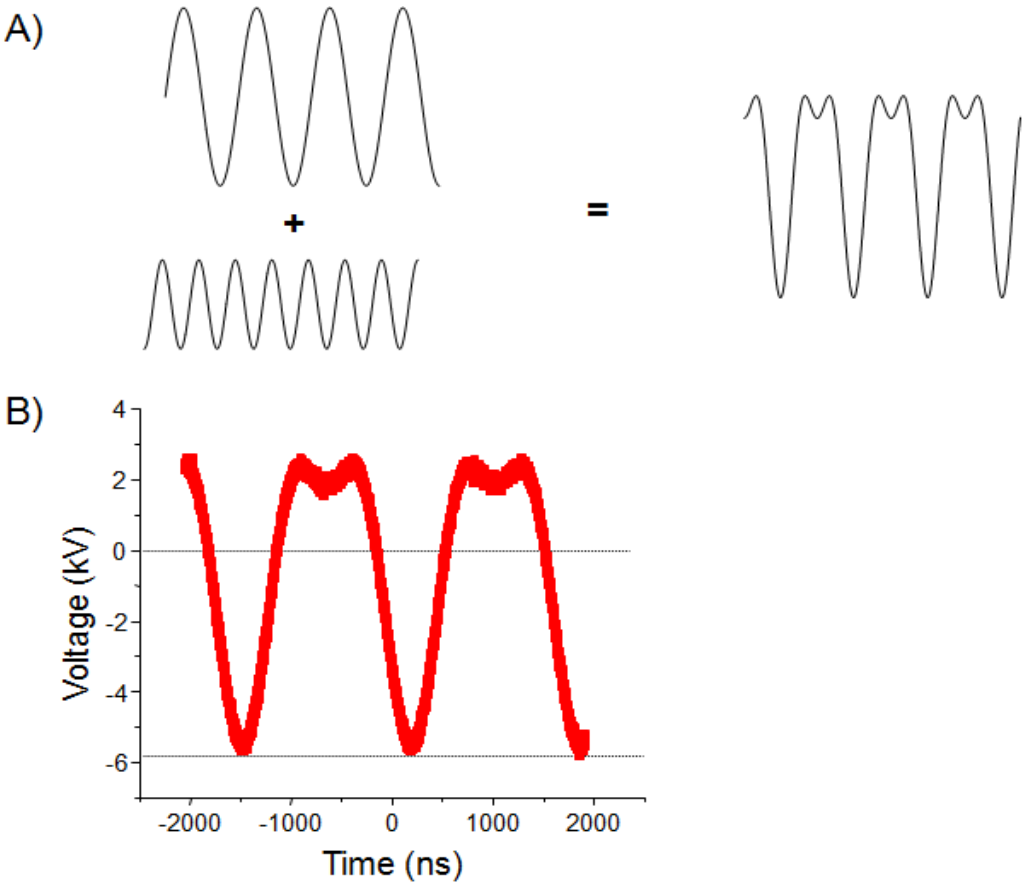

Figure 2.6 A) The summing of two sine waves of properly scaled frequency, phase, and amplitude to create an approximated asymmetric waveform. B) The output of the UNC supply during operation.

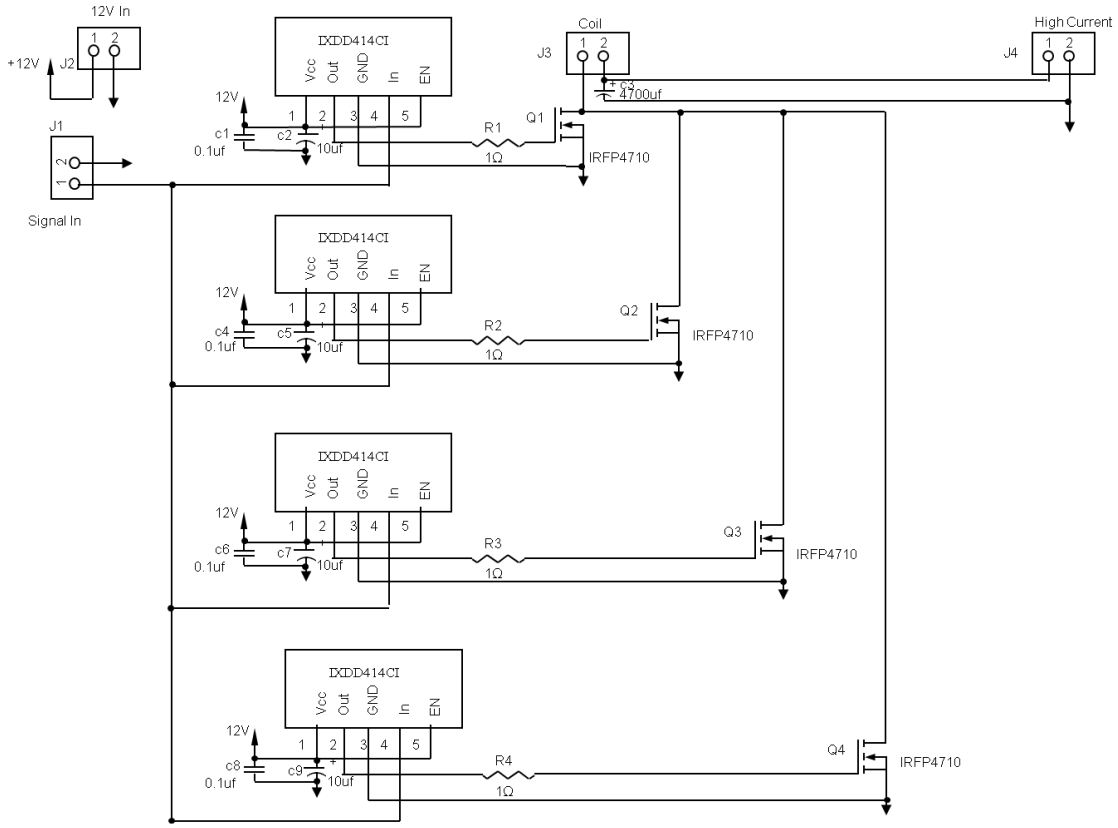

Figure 2.7 Detailed schematic of a FET driver module showing the parallel driver and power FET arrangement.

Each FET module (Figure 2.7) consists of four high current FETs (IRFP4710PdF, International Rectifier, El Segundo, CA) in parallel and four individual drivers (IXDD414CI, IXYS Corporation, Santa Clara, AC). The IRFP4710PdF FET was selected for the ability to handle high current; rated for 300 amps pulsed drain current, a low on resistance of 0.014 Ω, high drain-to-source voltage of 100 V, and high gate-to-source voltage of 20 V. Initially, an attempt was made to use discrete drivers to control the FETs; however, switching speeds proved inadequate. Subsequent testing showed that the IXDD414CI provided the best driver option, due to fast switching speed and a TO-220 package, which provides an optimal package type for connection to a heat sink. Between each driver and FET, a 1 Ω metal film,

non-inductive resistor rated at 2 W acts as a snubber and provides current limiting for the FET gates.

Figure 2.8 is a photograph of the assembled prototype supply. Each FET module can be seen in the foreground of the photograph. The FET modules are cooled through the use of heat sinks (Newark) and forced convection cooling via 120 V fans (4606, EBM-Papst Inc., Farmington, CT). DC power for the IXDD414CI drivers is provided by the 15 V dc supply (OLV15-15, Elpac Power Systems, Santa Ana, CA) located in the lower left hand corner of Figure 2.8. The PCB was designed with minimal trace lengths and maximized trace widths

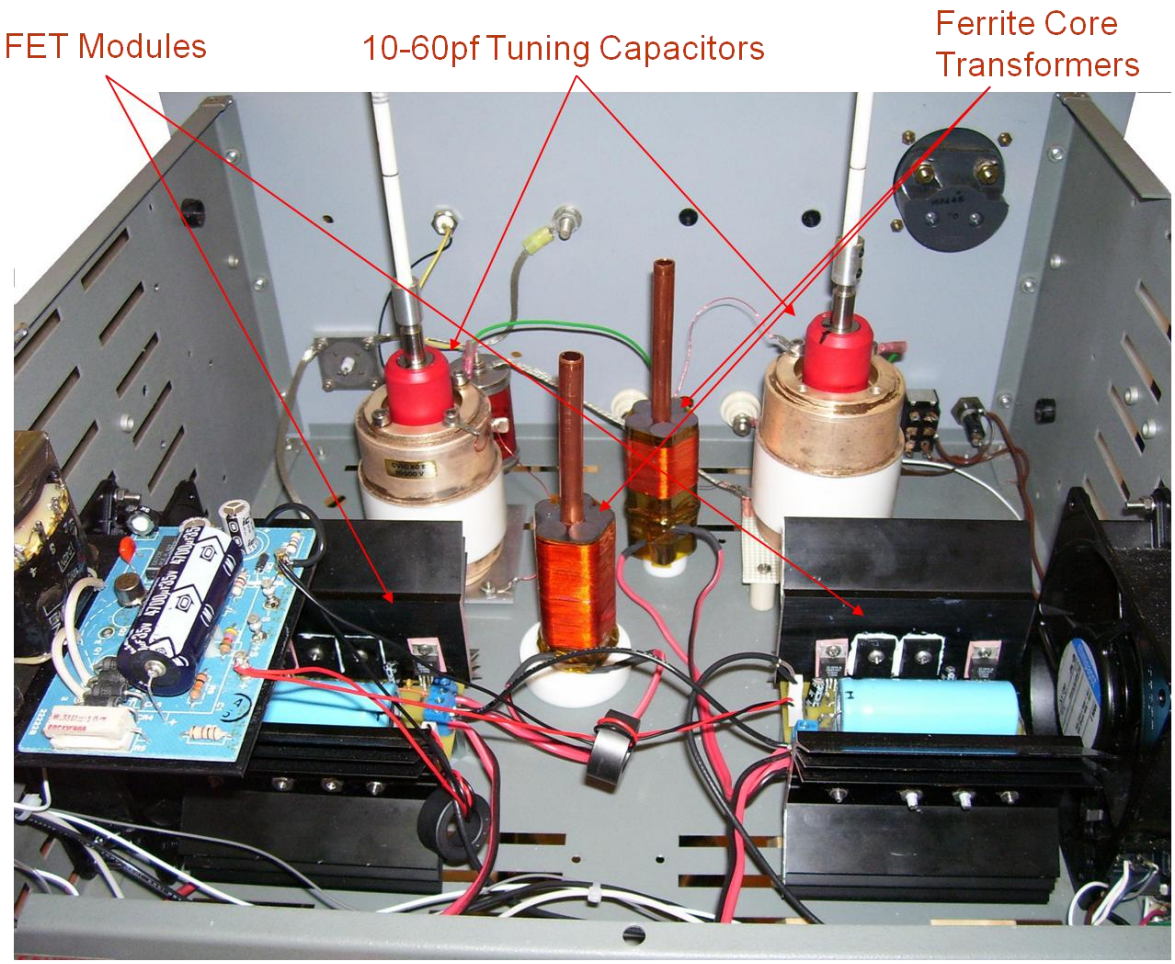

Figure 2.8 Photograph of the assembled UNC high amplitude asymmetric waveform supply with key components labeled

for the high current FETs. Additionally, the power leads from the low voltage, high current dc supplies were made as short and thick as possible to minimize resistive losses. Even so, due to the high instantaneous current drawn during operation, losses along the wires are considerable. To provide the instantaneous current a 4700 μF capacitor, labeled c3 in Figure 2.7 and visible in the center of each FET module in Figure 2.8, is used to provide the current locally and recharges between pulses. The entire power supply was installed in a 8U 19 inch rack-mountable box.

2.2.2 Transformer design

In Figure 2.8, the two rf coils are shown in the center of the enclosure. Each coil was custom made by placing five ferrite rods (R61-050-325, Amidon Inc, Costa Mesa, CA), measuring 12.7 mm diameter by 76.2 mm length, around a single piece of 12.7 mm diameter copper tubing. The primary winding of both coils consists of a single turn of 9 mm wide braid at the bottom of the ferrite rods. The secondary of each coil consists of AWG 7/36 Litz wire (a type of braided copper wire designed for high frequency applications) with the *f* frequency resonant coil having 60 turns in the secondary, and the *f/2* frequency resonant coil secondary consisting of 100 turns. The number of turns was determined experimentally to maximize the voltage output while keeping self-resonance significantly above the desired in-circuit resonance. The use of the linear ferrite rods allows for a separation of 13 mm between the primary and the high voltage secondary to prevent arcing, while retaining excellent magnetic coupling through the ferrite rods. Each coil assembly is isolated from ground via a 12.7 mm thick machined Teflon base. The copper tube through each coil allows the coils to be water-cooled, although under normal operating conditions this is not necessary.

The use of multiple ferrite rods was necessary to reduce heating in the coils due to core losses. Since core losses are proportional to flux density, increasing the total core area reduces the losses. A single ferrite core of the diameter desired in this application was not in current production so a bundle of coils was used to provide the desired diameter from commercially available 12.7 mm cores instead. Additionally, Litz wire was used to reduce the impedance of the secondary at high frequency due to the skin effect[13], which results in losses at high frequency due increased resistance.

2.3 Tuning

Each resonant circuit can be manually tuned with the use of a 10-60 pF variable capacitor (CV1C-60, Comet AG, Flamatt, Switzerland) to change the resonant frequency and phase of each coil. Maximum output from a coil is achieved when the resonant frequency of the LC circuit is matched to the output frequency from the waveform generator. Equation (2.4) demonstrates the necessity of controlling the phase between the two sinusoidal waveforms to construct the asymmetric waveform. This is achieved by use of both the variable capacitors for fine control and the use of a dual gate pulse generator to vary the delay between the two waveforms. The amplitude of each waveform is manually controlled through the use of two high current, low voltage dc power supplies. The *f* frequency coil is powered by a 25 A switching supply (MFJ-4225MV, MFJ Enterprises Inc, Mississippi State, MS) and the *f/2* frequency coil is powered by a 10 amp switching supply (TCR60S10-1, Electronic Measurements Inc., Neptune, NJ).

The procedure for tuning the supply is a three step process. When the supply is first powered on, only the *f/2* waveform 10 A supply is turned on. The capacitor for the *f/2* waveform is varied until maximum amplitude is achieved, and the amplitude of this

waveform is tuned to the desired level through control of the current output to the *f/2* frequency coil primary. At this point the *f* frequency low voltage, high current supply is turned on and the phase relationship relative to the *f/2* waveform is determined. If the two waveforms are close to having the desired phase relationship, then fine tuning is achieved through use of the variable capacitor for the *f* waveform. If the desired phase relationship cannot be achieved using the variable capacitors, the delay between the two waveforms can be varied using the dual gate pulse generator to change the delay time. Once the phase of the two waveforms has been properly set, the amplitude of each waveform is adjusted to the desired level through control of the current output from the dc supplies for both waveforms. Once tuned, the system can be operated for several days without retuning.

2.4 Supply performance

The output characteristics of the asymmetric waveform supply were evaluated using a digital oscilloscope (TDS 3012B, Tektronix, Portland, OR) and detailed in Figure 2.9. In this test, the power supply was connected to a planar FAIMS[14] device, the waveform was recorded by measuring the differential sum between the two plates of the FAIMS using two high voltage probes (HVP-15HF, Pintek Electronics Co. Ltd., Taipei Hsein, Taiwan), and acquired by the digital oscilloscope. In Figure 2.9a, it is shown that the output waveform is very low noise (less than 1% RSD) and that the amplitude and phase relationship between the *f* and *f/2* waveforms matches those conditions necessary to approximate an asymmetric square wave, described by Equation (2.4). Also of note is the amplitude of the DV, which is -5.5 kV. While in Figure 2.9a the DV is a negative voltage, a positive voltage of equal DV can be produced by changing the delay between the triggering waveforms. Maximum operational DV in the FAIMS device is determined by the materials of construction, carrier gas composition and the geometry of the FAIMS, which influences the voltage at which

dielectric breakdown occurs. When connected to a 15 pF high voltage capacitor, the supply is capable of producing over 8 kV of DV, although this voltage exceeds the dielectric breakdown barrier for FAIMS analyzer gaps of less than 2.5 mm.

Stability of the output is vital to any power supply that will be used to make scientific measurements. For this reason, the supply output was monitored during normal operation for approximately 15 hours. The data collected during this period of operation is shown in Figure 2.9b. Of note is that the 15 hours of operation is not continuous, but spread over two days of operation with the supply powered down for approximately 13 hours between periods of operation. This gives a true indication of stability in the supply showing the time necessary to come to stability and the amplitude of drift that occurs (less than 2% RSD). No tuning parameters where changed during the stability study. The waveform shown in Figure 2.9a was broken into components of interest, labeled A-E. While Figure 2.9b only shows the amplitude measured at points A-E, it also provides information on the stability of the phase difference between the two individual *f* and *f/2* waveforms. Component A is the DV of the waveform, shown in Figure 2.9 as being -5.8 kV. This is 1 kV higher than commercial supplies produced for the Thermo Electron FAIMS of similar analytical gap. Component C represents what is referred to as the low field "dip" and indicates that proper amplitude ratio of frequencies *f* and *f/2* are being applied to the FAIMS device. Component E provides peak to peak amplitude of the waveform which should be 50% greater than the DV alone if the supply is operating properly. The phase stability is indicated by monitoring parameters B and D. While graphically points B and D overlap and may seem redundant, any phase changes would cause the amplitude of B and D to shift in opposite direction and shift the peak value measured at C.

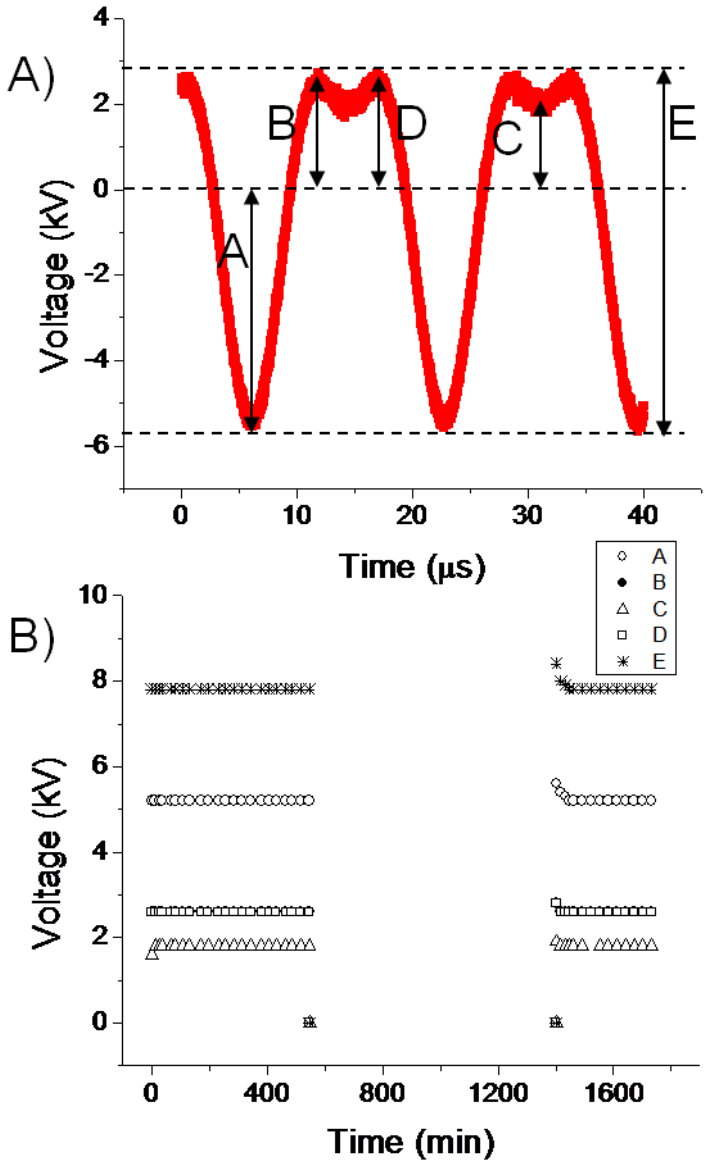

Figure 2.9 Plots demonstrating a) the output waveform and b) a plot analyzing the long term stability of the supply.

2.5 Conclusions

The power required to produce an ideal asymmetric square waveform to be used with standard FAIMS designs is too large for a supply which can be safely used in a laboratory setting. For that reason, multiple approaches exist to produce the desired waveform through the use of resonant circuits and the sinusoidal peak shape that they produce. Taking a different approach on the same theme, work between the Glish lab and the UNC electronics facility resulted in the development of an asymmetric waveform supply that uses the differential summing of sinusoidal waves across the capacitive load of the FAIMS electrodes to produce the desired asymmetric waveform. The supply is simple to build, consisting of two identical, independent FET amplifier modules, two resonant LC circuits using bundled ferrite cores, and two variable capacitors. The simple supply designed and constructed at UNC can produce waveforms of 1-5 MHz frequency, amplitudes of up to 8 $kV_{peak\text{-}to\text{-}peak}$. The UNC supply exhibits less than 2% drift with no tuning over multiple days, and can be constructed for less than $500. Simple high performance designs such as the one described in this chapter should assist future work in the custom instrumentation field of FAIMS analyzers by overcoming one of the most difficult instrumental challenges to building FAIMS analyzers. With further refinement of the supply layout, institution of feedback, and computer control, the UNC-designed supply could be competitive with any commercial supply in production.

2.6 References

1. Guevremont, R.; Purves, R. W., High field asymmetric waveform ion mobility spectrometry-mass spectrometry: An investigation of leucine enkephalin ions produced by electrospray ionization. *Journal of the American Society for Mass Spectrometry* **1999,** 10, (6), 492-501.

2. Purves, R. W.; Barnett, D. A.; Ells, B.; Guevremont, R., Elongated Conformers of Charge States +11 to +15 of Bovine Ubiquitin Studied Using ESI-FAIMS-MS. *Journal of the American Society for Mass Spectrometry* **2001,** 12, 894-901.

3. Guevremont, R. P., R., Atmospheric pressure ion focusing in a high-field asymmetric waveform ion mobility spectrometer. *Review of Scientific Instruments* **1999,** 70, (2), 1370-1383.

4. Krylov, E. V.; Coy, S. L.; Vandermey, J.; Schneider, B. B.; Covey, T. R.; Nazarov, E. G., Selection and generation of waveforms for differential mobility spectrometry. *Review of Scientific Instruments* 81, (2).

5. Miller, R. A.; Eiceman, G. A.; Nazarov, E. G.; King, A. T., A novel micromachined high-field asymmetric waveform-ion mobility spectrometer. *Sensors and Actuators B: Chemical* **2000,** 67, (3), 300-306.

6. Krylov, E. V., Pulses of Special Shapes Formed on a Capacitive Load. *Instruments and Experimental Techniques* **1997,** 40, 628-631.

7. Guevremont, R., High-field asymmetric waveform ion mobility spectrometry: A new tool for mass spectrometry. *Journal of Chromatography A* **2004,** 1058, (1-2), 3-19.

8. Potvin, L. B., Yves Patent#US 2007/0018629 Waveform Generator Electronics Based on Tuned LC Circuits. 2007/0018629, Jan 25, 2007, 2007.

9. Kouznetsov, V. Patent # 5801379 High Voltage Waveform Generator. 5801379, 1998.

10. Canterbury, J. D.; Gladden, J.; Buck, L.; Olund, R.; MacCoss, M. J., A High Voltage Asymmetric Waveform Generator for FAIMS. *Journal of the American Society for Mass Spectrometry* In Press, Accepted Manuscript.

11. McCracken, I. Patent #7058528 Automated Optimization of Asymmetric Waveform Generator LC Tuning Electronics. 7058528, June 6, 2006, 2006.

12. Eiceman, G. A.; Nazarov, E. G.; Miller, R. A.; Krylov, E. V.; Zapata, A. M., Micro-machined planar field asymmetric ion mobility spectrometer as a gas chromatographic detector. *Analyst* **2002,** 127, (4), 466-471.

13. Hsu, H. M., Effective series-resistance model of spiral inductors. *Microwave and Optical Technology Letters* **2005,** 46, (2), 107-109.

14. Shvartsburg, A. A.; Li, F. M.; Tang, K. Q.; Smith, R. D., High-resolution field asymmetric waveform ion mobility spectrometry using new planar geometry analyzers. *Analytical Chemistry* **2006,** 78, (11), 3706-3714.

Chapter 3
Modifications to conventional planar FAIMS devices

3.1 Introduction to FAIMS geometries

FAIMS analyzers may be constructed in any number of configurations, with only three major requirements: 1) A gap between two electrodes, across which a time-dependent asymmetric waveform composed of a high and low electric field component can be applied. 2) Surfaces on which ions can be neutralized when they do not meet the requirements for transfer through the device. 3) A force which transports the ions through the analyzer toward the detector. These minimum requirements for a viable design leave a great deal of flexibility in terms of electrode shape, length, gas composition, gas pressure, ion residence time, and materials used. Unfortunately, there is no single elegant solution currently available which simultaneously provides optimal resolution as well as optimum ion transmission. Rather, as is typical of scientific instruments, high resolution results in low signal intensity. The key is to find a compromise in terms of overall performance, which is further complicated by the need for the design to be built using available fabrication techniques. To date, two distinct analyzer types have been reported[1-4]. Each design has achieved variable levels of success in terms of sensitivity, resolution, and ease of construction. These two analyzer types are referred to as the planar[4] and cylindrical geometry[3] analyzers.

3.1.1 Cylindrical FAIMS analyzers

Cylindrical FAIMS analyzers are characterized by the use of two cylindrical electrodes with differing curvature, where the smaller radius electrode fits inside of the larger

(Figure 3.1). The analytical gap in FAIMS analyzers is defined as the distance between electrodes, and in the case of cylindrical analyzers is determined by the difference in radii of the inner and outer electrode. The curvature of the cylindrical FAIMS is determined by the

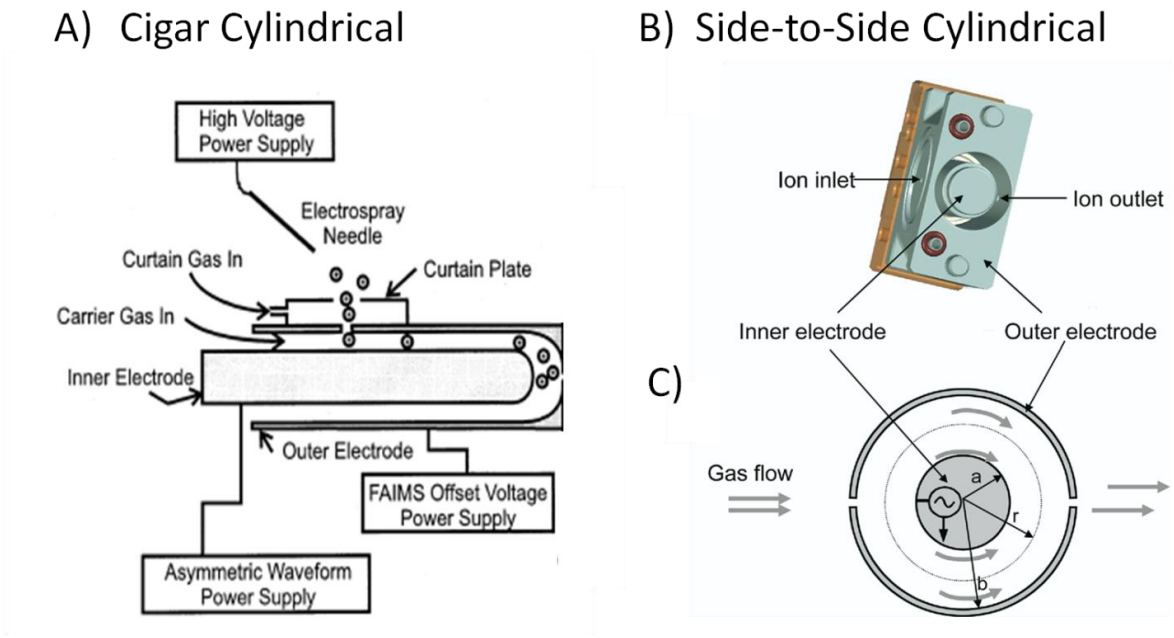

Figure 3.1 Schematic of A) Side on view of cigar type cylindrical FAIMS analyzer[5] B) an AutoCAD image of the Thermo side-to-side cylindrical FAIMS and C) An end on view schematic of the side-to-side FAIMS device[6].

average of the radii, and is a critical factor in the resolution and ion transmission of a device. Gap dimensions of cylindrical FAIMS devices range from 1.5 to 3 mm, with most devices having an median radius of curvature of 9mm[7]. There are two differing designs for cylindrical FAIMS devices. The most common is referred to as the "Cigar" type (figure 3.1A), and the newer version referred to as the side-to-side type (figures 3.1B and 3.1C)[6].

As the name implies, "cigar" type analyzers have a cigar shaped inner electrode, with the inlet end being flat and the exit end having a rounded dome. The outer electrode is machined as a cylinder with a slightly larger diameter than the inner electrode to create a constant analytical gap. Ions are injected orthogonally to the ion exit through a small hole in the outer electrode, which can be held at ground or have a small dc potential applied to it, while the

inner electrode is connected to the high amplitude asymmetric waveform and compensation voltage. Cigar type analyzers differ from all other FAIMS analyzers in that the distance between the dome of the inner electrode and the ion exit of the outer electrode is variable and is an important tuning parameter for device optimization. Varying the gap between the inner electrode and ion exit causes significantly different relative intensities and changes in resolution. As of yet, there is no means of calculating what exit gap distance is optimum for a given ion[8].

Side to side type analyzers are simple devices, with cylindrical inner and outer electrodes, and an ion inlet in line with the ion outlet. Although the inlet and outlet are co-linear, there is no line-of-sight for the incoming ions, and the ions must travel a minimum of one half the circumference of the inner electrode to reach the outlet. As with the "cigar" type analyzer, a high-amplitude asymmetric waveform and compensation voltage are applied to the inner electrode, while the outer electrode has only a dc bias voltage applied to assist in ion transmission into the mass analyzer. A feature of the side-to-side device is the ability to heat the electrodes. Originally instituted to provide temperature stability, it was quickly observed that an increase in temperature resulted in improved resolution. The observed improvements in performance are due to improved ion droplet desolvation and an increase in the E/N value.

Both analyzer types share similar operation, having four scan modes (Figure 3.2) which select for various ion types. These four modes (P1, P2, N1, and N2) refer to the polarity of the asymmetric waveform and polarity of the CV. Under conditions of a positive CV and

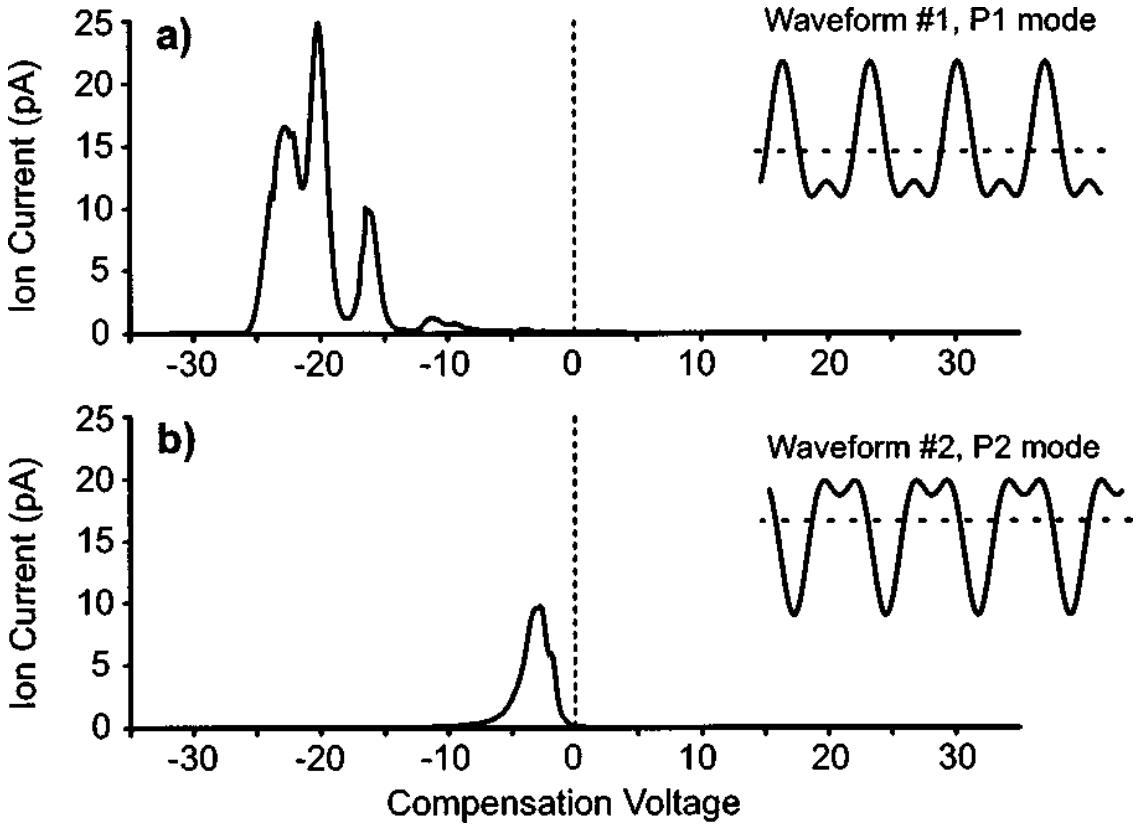

Figure 3.2 Operational modes for cylindrical FAIMS, the ions corresponding to mode P1 are completely lost in P2, those ions which are transmitted in each mode are totally unique with differing m/z values[9]

positive DV the analyzer is said to operate in mode P1, switching the DV to negative polarity results in P2 mode. Likewise a negative CV and negative DV is referred to as mode N2, and switching the CV to positive polarity while using a negative DV is N1 mode. Cylindrical devices are unique in that P2 and N1 are not equivalent to one another as would be expected, the ions in the left hand side of Figure 3.2 under P2 waveform conditions should appear in the right hand side of the N1 waveform plot. However, in cylindrical FAIMS ions may only be transmitted in a single mode. This is due to the inhomogeneous fields present in the analytical gap, which means that while fields in one mode have a focusing effect, fields in the opposite mode result in defocusing[9]. Cigar type analyzers have a longer ion path length and

hence, a longer residence time in the device. This longer residence time leads to higher resolution for a specific ion by the function of:

$$R = \frac{K(0)\langle F_3\rangle E_D\sqrt{t_{res}}}{4\sqrt{\bar{D}_{II}ln2}}\left(\frac{a_1 E_D^2}{N^2}\right) \quad \text{Equation (3.1)}$$

where R represents resolution, $K(0)$ the ions reduced mobility, E_D the dispersion field amplitude, t_{res} the residence time of the ion, D_{II} the diffusion coefficient for the ion and F_3 which is a form factor coefficient for the waveform, typically fixed at a value of 0.11 for a bisinusoidal waveform[7]. Due to the curved electrodes used in cylindrical FAIMS the electric fields are inhomogeneous which results in a focusing effect[10]. This is both an advantage and limitation, as the focusing results in higher ion transmission than that of planar devices, but limits resolution. In cylindrical FAIMS all ions of a similar structure feel the effect of the inhomogeneous fields and are focused together; resulting is a smaller spaceial distribution, and increased peak overlap relative to planar FAIMS. The focusing at atmospheric pressure in cylindrical FAIMS analyzers results in two advantages 1) higher dispersion voltages result in better focusing, resulting in an improvement in ion transmission at higher fields[9] and 2) ions can be trapped at atmospheric pressure[9]. While these are major advantages over planar FAIMS, the relative difficulty in the manufacture of cylindrical devices, the large number of variables which must be optimized to specific analyses, and lower resolution of the cylindrical devices are limitations which have lead researchers to pursue planar FAIMS technology[4].

3.1.2 Planar FAIMS Analyzers

The first paper published describing FAIMS used a set of parallel plates for FAIMS electrodes[1]. This is the simplest form of FAIMS device geometry and is currently referred to

as planar FAIMS. Shortly after the first published account of planar FAIMS, interest switched to cylindrical devices due to the higher ion transmission such devices offered. It was not until theoretical studies showed that resolution improved substantially with increasing electrode radius (to the limit that the radius is infinite) that interest was renewed in the simple planar FAIMS analyzer[4].

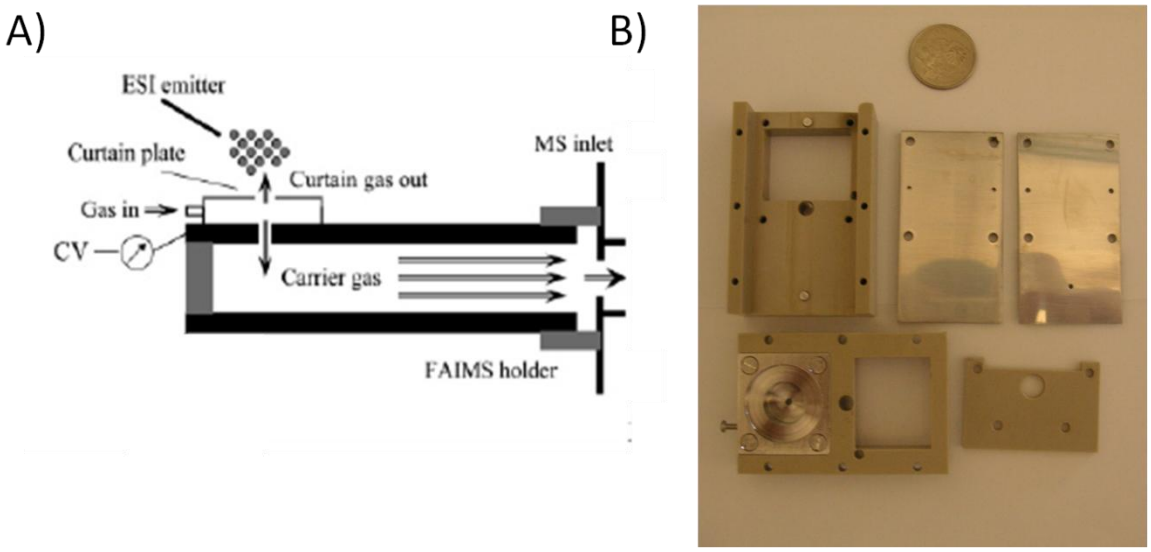

Figure 3.3 A) Schematic of PNNL design Planar FAIMS[4] and B) Photography of disassembled planar FAIMS with American quarter to give scale.

Planar analyzers consist of two flat parallel electrodes separated by an analytical gap through which ions are transported by gas flow perpendicular to the electric field (Figure 3.3). Analytical gaps range from 35 µm[11] to 2 mm[4] and electrode length ranges from 300 µm[11] to 50 mm[4]. In addition to the gap between electrodes and the length of the electrodes, the span (width) of the electrodes is an important parameter. To prevent ions from charging up the non-conductive surfaces which terminate the edges of the electrodes, the span of the electrodes must be a minimum of 6 times the gap width.

Asymmetric waveforms may be applied to a single electrode, or sine waves maybe applied to each electrode independently and summed across the analytical gap to produce the

desired waveform. Unlike cylindrical FAIMS, which has four scan modes, planar FAIMS has only two scan modes: either positive or negative scanning CV. Planar FAIMS devices have been developed with both heated[12] and cooled electrodes[13] which will be discussed later in this chapter.

3.1.3 Tradeoffs in sensitivity vs. resolution

. Planar devices have no trapping fields and operation of these devices at high resolution results in a decrease in sensitivity (Figure 3.4). However, the inhomogeneous fields in cylindrical FAIMS focus a range of ions rather than a single specific ion, resulting in peak broadening and overlap between different analytes as multiple compensation voltages transmit a broader range of ions through the device. The lack of focusing in planar FAIMS results in higher resolution than that of cylindrical FAIMS, given identical conditions[4].

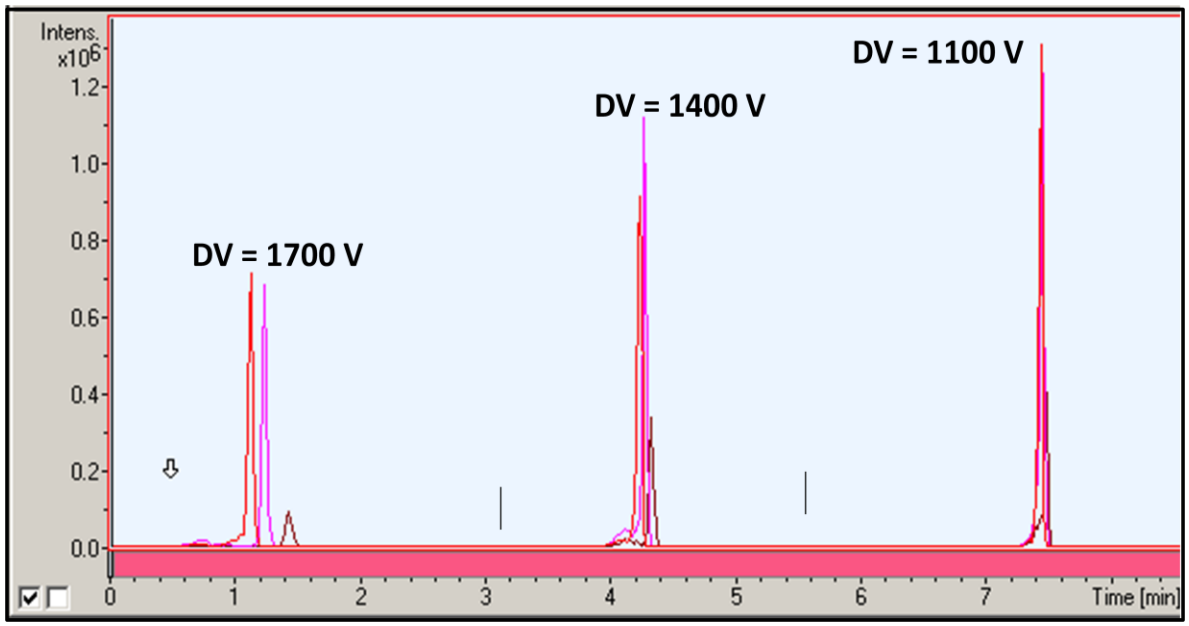

Figure 3.4 Three CV scans of a mixture of Hexakis (2,2-Difluoroethoxy) Phosphazene (622 m/z), Hexakis(1H, 1H, 3H-tetrafluoropropoxy)Phosphazene (922 m/z), and hexakis(1H, 1H, 5-Octafluoropentoxy)Phosphazene (1522 m/z) performed under differing dispersion voltages. With increasing dispersion voltage ion signal is attenuated while peak separation increases.

3.1.4 Advantages in operational modes and tuning

As mentioned in section 3.1.1, the cylindrical FAIMS has four modes of operation (P1, P2, N1, N2)[9]. This is not true for planar devices, where focusing due to inhomogeneous fields is not present. Planar FAIMS therefore have only two operation modes (P1=N2, P2=N1). With only two modes of operation, all ions may be observed by scanning from negative to positive CV without changing the waveform polarity as would be necessary in cylindrical FAIMS. The difficulty associated with switching between waveform polarities in order to acquire a complete spectrum depends on the cylindrical FAIMS analyzer design and the waveform generator used. In the best case scenario, physical connections to the device remain constant, and the waveform can simply be inverted. This can be accomplished with linear power amplifiers and waveform supplies, which use the sum of sinusoids to produce their output. With sinusoidal waveform generators, this is done by phase shifting the low frequency component relative to the high frequency component. The capability to shift phase through 360º is typically built into the supplies, but the resolution of the digital delays available are limited to ~5 ns increments. In the case of high frequency waveforms, this resolution proves insufficient to allow switching between positive and negative dispersion voltages without fine tuning through the use of variable capacitors. In the case of fly back power oscillator waveform generators, the polarity of the DV is a function of the design of the circuit. Changing the DV from positive to negative in these designs can be accomplished by modifications to the circuit or by switching connections to the FAIMS electrodes to modify the polarity of the field within the device. Switching the physical rf connection on the FAIMS analyzer is not possible in all device designs, as most are designed for the waveform to be applied to the inner electrode only, and do not provide sufficient electrical isolation between the outer electrode and the housing or ion source to allow application of

the FAIMS waveform. By comparison, all that is required to scan a complete spectrum in planar FAIMS is the ability to switch the polarity of the dc compensation voltage supply, which requires no tuning after initial calibration and setup.

Another drawback of the cylindrical FAIMS designs is that ion transmission occurs at high dispersion voltage. This is a problem when it is desirable for the FAIMS to operate in a "transparent" mode, where all ions are allowed to pass without separation. Using a co-linear ion injection with planar FAIMS, the device may be operated in a mode where both electrodes are connected to electrical ground, or with a low amplitude waveform insufficient to separate ions to transmit maximum ion current. Assuming the ion transmission in "transparent" mode can be nearly identical to the standard electrospray ion source (as will be shown in Chapter 4 and Chapter 6), planar FAIMS devices do not have to be removed from the instrument when not in use.

3.2 The PNNL device

Due to the advantages discussed above and the desire to use high resolution FAIMS to filter individual gas phase protein conformations, a planar geometry was determined to be the most desirable for our applications. At this time, few planar geometry devices were in use, most of which were small analyzers optimized for low molecular weight organic compounds[14-16]. Only one device appeared in the literature, which was a planar geometry designed to filter the gas phase structure of electrospray generated peptide and protein ions[4]. This planar FAIMS built at the Pacific Northwest National Laboratory (PNNL) was specifically designed for high resolution, with a residence time 20-100 times longer than previous planar FAIMS devices[4]. Modeling had been performed to optimize parameters for analytes which we were interested in studying (ubiquitin and bradykinnin)[4, 17-19], and the

device was simple to fabricate, with the tooling available at the UNC Chemistry Department machine shop.

3.2.1 Design

The PNNL planar geometry FAIMS device consisted of two mirror polished parallel electrodes, measuring two mm thick, 50 mm long, and 20 mm wide. These electrodes were separated by a two mm analytical gap, created by two mm thick alumina oxide spacers. The electrodes where not identical; one electrode had a hole through which ions could be injected orthogonal to the analytical gap. Both electrodes were held in outer casing constructed of two halves machined from polyether ether ketone (PEEK). The outer casing used for the orthogonal ESI source had additional machining to accommodate an ESI curtain plate, typically held at 1000 V relative to ground, and a carrier gas fitting. A carrier gas of variable temperature, composition, and flow rate was introduced into the outer casing into a mixing plenum between the ESI curtain plate and FAIMS electrode with the gas flow being partitioned between serving as carrier gas for the FAIMS (30%) and as counter current desolvation gas for the ESI emitter (70%). Electrical connections to the FAIMS electrodes were made through M2 screws, which were threaded directly into the electrodes via access points in the PEEK outer housing. A schematic and photograph of the planar FAIMS device constructed at UNC are shown in Figure 3.3. The entire device when assembled was press fit into a peak holder which was bolted to the mass spectrometer vacuum interface. The vacuum interface is also a specific PNNL design consisting of 11 circular 0.13 mm diameter parallel conductance limits in line with the analytical gap of the FAIMS device. The multi-hole inlet allowed sampling of ions distributed along the analytical gap where there are no electric fields to control ion motion[4].

3.2.2 PNNL device performance

The PNNL planar FAIMS device was tested by acquiring CV scans of ubiquitin, using a custom built mass spectrometer and the asymmetric waveform power supply described in chapter 2. The mass spectrometer consists of an atmospheric pressure interface designed to couple to planar FAIMS[4], an orthogonal ion funnel, an octopolar ion guide, an linear quadrupole mass filter (150-QC, Extrel, Pittsburgh, PA), and an rf only quadrupolar collision cell. A 25 μM bovine ubiquitin (U6253, Sigma, St. Louis, MO) solution composed of 49.95% water, 49.95% methanol, and .1% acetic acid was used for initial testing. Bovine ubiquitin was selected because it has been previously shown to have multiple gas phase ion conformations which can be separated by FAIMS[4, 5, 20, 21]. Samples were directly infused, using a syringe pump (model 22, Harvard Apparatus, Holliston, MA) coupled to a 75 μm diameter ESI tip. In this experiment, the mass spectrometer was set to pass selected ions, while the CV of the FAIMS was scanned to produce the CV spectra in Figure 3.5. The results show 5 conformations present in the +8 charge state and two conformations in the +7. These results agree favorably with those obtained using IMS instruments, although the resolution of the FAIMS analyzer is considerably lower[22]. Two conclusions can be drawn from Figure 3.5. First, the idea of using planar FAIMS for selection of gas phase ion conformations of proteins has been validated. This had been shown previously by other groups[5, 20, 21, 23-28], but this was a first in the Glish lab and was vital for moving forward with our own FAIMS analyzer designs. Second, none of the observed peaks are baseline resolved, and all of the peaks are low abundance, corresponding to 7% of the ion signal observed without the FAIMS analyzer being attached to the instrument. To improve transmission and resolution the PNNL device would require modification.

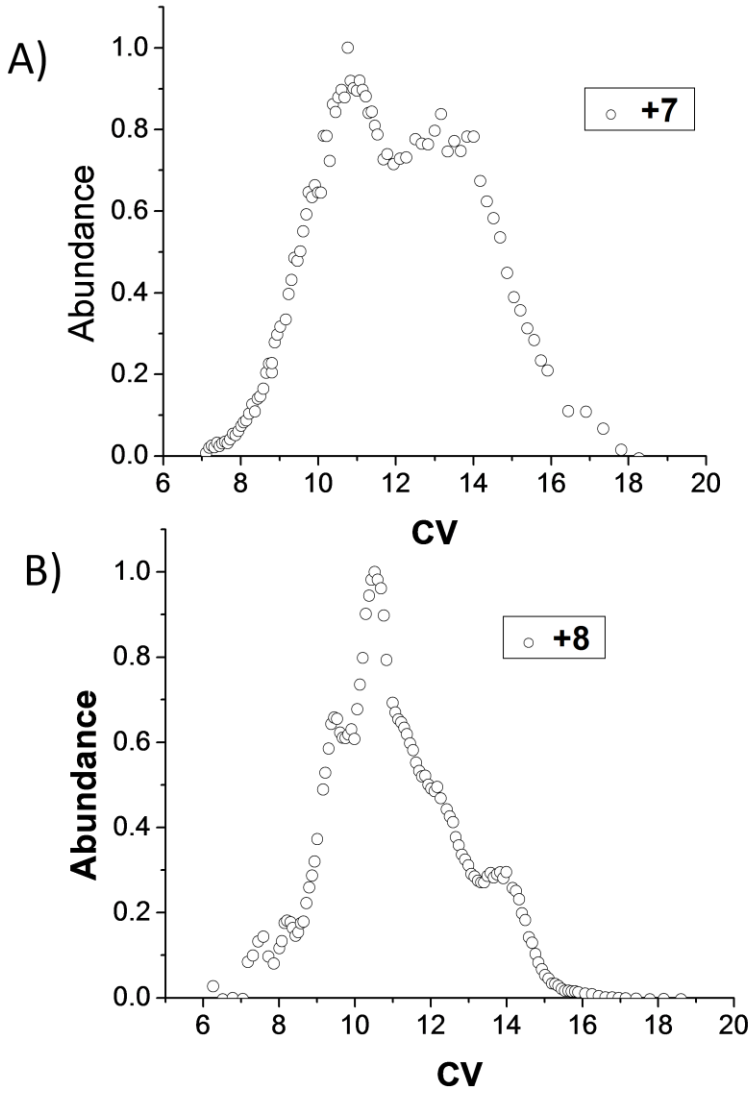

Figure 3.5 CV spectra showing multiple conformations present for the A) +7 and B) +8 charge state of bovine ubiquitin

3.3 Modifying the PNNL device

Given the results of the initial evaluation of the PNNL design, there were several disadvantages which became apparent. The most troubling problem with the PNNL FAIMS is the reduction in ion signal when the FAIMS is in use. Only 7% of ions observed with ESI

alone were observed with the FAIMS device. This problem is compounded by the fact that no ion signal can be observed when the device is attached to a mass analyzer but not actively performing a separation of ions. The ability to observe ion signal with the device turned off would more easily allow for the optimization of the electrospray before starting CV scans, troubleshooting for low ion abundances, and would enable the user to check for ion signal between CV scans without the removal of the FAIMS device. In addition, the presence of so many conformers and the lack of baseline resolution between peaks may be the result of isomerization within the FAIMS analyzer. Isomerization is possible due to high energy collisions between ions and carrier gas molecules in the FAIMS analytical gap. Ion heating is inherent to all FAIMS devices, not just the PNNL device.

Because the principle interest in using the PNNL design was to isolate individual gas phase ion structures for further study, improving resolution and limiting isomerization within the FAIMS analyzer are critical. Therefore, two modifications were proposed to solve these issues. The first was to give the ions a line of sight through the device in hopes of increasing ion transmission when performing gas phase separations and allowing ions to be transmitted through the FAIMS device when it is not actively filtering ions. The second was to cool the incoming carrier gas and device to reduce the effects of ion heating. By reducing the temperature in the device, isomerization would be reduced and resolution would be improved.

3.3.1 Converting from orthogonal to co-linear ion injection

Elimination of the orthogonal ion source and construction of a co-linear ion source required the fabrication of one replacement electrode and outer housing to replace the previous pieces which had been machined for the orthogonal ion source. Also, a new source

housing was machined which could attach to the back of the device. This rear piece would need to serve as the gas mixing plenum that the previous source design created, and to produce the same partitioning of incoming gas between desolvation and FAIMS carrier gas. Spacing between the curtain plate orifice and analytical gap was set at 2 mm (the minimum distance the metal curtain plate could be from the FAIMS electrodes without limiting the dispersion voltage, which could be applied between the FAIMS electrodes). Gas tight sealing of the new source was not possible due to the electrode and outer housing design. Gaskets where made from parafilm and placed in-between the curtain plate adaptor and FAIMS outer housing in an attempt to limit gas leakage in the ion source region.

3.3.2 Incorporating Peltier thermoelectric elements

In an effort to reduce the effective ion temperature for improved resolution and reduced isomerization, the FAIMS electrodes were cooled. This required slots to be machined into the PEEK outer housing of the FAIMS device. Alumina spacers between the FAIMS electrodes and Peltier thermoelectric cooling elements acquired from Melcor provide electrical isolation, while thermal conductivity remains suitable for cooling of the electrodes. Peltier thermoelectric coolers convert a voltage difference between dissimilar materials into a temperature difference. The temperature difference between the materials scales with the voltage difference and acts as a heat pump, pulling heat from one side of the device and transferring it to the other. Thermoelectric elements are small, typically having surface areas on the order of a few cm^2 and thickness of a few mm. With a maximum ΔT across a single element as high as 70 ºC, and element size on the same order as planar FAIMS electrodes, Peltier thermoelectric coolers seemed to be the ideal way to reduce the temperature of the FAIMS device. Control of the Peltier elements was achieved through the use of two Melcor

MTCC 1410 temperature controllers, which used feedback from platinum resistive temperature sensors placed in thermal contact with the FAIMS electrodes to control a variable dc power supply for cooling each electrode.

3.3.3 Cooling the carrier gas

Under normal operation, pure nitrogen carrier gas from the house nitrogen line was first routed through an Agilent RMSN-4 filter before being metered by a MKS 1179a flow controller and sent to the FAIMS device. To aid in cooling the FAIMS device, an additional segment of coiled aluminum tubing was added in series with the existing gas line and connected to the FAIMS device. The coiled tubing could be placed in a Dewar field with cryogen, and the temperature of the carrier gas could be reduced while aiding in the reduction of the temperature of the FAIMS device. By varying the cryogen used in the Dewar, the temperature of the carrier gas and the electrodes could be roughly varied as demonstrated by the measured values recorded in table 3.1. While not an extensive range of temperatures,

Table 3.1 List of Cryogens used to cool carrier gas for FAIMS device demonstrating the range of temperatures that can be reached by simply pre-cooling the carrier gas

Cryogen in dewar	Temperature of solution	Curtain plate temperature
Ice/water	0 °C	21.9 °C
Ice/salt water	-5 °C	20.9 °C
Dry Ice/acetone	-78 °C	2.9 °C
Liquid Nitrogen	-196 °C	0 °C

pre-cooling of the carrier gas provides an easy, low-tech way of reducing temperature within the FAIMS device, and demonstrated the ability to reach temperatures 25º below ambient laboratory temperatures.

3.4 Results and discussion of modified FAIMS

Modifications to the PNNL design FAIMS met with limited success. The orientation of the ion source was successfully changed (figure 3.6), allowing transmission of ions while inactive, but signal intensity was still very low. A calculated value for the relative increase in ion transmission between co-linear and orthogonal ion injection while FAIMS separation is inactive has no physical meaning because no signal is observed in the orthogonal ion injection mode and signal is observed in the co-linear mode, yielding an infinite percent increase. However, generally speaking, the losses with the FAIMS in place compared to the standard electro-spray interface are considerable, as greater than 70% of the ion signal is lost when the PNNL FAIMS is attached but inactive. The culprit for this loss of ion signal is the lack of gas tight seals in the FAIMS analyzer. Residence time for ions in the device is a function of the volume of the analytical gap and the pumping speed at the atmospheric pressure interface of the mass analyzer which the FAIMS is coupled too. By lacking gas tight seals where the FAIMS meets the mass spec, along the analytical gap, or between the two housing sections, the volume of gas which much be pumped by the mass analyzer increases slowing gas velocity through the analytical gap. Low gas velocities increase the residence time of ions, allowing for more time for the ions to diffuse into walls and be neutralized, decreasing ion transmission. This flaw in the PNNL design was not fully understood until the above modifications were made; ultimately leading to the design used in UNC developed systems (Chapter 4 and 6).

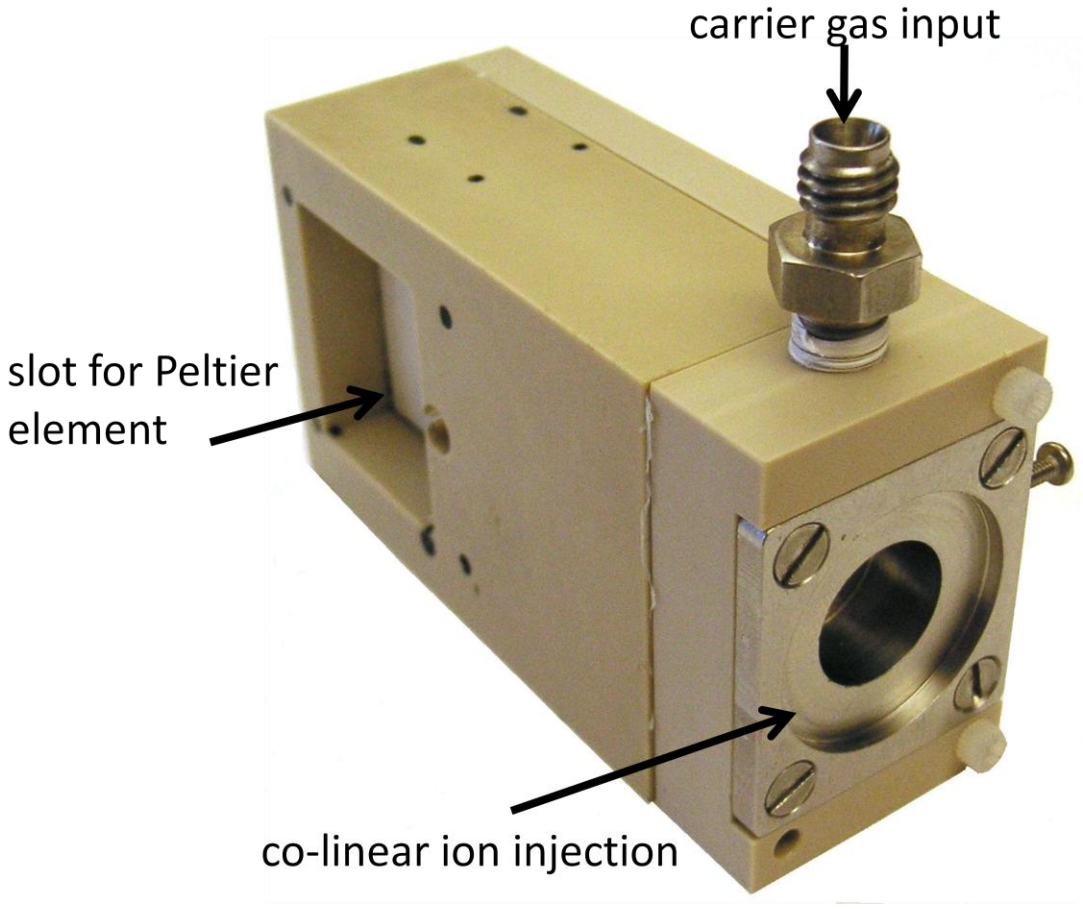

Figure 3.6 Image of the assembled modified PNNL designed FAIMS showing the added slots for Peltier thermoelectric coolers and the co-linear electrospray ESI plate

Cooling of the FAIMS proved problematic as well. Peltier thermoelectric coolers added capacitance to the FAIMS electrodes, exceeding the limitations of the asymmetric waveform supply. To reduce capacitance, alumina spacers where used to move the Peltier elements away from the electrodes, which limited the lowest temperature achievable by the Peltier elements to ~ 0ºC. Equal performance was achieved using liquid nitrogen to cool the incoming carrier gas, without the affecting the FAIMS high amplitude asymmetric waveform.

3.4.1 Increased signal intensity in active mode

Changing from orthogonal ion injection to a co-linear arrangement resulted in a doubling of signal intensity (figure 3.7). The use of a co-linear source also caused an increase in peak width. Both of these effects can be attributed to a lack of desolvation for the ions. While in both systems there is a counter-current gas, which in neither case is heated, in orthogonal ion injection, only desolvated ions are able to make the initial 90º turn into the FAIMS analytical gap. In a co-linear ion injection layout, all ions, desolvated or not, reach the analytical gap. Once ions enter the analytical gap, collisions between neutral carrier gas

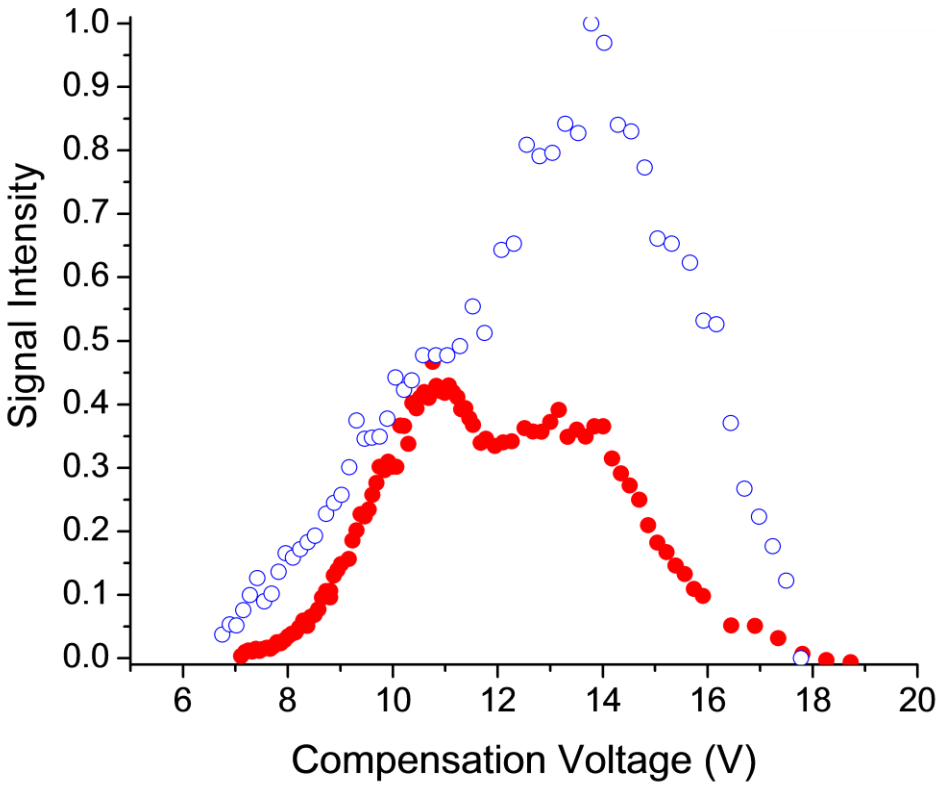

Figure 3.7 CV scans for the +7 charge state of ubiquitin for no cooling with orthogonal ion injection (red solid dots) and with device cooled to 0° C with co-linear ion injection (blue open circles).

molecules and solvated ion clusters cause the solvated ion clusters to evaporate as they traverse the analytical gap. A subsequent increase in noise, and peak broadening, due to solvated clusters changing size and cross section as they travel through the FAIMS device, are observed. These issues can be reduced or eliminated through the use of co-axial nebulizing gas for the ESI emitter, or by heating the carrier gas. However, heating of the carrier gas may result in potential structural isomerization.

3.4.2 Shifts in compensation voltage observed under cold conditions

A notable shift in figure 3.7 from two peaks of near equal abundance in the case of room temperature operation to a more favored peak at reduced temperature is observed. While the mathematical relationship between CV and cross sectional area is not fully understood, given the same class of ion, charge, and mass, CV roughly corresponds to the inverse of ion cross-sectional area. Higher CVs are necessary to provide more restoring force for ions with smaller cross sections because they undergo fewer collisions than larger conformations. If this is true, then the observation of shifts to higher CV intensities corresponds to a more compact structure, generally regarded as being more native-like than the highly extended structures which are observed in the case of harsh ion source conditions or extensive heating in the analyzer. At the very least, one can draw the conclusion that a reduction in the temperature of FAIMS results in changes in the relative proportion of structures. Therefore, temperature control (both heating and cooling) may be useful in future instruments as a way of controlling ion structure. These results represent the first sub-ambient temperature FAIMS spectra to be demonstrated and agrees favorably with previous theoretical work[12, 29]. It should be noted that the temperatures reached in these experiments never matched the temperatures calculated as being necessary to prevent structural

isomerization due to rf heating in FAIMS[29].

3.4.3 Is it worth it?

Ultimately, every attempted solution to problems observed with this device leads to yet another problem. At some point, the question becomes: is the design worth pursuing? For those in search of a tool to study ion structure, the answer is an unsure maybe. The PNNL device shows the ability to separate multiple conformations for a single mass-to-charge ratio of ubiqitin. In some cases, these results agreed with those observed using IMS, but most certainly the conditions in FAIMS are different than those used in IMS and are therefore only qualitatively comparable. Further, currently there is no means to allow structural determination from FAIMS separation, which is possible with IMS. However, FAIMS does show promise as a high speed gas phase filtering technique, similar in some ways to an atmospheric pressure quadrupole. For use as a fast gas phase separation, the PNNL design is badly designed. Lacking gas tight seals and designed for long residence time in order to achieve the maximum resolving power, the PNNL design has low ion transmission and scan times an order of magnitude longer than the designs discussed in chapter 4 and 6.

3.5 Summary

Based on the advantages of simple construction and high resolution, a planar electrode FAIMS analyzer design was acquired from the Pacific Northwest National Laboratory. The device was fabricated by the UNC chemistry machine shop, and then operated using the power supply detailed in Chapter 2. Low ion transmission and conformational isomerization due to rf heating lead to modifications to the original PNNL design. Those modifications resulted in notable changes in FAIMS spectra and improvements in ion transmission. Ultimately, the PNNL design provided validation of design concepts but was a limited design in terms of ion transmission.

3.6 References

1. Buryakov, I.; Krylov, E.; Nazarov, E.; Rasulev, U., A new method of separation of multi-atomic ions by mobility at atmospheric pressure using a high-frequency amplitude-asymmetric strong electric field. *International Journal of Mass Spectrometry and Ion Processes* **1993,** 128, 143-148
.

2. Guevremont, R.; Purves, R. W., High field asymmetric waveform ion mobility spectrometry-mass spectrometry: An investigation of leucine enkephalin ions produced by electrospray ionization. *Journal of the American Society for Mass Spectrometry* **1999,** 10, (6), 492-501.

3. Guevremont, R.; Purves, R., Comparison of experimental and calculated peak shapes for three cylindrical geometry FAIMS prototypes of differing electrode diameters. *Journal of the American Society for Mass Spectrometry* **2005,** 16, (3), 349-362.

4. Shvartsburg, A. A.; Li, F. M.; Tang, K. Q.; Smith, R. D., High-resolution field asymmetric waveform ion mobility spectrometry using new planar geometry analyzers. *Analytical Chemistry* **2006,** 78, (11), 3706-3714.

5. Purves, R. W.; Barnett, D. A.; Ells, B.; Guevremont, R., Investigation of bovine ubiquitin conformers separated by high-field asymmetric waveform ion mobility spectrometry: Cross section measurements using energy-loss experiments with a triple quadrupole mass spectrometer. *Journal of the American Society for Mass Spectrometry* **2000,** 11, (8), 738-745.

6. Barnett, D. A.; Belford, M.; Dunyach, J. J.; Purves, R. W., Characterization of a Temperature-Controlled FAIMS System. *J Am Soc Mass Spectrom* **2007,** 18, 1653-1663.

7. Shvartsburg, A. A., *Differential ion mobility spectrometry: nonlinear ion transport and fundamentals of FAIMS*. CRC Press: Boca Raton, 2009.

8. Guevremont, R., High-field asymmetric waveform ion mobility spectrometry: A new tool for mass spectrometry. *Journal of Chromatography A* **2004,** 1058, (1-2), 3-19.

9. Guevremont, R. P., R., Atmospheric pressure ion focusing in a high-field asymmetric waveform ion mobility spectrometer. *Review of Scientific Instruments* **1999,** 70, (2), 1370-1383.

10. Guevremont, R.; Ding, L. Y.; Ells, B.; Barnett, D. A.; Purves, R. W., Atmospheric pressure ion trapping in a tandem FAIMS-FAIMS coupled to a TOFMS: Studies with electrospray generated gramicidin S ions. *Journal of the American Society for Mass Spectrometry* **2001,** 12, (12), 1320-1330.

11. Shvartsburg, A. A.; Smith, R. D.; Wilks, A.; Koehl, A.; Ruiz-Alonso, D.; Boyle, B., Ultrafast Differential Ion Mobility Spectrometry at Extreme Electric Fields in Multichannel Microchips. *Analytical Chemistry* **2009,** 81, (15), 6489-6495.

12. Robinson, E. W.; Shvartsburg, A. A.; Tang, K.; Smith, R. D., Control of ion distortion in field asymmetric waveform ion mobility spectrometry via variation of dispersion field and gas temperature. *Analytical Chemistry* **2008,** 80, (19), 7508-7515.

13. Ridgeway, M.; Remes, P. M.; Glish, G. L. In *Planar High Field Asymmetric Ion Mobility Spectrometry Device Utilizing Temperature Control of Carrier Gas and Electrodes*, 57th ASMS Conference on Mass Spectrometry and Allied Topics, 2009; 2009.

14. Eiceman, G. A., Ion-mobility spectrometry as a fast monitor of chemical composition. *Trac-Trends in Analytical Chemistry* **2002,** 21, (4), 259-275.

15. Eiceman, G. A.; Nazarov, E. G.; Miller, R. A.; Krylov, E. V.; Zapata, A. M., Micro-machined planar field asymmetric ion mobility spectrometer as a gas chromatographic detector. *Analyst* **2002,** 127, (4), 466-471.

16. Eiceman, G. A.; Krylov, E. V.; Nazarov, E. G.; Miller, R. A., Separation of ions from explosives in differential mobility spectrometry by vapor-modified drift gas. *Analytical Chemistry* **2004,** 76, (17), 4937-4944.

17. Shvartsburg, A. A.; Tang, K. Q.; Smith, R. D., Understanding and designing field asymmetric waveform ion mobility spectrometry separations in gas mixtures. *Analytical Chemistry* **2004,** 76, (24), 7366-7374.

18. Shvartsburg, A. A.; Tang, K. Q.; Smith, R. D., Modeling the resolution and sensitivity of FAIMS analyses. *Journal of the American Society for Mass Spectrometry* **2004,** 15, (10), 1487-1498.

19. Shvartsburg, A. A.; Tang, K.; Smith, R. D., Optimization of the design and operation of FAIMS analyzers. *Journal of the American Society for Mass Spectrometry* **2005,** 16, (1), 2-12.

20. Purves, R. W.; Barnett, D. A.; Ells, B.; Guevremont, R., Elongated Conformers of Charge States +11 to +15 of Bovine Ubiquitin Studied Using ESI-FAIMS-MS. *Journal of the American Society for Mass Spectrometry* **2001,** 12, 894-901.

21. Robinson, E. W.; Williams, E. R., Multidimensional separations of ubiquitin conformers in the gas phase: Relating ion cross sections to H/D exchange measurements. *Journal of the American Society for Mass Spectrometry* **2005,** 16, (9), 1427-1437.

22. Myung, S.; Badman, E.; Lee, Y.; Clemmer, D., Structural transitions of electrosprayed ubiquitin ions stored in an ion trap over similar to 10 ms to 30 s. *Journal of Physical Chemistry A* **2002,** 106, 9976-9982.

23. Guevremont, R.; Barnett, D. A.; Purves, R. W.; Vandermey, J., Analysis of a tryptic digest of pig hemoglobin using ESI-FAIMS-MS. *Analytical Chemistry* **2000,** 72, (19), 4577-4584.

24. Purves, R. W.; Barnett, D. A.; Guevremont, R., Separation of protein conformers using electrospray-high field asymmetric waveform ion mobility spectrometry-mass spectrometry. *International Journal of Mass Spectrometry* **2000,** 197, 163-177.

25. Barnett, D. A.; Ells, B.; Guevremont, R.; Purves, R. W., Application of ESI-FAIMS-MS to the analysis of tryptic peptides. *Journal of the American Society for Mass Spectrometry* **2002,** 13, (11), 1282-1291.

26. Purves, R. W.; Ells, B.; Barnett, D. A.; Guevremont, R., Combining H-D exchange and ESI-FAIMS-MS for detecting gas-phase conformers of equine cytochrome c. *Canadian Journal of Chemistry-Revue Canadienne De Chimie* **2005,** 83, (11), 1961-1968.

27. Venne, K. B., Eric; Eng, Kevin; Thibault, P., Improvement in Peptide Detection for Proteomics Analyses Using Nano LC-MS and High-Field Asymmetry Waveform Ion Mobility Mass Spectrometry. *Analytical Chemistry* **2005,** 77, (7), 2176-2186.

28. Shvartsburg, A. A.; Li, F. M.; Tang, K. Q.; Smith, R. D., Characterizing the Structures and Folding of Free Proteins Using 2-D Gas-Phase Separations: Observation of Multiple Unfolded Conformers. *Analytical Chemistry* **2006,** 78, (10), 3304-3315.

29. Shvartsburg, A. A. L., Fumin ; Tang, Keqi ; Smith, Richard D., Distortion of Ion Structures by Field Asymmetric Waveform Ion Mobility Spectrometry. *Analytical Chemistry* **2007,** 79, 1523-1528.

Chapter 4
Development of a planar FAIMS device for high ion transmission and high resolution

4.1 Introduction to the problems of planar FAIMS

As stated in the previous chapter when compared to more mature technology such as mass spectrometry few FAIMS designs are published in literature or commercially available. The designs that are available[1-12] present two major problems: 1) Low ion transmission during operation in front of a mass analyzer and 2) No ion signal when the FAIMS device is attached to an instrument but is not actively filtering ions. Cylindrical FAIMS analyzers have seen more widespread use and commercialization[4, 11-13] than planar designs because they offer higher ion transmission during operation, albeit at a lower resolution than planar designs. However, cylindrical FAIMS analyzers still must actively perform a separation in order to observe ion signal, requiring removal of the device when not in use. Removal of these devices may seem trivial or little more than an irritating use of time; but device alignment, tuning of the waveform generators, and damage to delicate electro spray emitters all become issues when the source of an instrument is continually being assembled and disassembled. This chapter will focus on the design and development of a FAIMS device which solves these two major problems while offering higher resolution than any cylindrical FAIMS known to date.

4.1.1 Poor ion transmission for planar FAIMS

Ion transmission in planar FAIMS devices is lower than cylindrical FAIMS analyzers due to the lack of two dimensional focusing when using parallel plates[10, 14-16]. Ions entering

the analytical gap of the FAIMS begin with an initial spatial distribution from the ion source. Once in the device, diffusion and Coulombic repulsion further spread ions out along the analytical gap. Ion losses occur when ions either collide with an electrode or move outside of the effective sampling area for the device. In planar FAIMS devices ions which do not enter the analytical gap at the center will not be brought to the center due to the lack of two dimensional focusing, and those that enter too close to an electrode will be neutralized if the distance traveled during either the high or low field portion of the waveform brings the ion in contact with the electrode surface. This creates a reduced effective analytical gap (g_e) which maybe calculated using equation 4.1. The (g_e) is determined by subtracting the distance that an ion will travel during one cycle of the waveform from the measured distance between

$$g_e = g - K_0 E_D t_h \Delta F \qquad \text{(Equation 4.1)}$$

electrodes (g). The distance an ion travels during one portion of the waveform is related to the reduced mobility (K_0) of the ion, the electric field strength during the high field portion of the asymmetric waveform (E_D) and the period of the high electric field strength (t_h). Calculating the distance traveled during one cycle of the waveform using only $K_0 E_D t_h$ assumes an ideal square wave, so a correctional form factor (ΔF) is used to compensate for different waveform shapes. In the case of a bisinusoidal waveform used in the devices discussed below, ΔF is equal to 0.234[17]. Calculations based on a 750 kHz waveform with a 3 kV DV across a 1 mm gap and an ion of moderate K_0 (1.5 $cm^2/(V\ s)$) the distance traveled during one cycle of the waveform would be 0.5 mm, reducing g_e to 0.5 mm. If the electrode gap were to be reduced to 0.3 mm then ion transmission would be significantly reduced unless the field is reduced or the frequency of the waveform increased.

Another reason for reduced ion transmission in planar devices is that much of the ion beam does not overlap with the effective sampling area of the detector. Early FAIMS devices used Faraday cups or electrometers for detection, these detectors could sample the entire area of the FAIMS analytical gap[2-4, 18]. However, when FAIMS is coupled with a mass analyzer, a conductance limit must exist to maintain the pressure differential between the first vacuum region of the mass analyzer (~10 - 0.1 Torr) and the FAIMS analytical gap (~760 Torr). This conductance limit is typically small (< 0.6 mm diameter) and circular in cross section. Cylindrical FAIMS devices focus the ion beam to a circular point at the exit of the device[19]. Planar FAIMS devices produce a rectangular beam of ions at the exit, with only a small percentage (< 10%) of the ions distribution overlapping with the standard mass analyzer's circular conductance limit[10, 12].

4.1.2 FAIMS must always be active

While cylindrical geometry FAIMS designs may have an advantage in ion transmission when performing separations, neither planar nor cylindrical geometry devices have been designed to transmit ions when not performing an active separation. In cylindrical FAIMS devices ion transmission increases with dispersion voltage, resulting in highest ion signal occurring at the maximum separation conditions[19]. Similarly, LC/MS and GC/MS analyzers have optimal limits of detection when the separation removes interfering analytes which would otherwise complicate the mass spectra. However, with LC/MS and GC/MS systems there are typically provisions which allow a user to bypass the chromatography step and perform direct infusion into the ion source without disassembling the GC or LC and moving it away from the mass analyzer. This option currently does not exist with FAIMS analyzers. The FAIMS analog of direct infusion requires removal of the FAIMS device and

repositioning of the electro-spray emitter. FAIMS analyzers are much smaller than chromatography systems, and removal of the device may require only a matter of seconds if intelligently engineered, but several potential problems arise when the ion source is constantly being taken apart and reassembled. These problems range from minor, such as reconnecting FAIMS analyzers incorrectly leading to loss of signal, to moderately expensive, such as damage to delicate electrospray emitters or the glass transfer capillary used in the source.

A simple solution which prevents potential mistakes and saves time for users is to create a FAIMS device which has 100% ion transmission when not active. Previous work discussed in chapter three provided two key design criteria for high transmission in FAIMS devices. First, a co-linear ion source improves ion transmission, with limited adverse effects to analyzer performance. Those adverse effects can be eliminated by ensuring that ions entering the analytical gap are desolvated through the use of nebulizing or heated counter current gas, both of which are found in commercial mass spectrometer sources. Second, the device must be gas tight to optimize ion transport into the analyzer. The following chapter will focus on the first three generations of planar FAIMS analyzers developed in collaboration with Bruker Daltonics.

4.2 Generation one (G1)

The first planar FAIMS constructed in the Bruker-UNC collaboration consisted of a polyether ether ketone (PEEK) capillary with 20 individual, electrically isolated, electrodes vapor deposited in a rectangular inner bore (figure 4.1A). To deposit these electrodes on the interior of the capillary and provide conductive surfaces for the neutralization of ions which did not meet the requirements for stable transmission the capillary was split into two halves.

After the electrodes where vapor deposited onto the surface the capillary was reassembled using an adhesive. The capillary when assembled had identical physical dimensions to the standard glass capillaries used in Bruker electrospray ion sources to transition ions from atmospheric pressure to the first vacuum region (~10 mTorr) (figure 4.1B). The inner bore of the capillary was a different shape than standard capillaries (rectangular 0.5 mm X 1 mm vs. round 0.6 mm diameter), but the conductance of the two capillaries is similar (within a factor of 2), and the first vacuum region does not require additional pumping to maintain normal pressure.

20 individual electrodes where used in an attempt to correct for pressure gradients through the capillary. Because the separation in FAIMS is dependent on the ratio of electric field (E) to gas number density (N), changes in pressure will result in changes in the ratio of K_h/K_l. By using electrically isolated electrodes a varying electric field could be applied through a fixed voltage dividing network to accommodate any change in N. Alternatively the change in N could be negligible along the capillary in which case the individual elements could simply be wired together and act as a set of two parallel electrodes. Interestingly only one low pressure FAIMS device has ever been published[20], and while theoretically advantageous, no device has ever been integrated into a sub ambient pressure region of a mass analyzer. Given the low N present in transfer capillaries the electric field amplitude necessary for in-capillary FAIMS should be 2-3 orders of magnitude lower than at atmospheric pressure. Asymmetric waveform generation is much simplified at such low amplitudes (tens of V/mm), and the waveform amplifiers discussed in chapter 2 become unnecessary. However, the advantage of reduced power requirements comes with short ion

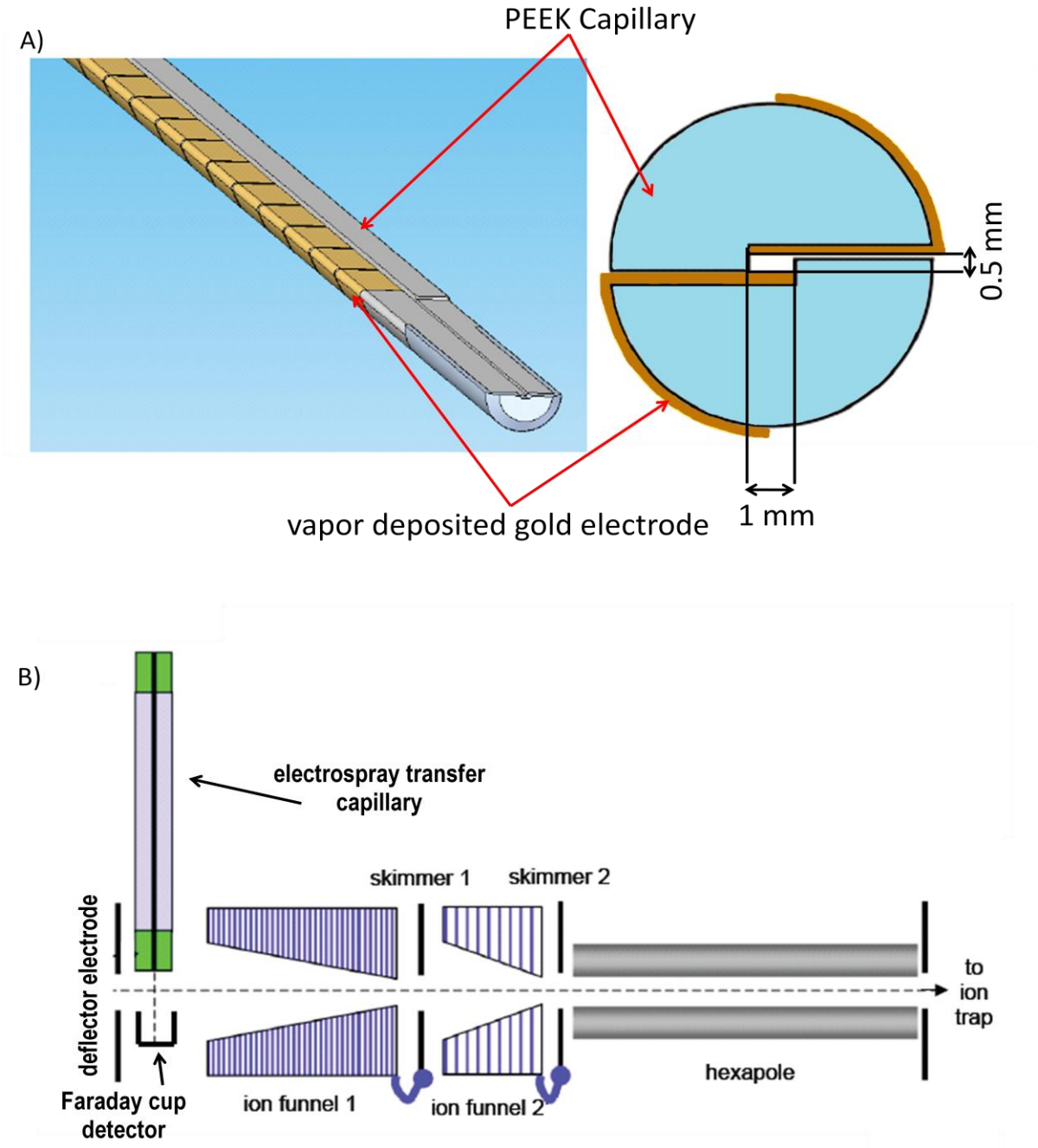

Figure 4.1 Generation 1 FAIMS with the image on left of one half of the assembly showing individual isolated electrodes. The image on the right is a cross section of the assembled capillary including analytical gap dimensions A). Bruker Apollo II ion source showing the position of the Faraday cup used for current measurement and the orthogonal orientation of the electrospray transfer capillary B)

residence times (< 1 ms) in the capillary and the difficulty of engineering gas tight seams for multi-component capillaries.

4.2.1 Results

Initial testing of the G1 FAIMS was carried out by measuring current at a Faraday cup placed at the capillary exit in the first vacuum region of the electrospray ion source. Measured ion current at the Faraday cup for the G1 device was considerably lower (4 pA) than the standard glass capillary of identical length (250 pA). Numerous differences existed between the standard capillary and the FAIMS capillary and a systematic evaluation of those differences showed that the major factors were the presence of electrodes in the capillary, the rectangular shape, and the larger cross sectional area of the capillary (figure 4.2). The ion losses observed with rectangular bore shape and 0.5 mm^2 cross section are also convoluted with losses associated with leaks arising from poor sealing in capillaries assembled from two

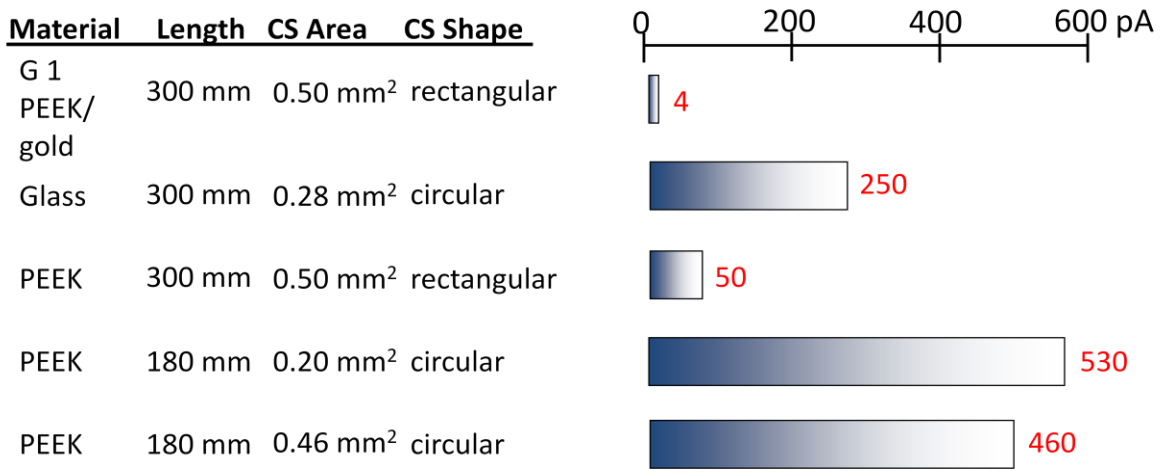

Figure 4.2 Ion current measured for capillaries of differing cross sectional area, cross sectional shape, material and length. Ion current is independent of material, but highly dependent on cross sectional area, and length. Correlation between ion current and shape maybe convoluted with leaks due to longitudinal seams.

PEEK segments. The 30 cm rectangular bore capillary used to evaluate the effects of rectangular vs. circular bore was identical to the FAIMS capillary, but without the 20 gold plated electrodes. No separation was ever acquired with the G1 design, as ion transmission was too low to observe any signal.

4.2.2 G1 lessons learned

The most important lesson learned from the G1 is a reiteration of the key design rule acquired from the PNNL device, that FAIMS devices must be gas tight to achieve high ion transmission. The longitudinal seams bonding the halves together resulted in leaks, causing severe ion loss. A second lesson is that multi-segment designs lead to ion losses due to electrically dissimilar materials, which result in unintended intra-capillary electric fields. Of the ions which could be accounted for 62% of the losses occurred at the first electrode. This is believed to be due to ions charging the non-conducting surfaces surrounding the first electrode. As the non-conductive surfaces acquired and stored charge, the potential difference between the non-conductive capillary and the electrodes increased until electrostatic forces began to drive ions into the electrodes. Attempts to apply dc potentials up to 500 V on the electrodes to prevent ions from being neutralized on these surfaces proved unsuccessful and subsequent designs eliminated the segmented electrode design to avoid this source of ion loss.

4.3 Generation two (G2)

Building on the lessons learned from G1 a second in-capillary planar FAIMS was designed which consisted of two planar electrodes in a much larger and more rigid design to eliminate leaks. The G2 capillary was constructed from four components: two stainless steel electrodes and two PEEK spacers (figure 4.3). This assembly had a greater surface area for

bonding the components together and used screws to tighten and reinforce the capillary. The result was a capillary of identical length, and conductance to the generation 1 design but with significantly increased thickness and weight. The G2 capillary would not fit in the commercial source due to the increased size, and a special adapted version was shipped from Bruker with the new capillary (figure 4.3).

Initial testing showed 75 pA of ion current when tested using the same in source faraday cup used to evaluate the generation 1 design. While low compared to the 250 pA of ion current from the conventional glass capillary, the performance of the G2 design was a positive result. FAIMS separations using the G2 design proved to be low resolution but

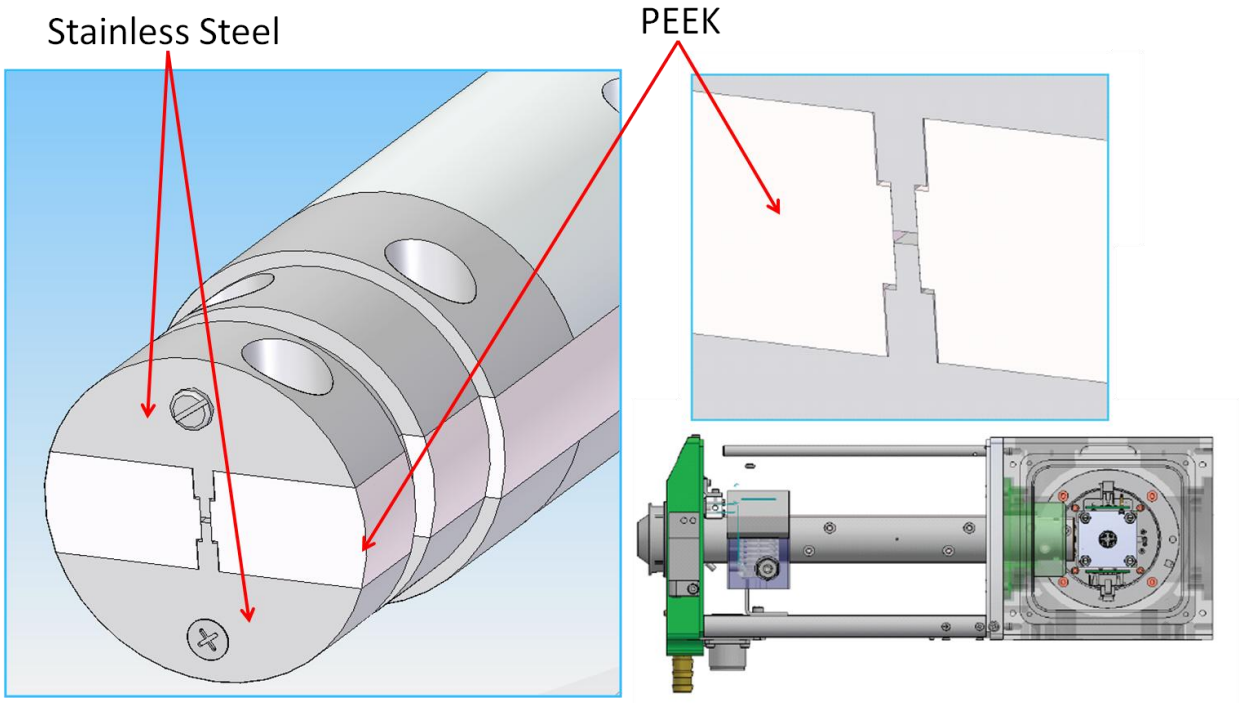

Figure 4.3 Image on left shows the construction of the G2 capillary using two parallel stainless steel electrodes and two PEEK spacers. Top right is a zoom in image of the rectangular gap measuring 1 mm X 0.5 mm. The bottom right image is the Bruker Apollo II source modified for the G2. Components in green were redesigned to accommodate the larger diameter capillary.

successful, and the design served to provide insight into what other factors influenced ion transmission through FAIMS devices.

4.3.1 G2 Results

With the G2 capillary installed and the planar electrodes grounded, ion transmission was measured at 30% of the standard ESI transfer capillary. Ion current measured in the source would spike when the electro spray source was first turned on, and then slowly drop until reaching a steady state value of 30%. Attributing this to charging, the PEEK surfaces were coated with carbon black. The carbon black coating served to provide a means of discharge for current striking the PEEK spacers, while maintaining the isolation between FAIMS electrodes (40 MΩ measured impedance between electrodes). After coating the PEEK surfaces ion transmission doubled to 150 pA (60% of standard glass capillary). Low amplitude asymmetric waveforms, generated by a linear amplifier, were applied to the G2 FAIMS electrodes and CV scans performed. The results were encouraging, demonstrating that the ion signal responded to the application of asymmetric waveforms. Furthermore, ion signal could be increased by the addition of a compensation voltage to correct for net drift when a dispersion voltage as of > 76 V was applied to the FAIMS electrodes (figure 4.4).

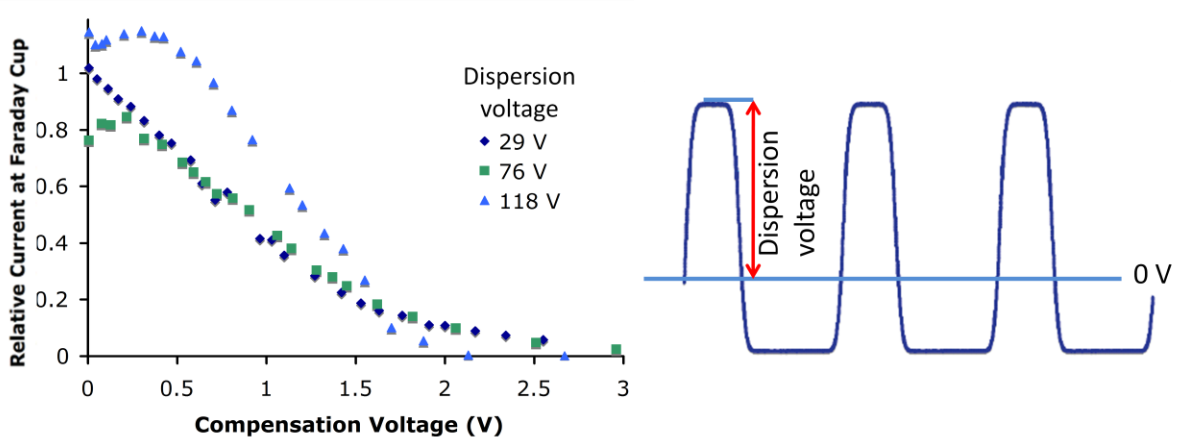

Figure 4.4 Plot on left show compensation voltage scans of the peptide YGGFL at three dispersion voltages. The waveform displayed on the right is an image of the waveform used in the G2 device

4.3.2 G2 lessons learned

With ion losses from leaks largely eliminated, the G2 FAIMS provided two more valuable pieces of information. Planar FAIMS analytical gaps require several times the distance between opposed insulating surfaces than between conductive surfaces to reduce the effect of charging insulators on ion transmission. G1 and G2 used an analytical gap width to height ratio of 2:1, due to limitations in capillary dimensions required for the mass analyzers vacuum system. This aspect ratio proved too low and cut ion transmission by half in the non-resistively coated G2 device relative to the G2 after coating with carbon black. A search of literature for the dimensions of planar FAIMS devices indicated that the minimum width to height aspect ratio for the analytical gap of successful designs was 6:1[2, 7, 10, 21-25], and all designs built at UNC since this work have used a minimum of 10:1.

4.4 Generation three (G3)

The G3 device (figure 4.5) departs from the G1 and G2 designs in that it mounts directly to the ion source of the mass analyzer (figure 4.6) but is not built into the ESI transfer capillary. The device consists of an outer housing machined from Macor (a machinable ceramic) with stainless steel fixtures to attach the ESI curtain plate to the FAIMS

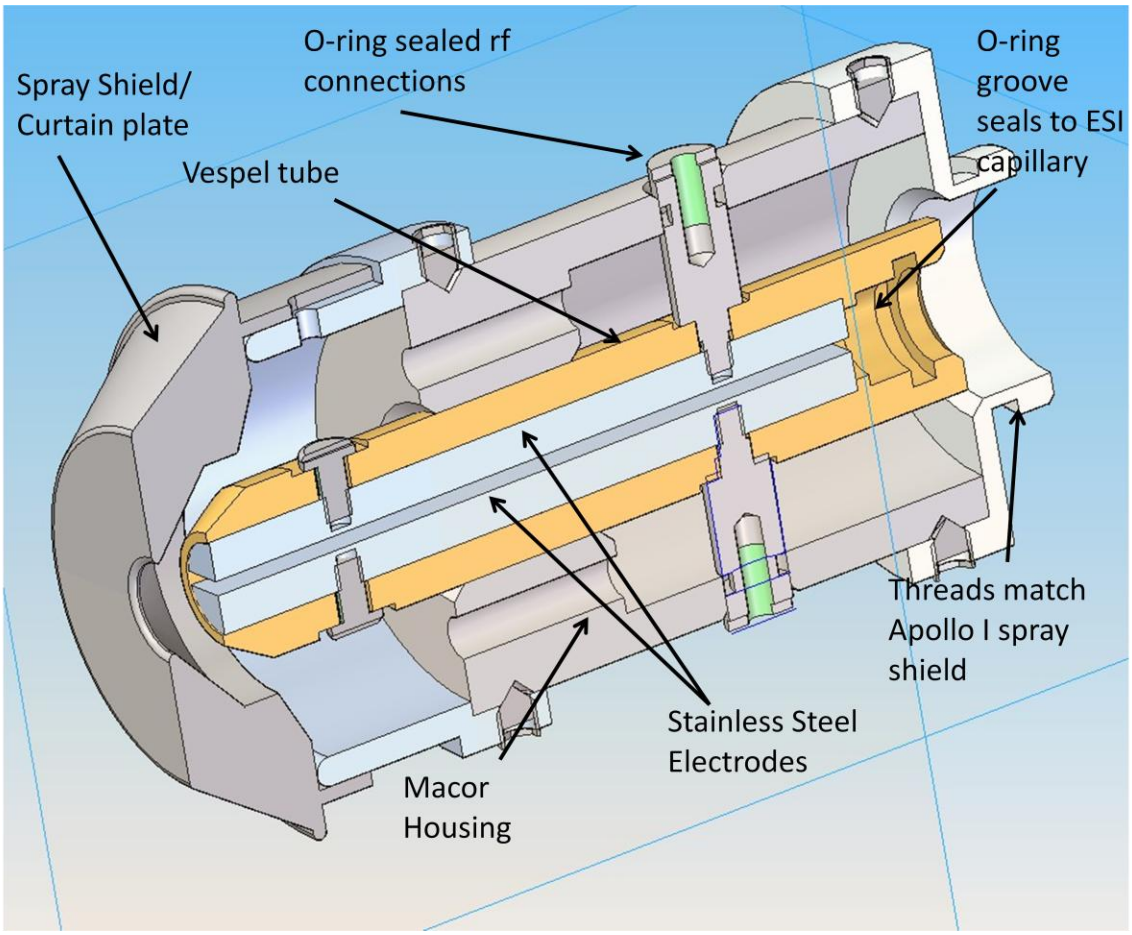

Figure 4.5 Cutaway of G3 device with major components labeled.

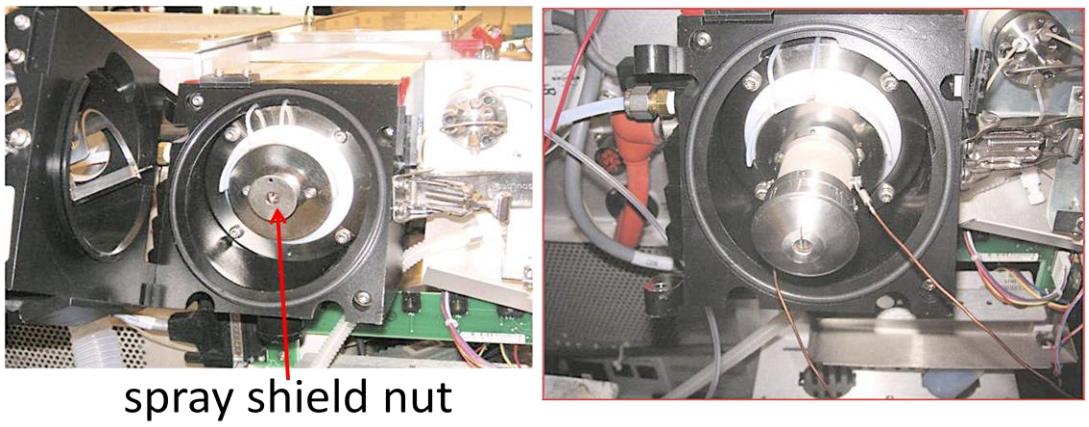

Figure 4.6 Photograph on left is the standard Bruker Esquire 3000 electrospray source. The spray shield nut is removed and replaced with the G3 device as pictured on the right.

and allow the G3 device to screw into the ESI ion source. The curtain plate placed on the front of the analyzer partitions heated drying gas between countercurrent desolvation gas and carrier gas for the FAIMS. The curtain plate also serves as the counter electrode to the ESI emitter. In the G3 design, the curtain plate is always held at ground while the ESI emitter is held at +/- 4 kV. The hemispherical stainless steel FAIMS electrodes are held in a cylindrical bore tube made of Vespel, a polymer with excellent electrical properties and high temperature stability. The Vespel tube also serves to couple the electrodes to the ESI transfer capillary, seal the assembly together with an o-ring, and provide electrical isolation between the electrodes and the capillary.

The G3 Device is 40 mm in length with an outer diameter of 35 mm. The electrode design is modular, allowing for variation of the analytical gap by simply changing electrode sets without further modification. The G3 assembly can be installed or removed from the mass spectrometer in approximately 30 seconds, and requires only two external electrical connections. However, removal of the device often is unnecessary because ion transmission when the FAIMS electrodes are held at ground is nearly 100% for ions above a minimum mass-to-charge ratio.

4.4.1 Ion transmission in "transparent mode"

As discussed previously, high ion transmission when operating in "transparent mode" eliminates the need to remove the FAIMS when not in use. Ion transmission in "transparent mode" was evaluated using samples of bovine ubiquitin in a 49.95/49.95/0.1 percent by volume solution of methanol/water/acetic acid. The G3 was installed on a Bruker Esquire 3000 ion trap with the FAIMS electrodes held at ground potential. A comparison of

ion signal with the FAIMS attached and with no FAIMS (normal spray conditions) showed that ion transmission was < 10% of the normal spray conditions (figure 4.7). While ion transmission was considerably better than the G1 or the PNNL device, it fell far short of anticipated results.

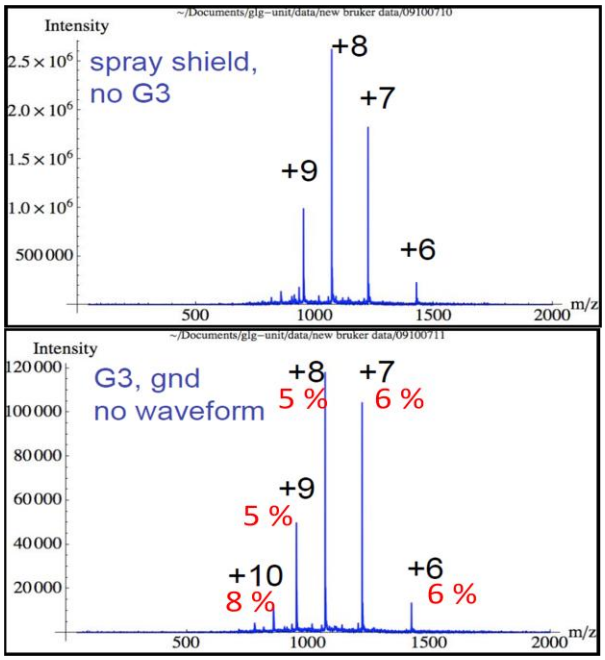

Figure 4.7 Mass spectrum on top of bovine ubiquitin under conventional electrospray conditions with no FAIMS device attached. Mass spectrum on bottom is of the same bovine ubiqitin sample with the G3 FAIMS in place in passive mode, percent ion transmission numbers are given in red below the charge state of each peak.

4.4.2 Improved ion transmission

Other planar designs improved ion transmission by changing the conductance limit design from a single circular conductance limit to a line of circular orifices in an attempt to sample more of the analytical gap of the FAIMS[10, 21]. In the G2 design this had not been an issue because the conductance limit was the analytical gap. The conductance limit in the G3 device is the standard Bruker glass electrospray transfer capillary which measured 0.6 mm in diameter and 18 cm in length. Producing a multi-holed inlet capillary would have been an expensive and complex task considering the diameter and length of the holes which would be

required to maintain the same conductance as the standard capillary. Instead a "flared" capillary similar to those used in previous work replaced the standard capillary[26]. The flared capillary has identical conductance to the standard capillary, but a wider acceptance area created by grinding the face of the capillary into a three dimensional funnel shape (figure 4.8)

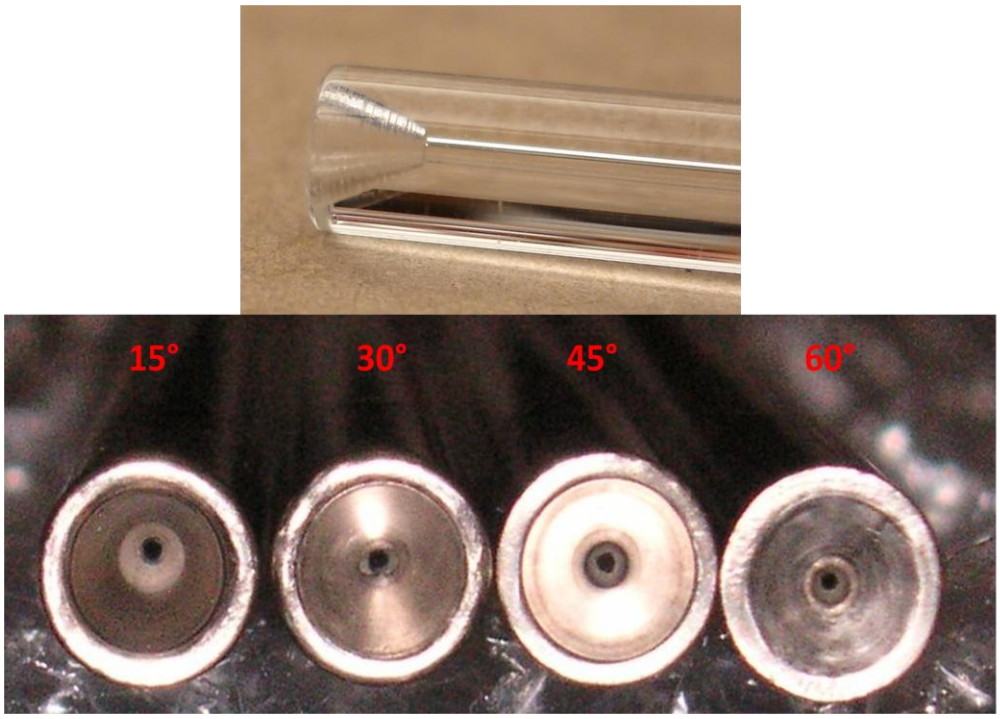

Figure 4.8 Top photograph is of a flared glass capillary prior to metal coating showing the three dimensional funnel. Bottom photograph is of the 15°, 30°, 45°, and 60° flared capillaries after metal coating.

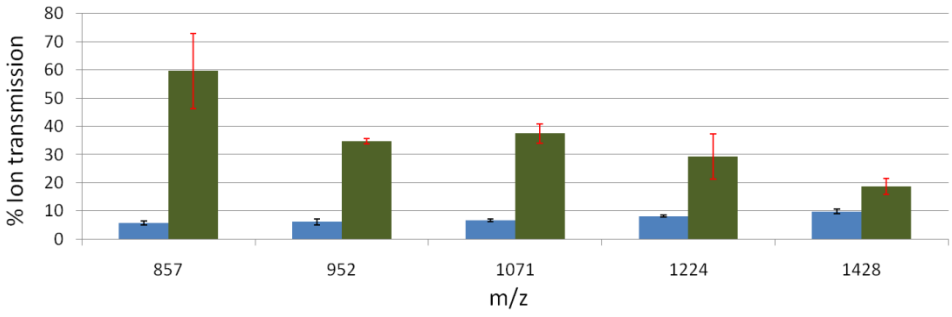

Figure 4.9 Increases in percent ion transmission for bovine ubiquitin using conventional electrospray source with standard capillary (blue) and 60° capillary (green) installed. Improvements in ion transmission are greatest for ions with high diffusion losses with the standard capillary.

After machining, the capillaries are metal coated and installed into the Bruker Esquire 3000 ion trap mass spectrometer without further modification. Because diffusion causes ions to move away from the center of the FAIMS device and thus the transfer capillary, signal improvement (figure 4.9) is a function of the ion mobility and diffusion distance. Ion signal is improved by a factor of 2X for most analytes, with over 10X improvement for ions with higher diffusion rates.

4.4.3 Resolution increases when gap size decreases

Separation performance (figure 4.9a) achieved with the first set of electrodes installed (1 mm analytical gap) was moderate with a resolving power of 12.5 for *m/z* 622 (Hexakis (2,2-difluoroethoxy) Phosphazene (CAS No. 186817-57-2) from the Agilent ESI tune mix. This was on par with cylindrical FAIMS analyzer performance. The ion residence time (t_{res}) for the 1 mm device is 5 ms, $1/20^{th}$ of t_{res} for the PNNL analyzer, so the low resolution intuitively made sense. The end goal of the Bruker-UNC collaboration remained an in-capillary device, and testing of the G3 with reduced analytical gaps on the order of capillary dimensions proceeded.

When the 1 mm electrode set was exchanged for a 0.5 mm gap resolving power improved to 21 for *m/z* 622. Reducing the distance between electrodes to 0.5 mm (figure 4.9b) caused t_{res} to further decrease from 5.0 ms to 2.5 ms, while dispersion voltage had to be decreased from the 3 kV used with a 1mm gap to 2.2 kV to prevent arcing between electrodes. Ion transmission had no observable change between the 1 mm and 0.5 mm gaps. Why then did decreasing every parameter known to be proportional to resolution increase the resolving power of the analyzer?

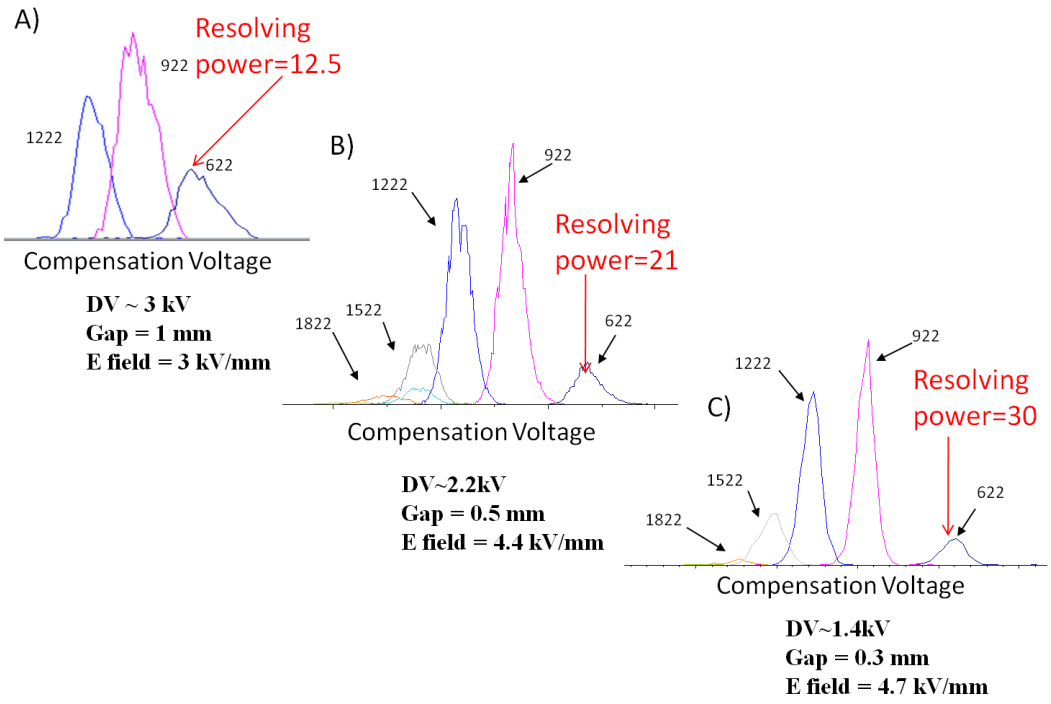

Figure 4.10 CV scans of ESI tune mix for the A) 1mm gap G3 B) 0.5 mm gap G3 and C) 0.3 mm gap G3

While the gap dimension was reduced by a factor of two, the dispersion voltage was only reduced by 2/3, actually increasing the electric field strength. The equation for FAIMS resolving power (R) (equation 4.2) indicates that (R) is proportional to the square root of t_{res} but to the cube of electric field during the DV portion of the waveform (E_D) assuming all

$$R = \frac{K(0)\langle F_3\rangle E_D\sqrt{t_{res}}}{4\sqrt{\overline{D}_{II}}ln2}\left(\frac{a_1 E_D^2}{N^2}\right) \qquad \text{Equation 4.2}$$

other factors such as the waveform factor $\langle F_3\rangle$, gas number density (N), diffusion parallel to the electrodes ($\overline{D}_{II}$) and alpha function for a specific ion (a_1) are held constant. Based on the increase in E_D achieved by reducing electrode spacing from 1 mm to 0.5 mm, resolving power for the *m/z* 622 peak using the 0.5 mm device should be approximately 39. However t_{res} also decreases by a factor of two with the reduction in gap size, leading to a calculated

resolving power of 20 for the *m/z* 622 peak, which compared favorable to the measured resolving power of 21.

The analytical gap was further reduced to 0.3 mm (figure 4.9c) with a subsequent increase in resolution due to yet higher electric fields. The gap has not been further reduced as 0.3 mm is small enough to fit in a conventional capillary. Smaller gaps require more precise assembly tolerances to assure parallelism (section 6.3.1) and also an increase in waveform frequency (Equation 4.1). Very small gap devices have been built using micro fabrication techniques by other groups, with extremely high electric fields (60,000 V/cm), but have limited resolution due to extremely short residence times[22].

4.4.4 Increased electric fields at smaller gaps

Increasing field strengths with decreasing gap distance has been observed previously. Paschen's curve describes the relationship (equation 4.3) between gas pressure (*P*), distance between plates (*d*), and the voltage (*V*) necessary for discharge between two plates[27]. The curves generated are gas specific and require the input of two coefficients, a and b, for each gas. When the pressure and composition of the gas is held constant, as is the case of

$$V = \frac{a(Pd)}{ln(Pd)+b} \qquad \text{Equation 4.3}$$

atmospheric pressure FAIMS devices, the absolute voltage which causes discharge decreases, but because of the *ln(Pd)* factor in the denominator the decrease in voltage with distance is non-linear. Figure 4.11 is a plot of Pashen's curve for nitrogen, with lines drawn in to show the maximum electric fields with 1 mm and 0.3 mm gaps.

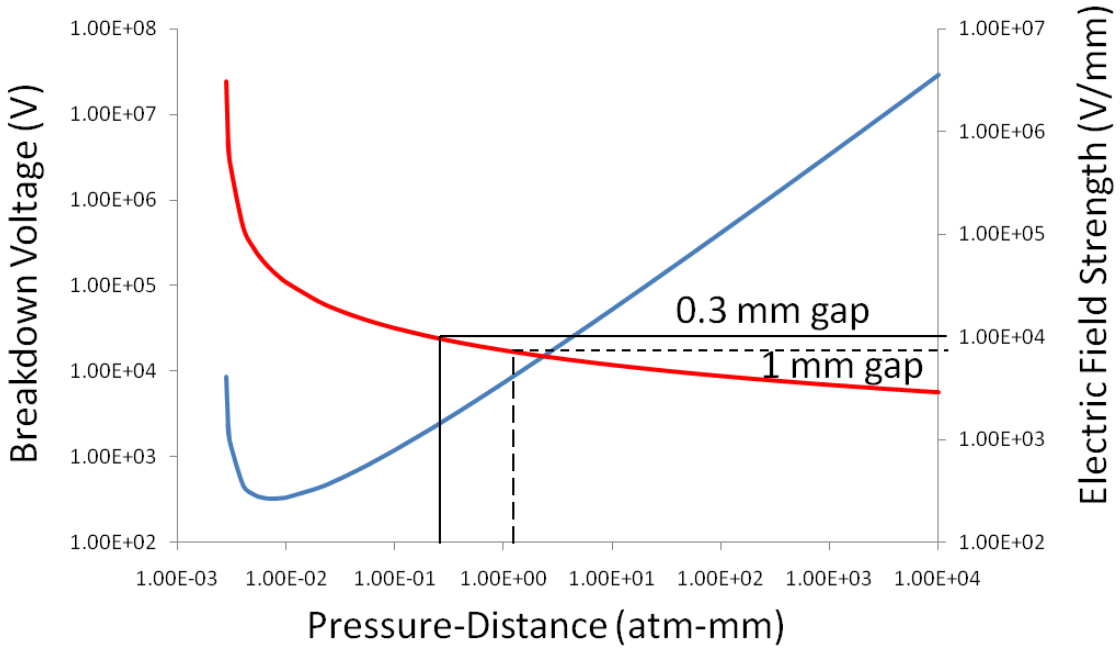

Figure 4.11 Paschen's curve for nitrogen gas (blue trace) and the corresponding electric field strength (red trace). Lines representing the 1 mm (dashed) and 0.3 mm (solid) electrode gaps are inserted to show relative scale of the electric fields which can be obtained.

A second advantage to decreasing the analytical gap is that the power requirement for the waveform generator is further reduced. Chapter 2 discussed the difficulty of producing the high frequency high voltage waveforms used in typical FAIMS devices with gaps of 2-2.5 mm. Reducing gap dimensions to 0.3 mm requires only 15 % of the voltage of traditional 2 mm gaps to generate an identical electric field. With a 0.3 mm gap the normal operating DV is 1400 V which is almost within reach of linear power amplifier waveform generators. Improvements in solid state power amplifiers or further reduction in FAIMS analyzer size would allow the use of ideal square waves and simplify production and control of FAIMS waveforms.

4.4.5 Simplification of spectra

With improvements in ion transmission and resolving power over previous designs the G3 FAIMS has the ability to separated complex mixtures and provide improved limits of

detection for samples in complex matrixes. To demonstrate this, a mixture of 1:1 bovine ubiquitin and bovine serum albumen (BSA) was prepared in a 49.95/49.95/0.1 percent by volume solution of methanol/water/acetic acid. The sample was ionized using standard electrospray source conditions on a Bruker Esquire 3000 ion trap mass spectrometer. Figure 4.12a is a spectrum of the mixture with the G3 attached but operated in passive mode. BSA is a 66.4 kDa protein and appears in ESI spectra as a broad range of charge states which can appear as one large noisy peak due to insufficient resolution to separate individual peaks. Figure 4.12b is a mass spectrum of the same sample with the FAIMS device actively filtering ions from BSA while transmitting ubiquitin ions. The majority of ubiqitin peaks fall outside the mass envelope of BSA. However, the +6 ubiquitin peaks at m/z 1428 does not and is undetectable in figure 4.12a while clearly visible in 4.12b.

More interesting than the ability to observe a peak previously covered by BSA is the increase in signal of most charge states of ubiquitin (all but the +7 charge state) when BSA is filtered out. This is due to the limited space charge capacity of ion traps. By removal of unwanted ions the desired signal can be increased. This is exemplified by figure 4.13, where a sample of ubiquitin contains trace amounts of the peptide angiotension I. In figure 4.13a only the charge states of ubiqitin observed in the mass spectrum along with an undetermined low mass noise. In figure 4.13b with the G3 analyzer being used to selectively transmit agiotension I no other ions are observed, and the signal intensity for angiotension surpasses the ion signal intensity observed for the most abundant of the ubiquitin peaks.

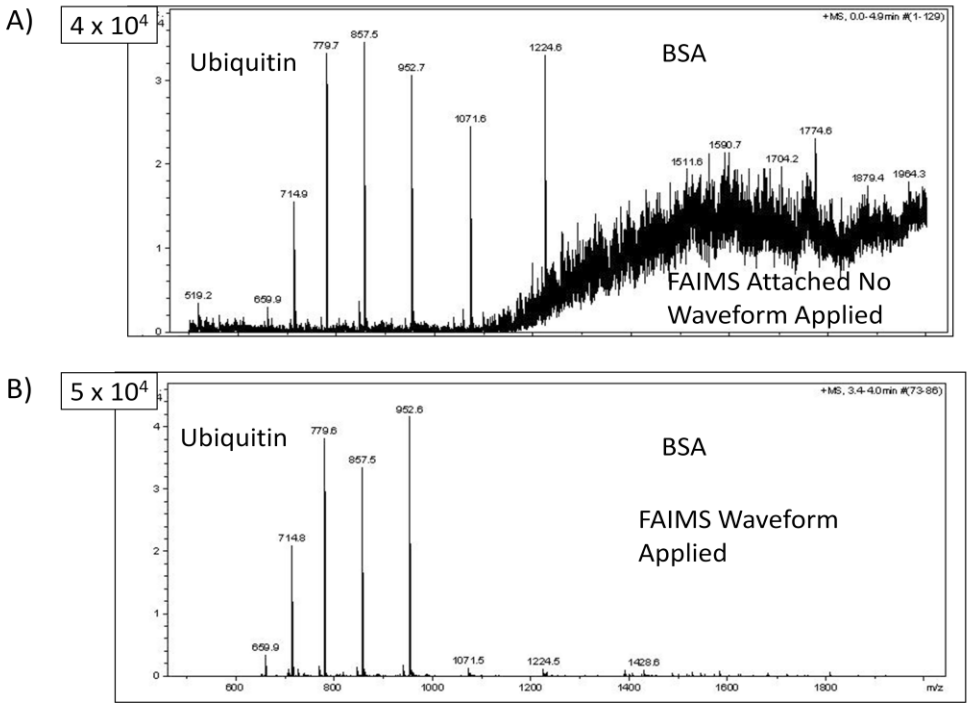

Figure 4.12 Mass spectra of BSA/bovine ubiquitin mixture with G3 FAIMS in passive mode A) and actively filtering ions corresponding to BSA B). Signal intensity increases in spectrum B for the ubiquitin ions because of reduced space charge in the ion trap.

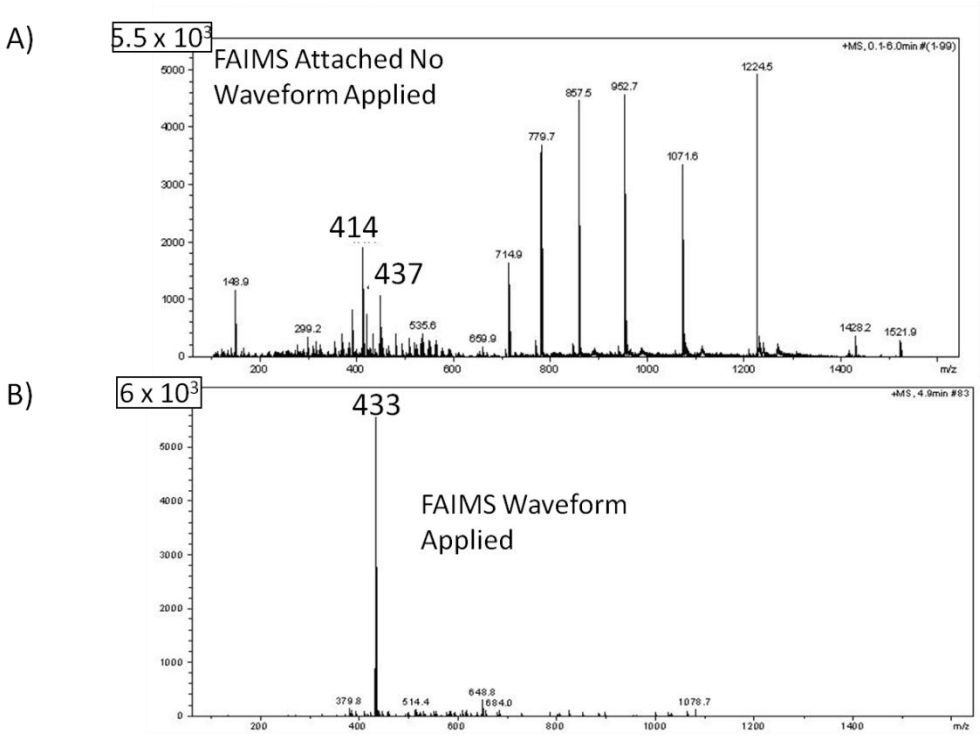

Figure 4.13 Mass spectra of a) ubiqitin and angiotension I (433 m/z) with G3 attached but in passive mode b)mass spectrum of the angiotension I with the G3 active.

4.4.6 High speed analysis

The small gap volume of the G3 FAIMS analyzer results in short t_{res} for ions in the analytical gap, which to this point has been discussed only with relation to resolution. Maximum FAIMS scan speeds are limited by the transit time for ions through the device. Unlike many FAIMS analyzers, the G3 scan speed is limited by the acquisition speed of the mass analyzer, in this case show for a 3D ion trap but equally true for faster Q-TOF instruments, rather than the FAIMS residence time. As an example, the calculated t_{res} is 1.5 ms for the 0.3 mm gap G3. Ion gate time for the Bruker Esquire 3000 ion trap mass analyzer on which the G3 is installed ranges between .1 ms and 200 ms, with a typically ion gating event of 5 ms. Following ion gating, a cool time and mass scan follow adding another 15-20 ms for a mass scan of 50-2000 Da. 20 ms per CV step scans would not be possible in many FAIMS devices, some commercial devices operate at $1/10^{th}$ that scan speed, requiring the mass analyzer to slow down and wait on the FAIMS device . Figure 4.14 shows a CV scan performed at the maximum scan rate of the mass analyzer using no signal average. To scan the entire range of compensation voltages takes 12 seconds. While far from optimal resolution the plot demonstrates the high scan speeds small FAIMS analyzers are capable of while maintaining baseline resolution for the majority of the components in the Agilent ESI

tune mix.

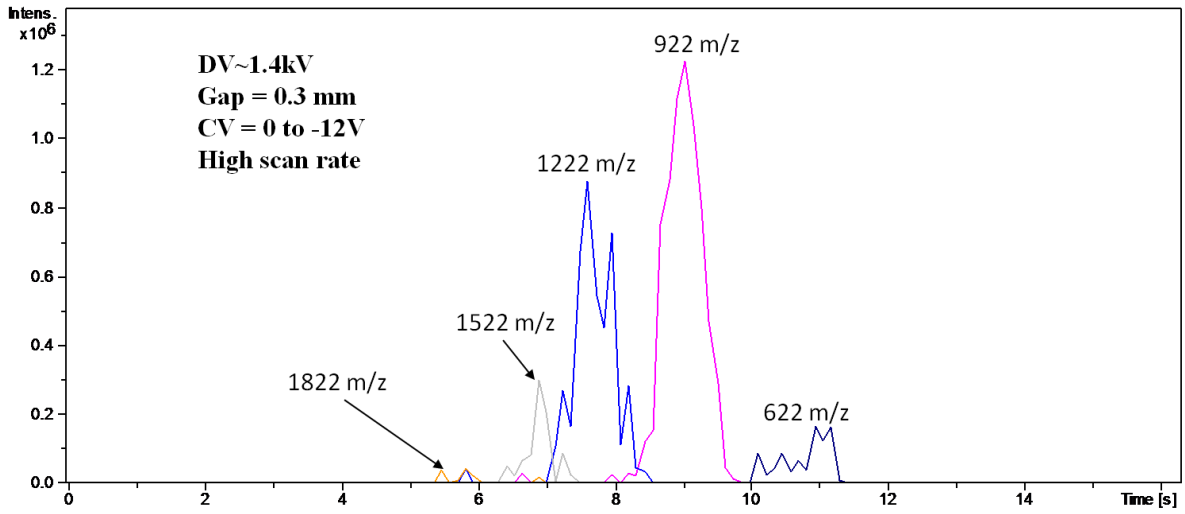

Figure 4.14 Complete FAIMS chromatogram acquired in 12 seconds. Peaks shapes show some distortion due to reduced signal averaging but resolution remains similar to slower scans, and sensitivity is unchanged.

4.5 Summary

Collaborative efforts between Bruker Daltonics and the Glish lab at UNC resulted in the development of three generations of planar FAIMS analyzers. The G1 design was a failure due to the design of the multi-segmented electrodes and poor sealing of the seams along the two halves of the capillary. Lessons learned from G1 lead to a second in-capillary FAIMS design the G2 which had significantly improved ion transmission over the G1, but modest performance as a FAIMS analyzer. To simplify analyzer design and create a modular design which could be used to optimize device geometry the G3 device was designed to mount to the source of a commercial mass analyzer. With several rounds of device improvement the G3 proved to be capable of resolving power of over 30, close to 100% ion transmission in the passive mode, and scan speeds on the order of most mass analyzers.

4.6 References

1. Canterbury, J. D.; Gladden, J.; Buck, L.; Olund, R.; MacCoss, M. J., A High Voltage Asymmetric Waveform Generator for FAIMS. *Journal of the American Society for Mass Spectrometry* In Press, Accepted Manuscript.

2. Buryakov, I.; Krylov, E.; Nazarov, E.; Rasulev, U., A new method of separation of multi-atomic ions by mobility at atmospheric pressure using a high-frequency amplitude-asymmetric strong electric field. *International Journal of Mass Spectrometry and Ion Processes* **1993,** 128, 143-148.

3. Krylov, E. V., Pulses of Special Shapes Formed on a Capacitive Load. *Instruments and Experimental Techniques* **1997,** 40, 628-631.

4. Barnett, D. A.; Ells, B.; Guevremont, R.; Purves, R. W., Separation of leucine and isoleucine by electrospray ionization-high field asymmetric waveform ion mobility spectrometry-mass spectrometry. *Journal of the American Society for Mass Spectrometry* **1999,** 10, (12), 1279-1284.

5. Guevremont, R.; Ding, L. Y.; Ells, B.; Barnett, D. A.; Purves, R. W., Atmospheric pressure ion trapping in a tandem FAIMS-FAIMS coupled to a TOFMS: Studies with electrospray generated gramicidin S ions. *Journal of the American Society for Mass Spectrometry* **2001,** 12, (12), 1320-1330.

6. Eiceman, G. A., Ion-mobility spectrometry as a fast monitor of chemical composition. *Trac-Trends in Analytical Chemistry* **2002,** 21, (4), 259-275.

7. Eiceman, G. A.; Nazarov, E. G.; Miller, R. A.; Krylov, E. V.; Zapata, A. M., Micro-machined planar field asymmetric ion mobility spectrometer as a gas chromatographic detector. *Analyst* **2002,** 127, (4), 466-471.

8. Cui, M.; Ding, L. Y.; Mester, Z., Separation of cisplatin and its hydrolysis products using electrospray ionization high-field asymmetric waveform ion mobility spectrometry coupled with ion trap mass spectrometry. *Analytical Chemistry* **2003,** 75, (21), 5847-5853.

9. Guevremont, R.; Purves, R., Comparison of experimental and calculated peak shapes for three cylindrical geometry FAIMS prototypes of differing electrode diameters. *Journal of the American Society for Mass Spectrometry* **2005,** 16, (3), 349-362.

10. Shvartsburg, A. A.; Li, F. M.; Tang, K. Q.; Smith, R. D., High-resolution field asymmetric waveform ion mobility spectrometry using new planar geometry analyzers. *Analytical Chemistry* **2006,** 78, (11), 3706-3714.

11. Barnett, D. A.; Belford, M.; Dunyach, J. J.; Purves, R. W., Characterization of a Temperature-Controlled FAIMS System. *J Am Soc Mass Spectrom* **2007,** 18, 1653-1663.

12. Saba, J.; Bonneil, E.; Pomies, C.; Eng, K.; Thibault, P., Enhanced Sensitivity in Proteomics Experiments Using FAIMS Coupled with a Hybrid Linear Ion Trap/Orbitrap Mass Spectrometer. *Journal of Proteome Research* **2009,** 8, (7), 3355-3366.

13. Robinson, E. W.; Williams, E. R., Multidimensional separations of ubiquitin conformers in the gas phase: Relating ion cross sections to H/D exchange measurements. *Journal of the American Society for Mass Spectrometry* **2005,** 16, (9), 1427-1437.

14. Shvartsburg, A. A.; Tang, K. Q.; Smith, R. D., Modeling the resolution and sensitivity of FAIMS analyses. *Journal of the American Society for Mass Spectrometry* **2004,** 15, (10), 1487-1498.

15. Shvartsburg, A. A.; Tang, K.; Smith, R. D., Optimization of the design and operation of FAIMS analyzers. *Journal of the American Society for Mass Spectrometry* **2005,** 16, (1), 2-12.

16. Shvartsburg, A. A.; Smith, R. D., Scaling of the Resolving Power and Sensitivity for Planar FAIMS and Mobility-Based Discrimination in Flow- and Field-Driven Analyzers. *J Am Soc Mass Spectrom* **2007,** 18, 1672-1681.

17. Shvartsburg, A. A., *Differential ion mobility spectrometry : nonlinear ion transport and fundamentals of FAIMS*. CRC Press: Boca Raton, 2009.

18. Guevremont, R.; Purves, R. W., High field asymmetric waveform ion mobility spectrometry-mass spectrometry: An investigation of leucine enkephalin ions produced by electrospray ionization. *Journal of the American Society for Mass Spectrometry* **1999,** 10, (6), 492-501.

19. Guevremont, R. P., R., Atmospheric pressure ion focusing in a high-field asymmetric waveform ion mobility spectrometer. *Review of Scientific Instruments* **1999,** 70, (2), 1370-1383.

20. Nazarov, E. G.; Coy, S. L.; Krylov, E. V.; Miller, R. A.; Eiceman, G. A., Pressure effects in differential mobility spectrometry. *Analytical Chemistry* **2006,** 78, (22), 7697-7706.

21. Mabrouki, R.; Kelly, R. T.; Prior, D. C.; Shvartsburg, A. A.; Tang, K. Q.; Smith, R. D., Improving FAIMS Sensitivity Using a Planar Geometry with Slit Interfaces. *Journal of the American Society for Mass Spectrometry* **2009,** 20, (9), 1768-1774.

22. Shvartsburg, A. A.; Tang, K. Q.; Smith, R. D.; Holden, M.; Rush, M.; Thompson, A.; Toutoungi, D., Ultrafast Differential Ion Mobility Spectrometry at Extreme Electric Fields Coupled to Mass Spectrometry. *Analytical Chemistry* **2009,** 81, (19), 8048-8053.

23. Rorrer, L.; Yost, R. A. In *Solvent Vapor Effects in Planar FAIMS*, American Society for Mass Spectrometry, 2010; 2010.

24. Shvartsburg, A. A.; Danielson, W. F.; Smith, R. D., High-Resolution Differential Ion Mobility Separations Using Helium-Rich Gases. *Analytical Chemistry* **2010,** 82, (6), 2456-2462.

25. Shvartsburg, A. A.; Tang, K. Q.; Smith, R. D., Differential Ion Mobility Separations of Peptides with Resolving Power Exceeding 50. *Analytical Chemistry* **2010,** 82, (1), 32-35.

26. Bushey, J. M.; Kaplan, D. A.; Danell, R. M.; Glish, G. L., Pulsed Nano-Electrospray Ionization: Characterization of Temporal Response and Implementation with a Flared Inlet Capillary. *Instrumentation Science & Technology* **2009,** 37, (3), 257-273.

27. Friedrich, P., Ueber die zum Funkenübergang in Luft, Wasserstoff und Kohlensäure bei verschiedenen Drucken erforderliche Potentialdifferenz. *Annalen der Physik* **1889,** 273, (5), 69-96.

Chapter 5
Unconventional Carrier Gas Compositions in Planar FAIMS

5.1 Carrier gasses in ion mobility

An ion placed in a uniform electric field (*E*) has a constant force (*F*) equal to the charge of the ion (*q*) multiplied by *E* and will undergo constant acceleration (*a*) which is proportional to the mass-to-charge ratio of the ion (equation 5.1). In the case where no collisions occur only the

$$F = ma = qE \qquad \text{Equation 5.1}$$

mass (*m*), *q* and *E* determine the velocity of the ion. By accelerating ions across a fixed distance (*L*) under a fixed E, as is done in a time-of-flight mass analyzer, the mass-to-charge ratio for an ion can be determined by measuring the time (*t*) it takes an ion to travel a fixed field free flight distance (*d*) (equation 5.2). However, if collisions between ions and neutrals occur during the

$$t = \frac{d}{\sqrt{2qEL/m}} \qquad \text{Equation 5.2}$$

flight, the arrival time of the ion becomes a function of the force imparted by the *E*, but also on the energy lost per collision with neutrals and the number of collisions which occur[1]. By increasing the pressure (to 2-20 Torr) and applying a fixed *E* (~ 2-20 V/cm) in the drift tube the number of collisions which occur increases to the point where the acceleration of the ion between collisions is balanced by the velocity lost per collision and the ion moves along the

drift tube at constant velocity (v) (Equation 5.3). The equilibrium of frictional forces between the

$$t = \frac{L}{v} = \frac{L}{KE} \qquad \text{Equation 5.3}$$

ion, carrier gas, and the acceleration due to the electric field is referred to as the mobility (K), and leads to the separation of ions based on shaped-to-charge ratio in ion mobility spectrometry (IMS).

FAIMS operates at higher pressures (760 Torr), shorter distances (50 mm), and with time dependent electric fields, yielding a separation technique that is complementary to conventional IMS[2]. While different than IMS, the equilibrium between acceleration under an electric field, and energy lost through collisions with a neutral gas is still the physical means underlying separation of ions of different shape and charge in the low field portion of the asymmetric waveform[3]. A major difference between FAIMS and IMS is that FAIMS asymmetric waveforms also include a high field portion in which the force due to the electric field and the friction force due to collisions are not in equilibrium. Under high E/N conditions, the energy associated with collisions between ions and neutrals results in an increase in the ion internal energy, and a field dependent change in K. Because of this, the interaction between carrier gas and ions in both low and high field collisions has large effects on performance, in terms of sensitivity, resolution and peak capacity in FAIMS separations. Unfortunately, FAIMS performance as a function of gas composition is not well understood[1, 4-7]. This chapter focuses on the use of alternative carrier gas compositions in the G3 FAIMS device as a means of improving performance.

5.1.1 Characteristics of gases in low field mobility

The interaction between an ion and a gas molecule is largely governed by the relative mass of collision partners, and the polarizability of the gas molecule. Increasing the mass of the neutral collision gas relative to the mass of the ion will result in a decrease in an ion's mobility. As the mass of the carrier gas increases the collision cross section for the gas typically increases as well. An ion traveling through two gases at identical pressure but differing collision cross sections will travel slower through the larger collision cross section gas because collisions are more likely to occur. A second reason that higher molecular mass collision gases tend to result in lower ion mobility is because according to the laws of momentum conservation (equation 5.4) the center of mass collision energy, or the maximum amount of kinetic energy which can be converted to internal energy from a collision between ion and neutral gas, (E_{com}) is a function of the laboratory kinetic energy of the ion (E_{lab}), the mass of the ion (m_1), and mass of the gas (m_2). Increasing m_2 results

$$E_{com} = \frac{E_{lab} m_2}{m_1 + m_2} \qquad \text{Equation 5.4}$$

in a larger percentage of E_k being transferred to the collision gas[8]. Larger E_t values result in lower ion velocities through the carrier gas as more kinetic energy is lost by the ion during collisions with the carrier gas.

The polarizability of a molecule is a measure of the distortion of the electron cloud by an electric field. As ions travel through a polarizable gas the electron cloud of the gas becomes distorted which leads to an increase in the collision cross section of the neutral gas molecule, and makes collisions between ion and neutrals "sticky". These "sticky" collisions lead to an to cluster formation, and decreased acceleration between collisions due to the

increased mass of the ion-neutral gas cluster[9]. Comparison between the mobility of lithium ions measured using a polarizable gas such as hydrochloric acid and a non-polar gas of similar molecular mass such as argon yield a reduced mobility coefficient (K_0) which is lower by a factor of 2.5 for hydrochloric acid[10, 11].

5.1.2 Carrier gas influence on high electric field mobility

The ratio of (E) and gas number density (N) at which ions transition from (E/N) independent K, the low field condition, to a K which is dependent on E/N, the high field condition, referred to as the E/N_{critical} varies with the carrier gas used. Equation 5.5 although not quantitative without knowledge of the correction factor (y) provides some insight into ($E/N_{critical}$) as a function of temperature (T), the Boltzmann's constant (k_B), m_1, m_2, the collision

$$E/N_{critical} = 8k_B T \frac{\Omega}{q}\sqrt{\frac{2ym_1}{3\pi(m_1+m_2)}} \qquad \text{Equation 5.5}$$

integral (Ω) and q for an ion[1]. At first glance equation 5.5 seems to indicate that by increasing the mass of the carrier gas (m_2), $E/N_{critical}$ would decrease. This is actually opposite of data observed with lithium and cesium ions in noble gases, where $E/N_{critical}$ always increases with increasing carrier gas mass[12, 13]. The reason for this is the Ω term which is increasing with m_2 faster than the $\sqrt{\frac{m_1}{(m_1+m_2)}}$ term is decreasing. Additionally the increase in $E/N_{critical}$ as a function of m_2 makes intuitive sense, because the difference for K under low and high field conditions is largely a function of how much internal energy the ion absorbs per collision. Under low field conditions the ion remains in thermal equilibrium and ion velocity remains constant because the energy transferred per collision is sufficient to

remove the energy gained between collisions from the electric field. From equation 5.4 it can be seen that more energy per collision is transferable with higher mass carrier gases, and thus low field behavior will be maintained for higher E/N conditions.

5.2 Nitrogen with modifiers

Nitrogen (N_2) is the carrier gas predominately used in FAIMS analyzers due to a relatively high dielectric breakdown potential, low cost, and availability. Most mass analyzer electrospray ionization (ESI) sources are designed with N_2 as a nebulizer and/or drying gas, making N_2 readily available to use as a FAIMS carrier gas. However no FAIMS analyzer using pure N_2 has ever exceeded a resolving power of 45 for any analyte, while resolving powers of over 200 have been shown for FAIMS systems using gas blends[6, 14].

The introduction of additional gases into the drying gas line of the generation 3 (G3) FAIMS device is straight forward. Dry house N_2 is filtered and sent to the Bruker Esquire 3000 ion trap mass analyzer through a ¼ inch Swagelok connection. Once N_2 is brought into the Esquire it is divided into nebulizer gas and counter current drying gas, which are electronically metered through software control. Nebulizer gas is used in the electrospray emitter to reduce the size of ESI droplets therefore speeding droplet evaporation and improving sensitivity. Counter current drying gas is heated in the source block, and flows out of the ion source to further assist in desolvation of droplets. With the G3 in place, the counter current drying gas also serves as the FAIMS carrier gas. For addition of gases in addition to N_2 a ¼ inch Swagelok "tee" fitting was place in the house N_2 line after filtering. Gases were metered by an MKS model 1179 flow controller, which was software controlled through a modified version of the LabView program written for compensation voltage scans.

5.3 Nitrogen/argon blends

Argon (Ar) is heavier, less polarizable, and has a smaller collisional cross section than N_2. While almost no work has been published using Ar as a carrier gas in FAIMS, a number of papers have used Ar in IMS to improve the separation of compounds which are not resolvable using N_2[15-17]. With so little information available prediction of $E/N_{criticial}$ for test compounds relative to pure N_2 is difficult. With the increased mass of Ar ion transmission might be improved through reduced diffusion in the low field or collisional cooling, similar to the use of Ar as a collision gas in ion traps[18, 19], under high field conditions. Since resolution in IMS is largely unchanged between Ar and N_2 there was hope that improved sensitivity could be achieved without reducing resolving power[15-17].

When blends of up to 60% Ar with 40% N_2 where tested with the G3 in passive mode ion signal rapidly decreased with greater than 20% Ar added to the carrier gas. CV scans were then performed using a mixture of Hexakis(2,2-Difluoroethoxy)Phosphazene (622 m/z), Hexakis(1H, 1H, 3H-tetrafluoropropoxy)Phosphazene (922 m/z), and hexakis(1H, 1H, 5-Octafluoropentoxy)Phosphazene (1522 m/z) at 20% Ar and 80% N2 carrier gas composition (figure 5.1). Peak CV increases for all compounds by roughy 5% with virtually no loss in sensitivity. However, the minor increase in CV is hardly worth the added complexity or cost of using a blend of AR with N_2.

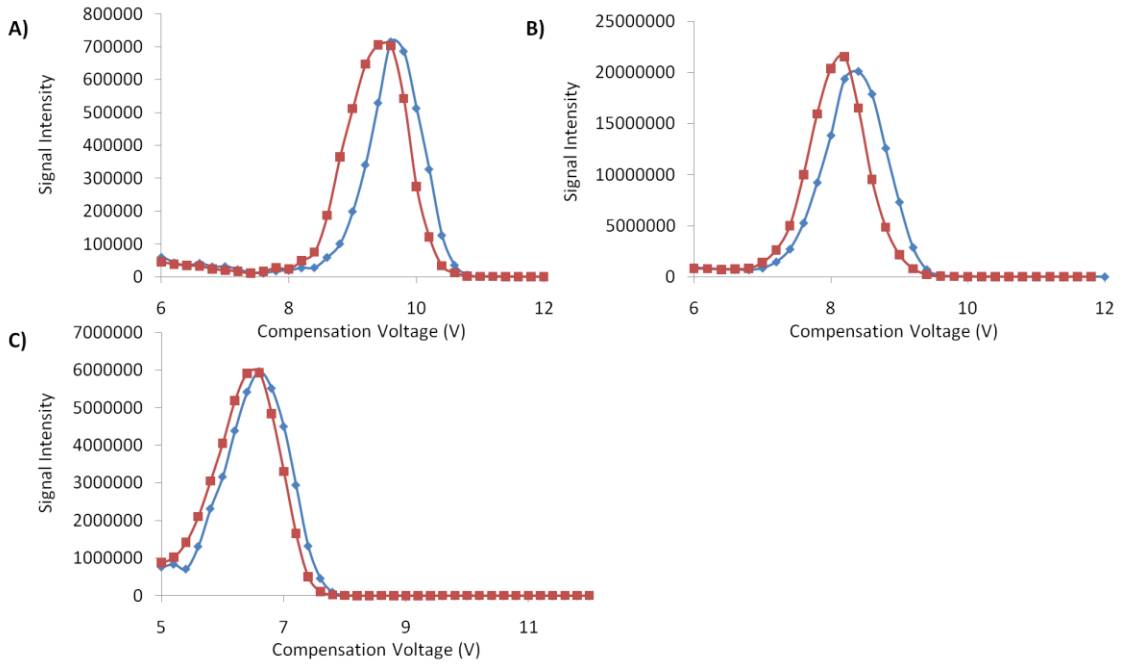

Figure 5.1 CV scans with 100% N_2 (red squares) and 20% Ar (blue diamonds) for Hexakis(2,2-Difluoroethoxy)Phosphazene (622 m/z) A) Hexakis(1H, 1H, 3H-tetrafluoropropoxy)Phosphazene (922 m/z) B) and hexakis(1H, 1H, 5-Octafluoropentoxy)Phosphazene (1522 m/z) C). In all cases peak CV voltages show slight increases (<5%) with identical ion transmission for all spectra except plot B shows a 7% signal decrease in absolute intensity.

5.4 Nitrogen/carbon dioxide blends

Another commonly used collision gas in IMS is carbon dioxide (CO_2) has a similar mass to Ar, a 20% large collision cross section and nearly twice the polarizability of Ar. CO_2 has been used in FAIMS previously and was shown to improve sensitivity and resolution for the ortho, meta, and para isomers of phthalic acid when used in a low percentage blend with N_2[5]. Following the failure of Ar to make any noticeable improvement in resolution or ion transmission CO_2 seemed like a good candidate to improve sensitivity due to its large cross section and mass. Initially interest in CO_2 as a carrier gas for the G3 was to improve ion transmission for low mass-to-charge ions in passive mode, but the addition of any percentage of CO_2 resulted in decreased signal relative to pure nitrogen for a wide range of +1 ions generated by electrospraying a solution of polyethyleneglycol (figure 5.2).

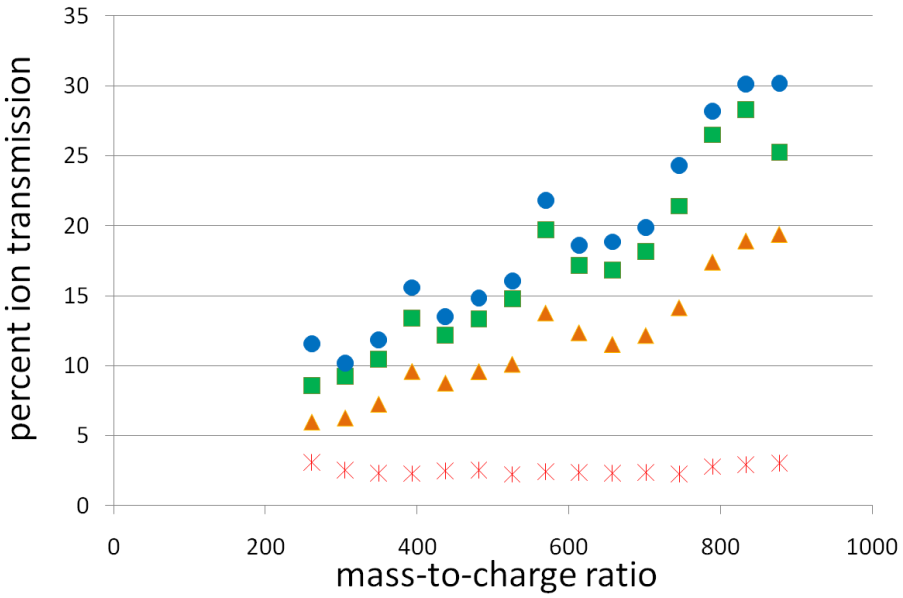

Figure 5.2 Ion transmission for +1 ions genereated by electrospray ionization of a mixture of Poly Ethylene Glycol polymers with average molecular mass 600 (PEG 600). Pure N_2 (blue dots) provides the highest ion transmikssion in passive mode while mixtures of N2 and 20% CO_2 (green squares), 45% CO_2 (orange triangels) and 59% CO_2 (red astriscks) show decreased signal relative to the standard ESI source (without the G3 attached).

While in passive mode the addition of CO_2 only reduce ion transmission, in active mode CO_2 can increase either the CV at which an ion transmits when used in small percentages with N_2 or improve transmission for ions at reduced CV by increasing the concentration of CO_2 relative to N_2 (figure 5.3). By using a gas blend of 20% CO_2 and 80% N_2 the CV values for the mixture of Hexakis(2,2-Difluoroethoxy)Phosphazene (622 m/z), Hexakis(1H, 1H, 3H-tetrafluoropropoxy)Phosphazene (922 m/z), and hexakis(1H, 1H, 5-Octafluoropentoxy)Phosphazene (1522 m/z) all increased, with the largest increase for higher mass ions. Further increases in CO_2 concentration in the carrier gas caused a shift towards lower CV values for all the ions in the test mixture and increases in ion signal for the low mass-to-charge component. While the mechanism for these changes due to gas composition are still not understood it seems that the changes are largely dependent on the relative mass

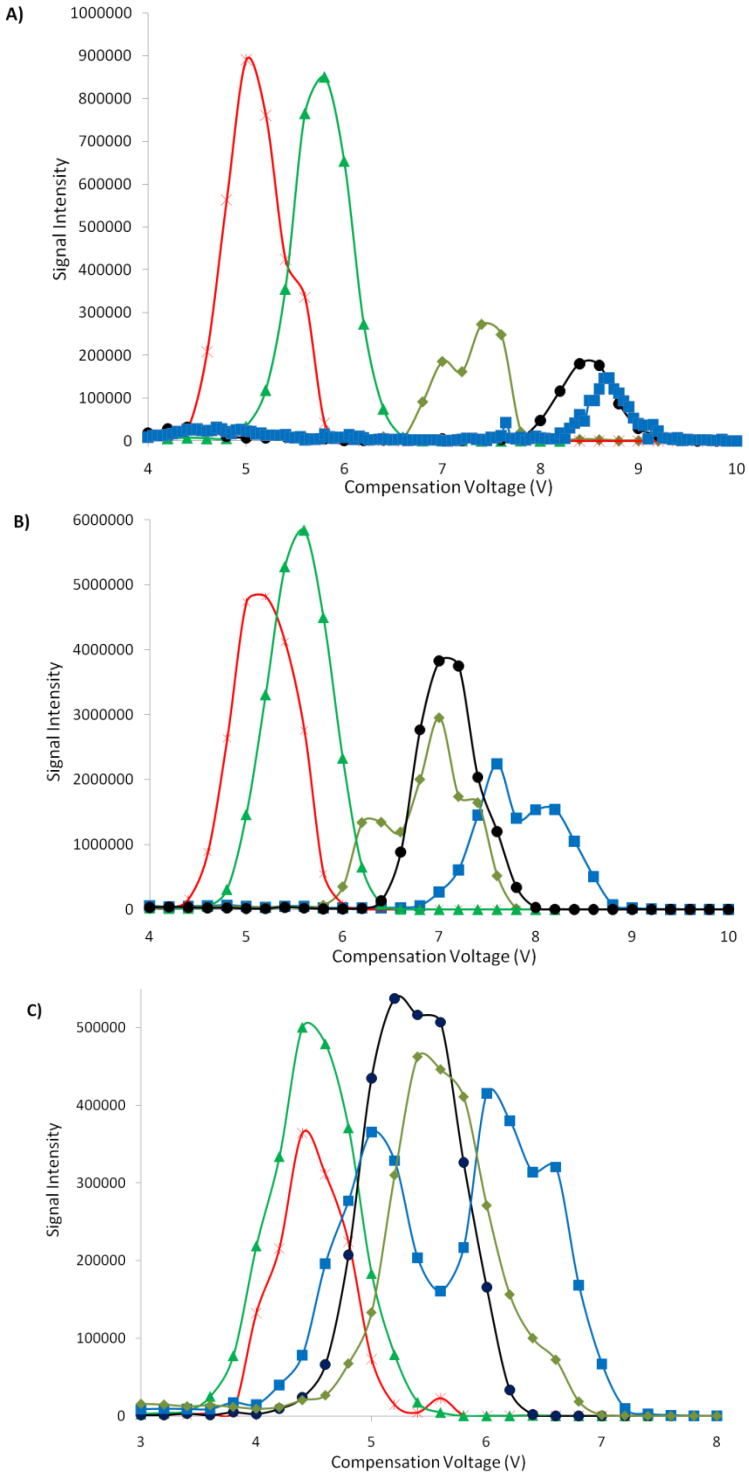

Figure 5.3 CV scan plots of A) Hexakis(2,2-Difluoroethoxy)Phosphazene (622 m/z) B) Hexakis(1H, 1H, 3H-tetrafluoropropoxy)Phosphazene (922 m/z) and C) hexakis(1H, 1H, 5-Octafluoropentoxy)Phosphazene (1522 m/z) in 100% N_2 (black circles), 80% N_2 20% CO_2 (blue squares), 66% N_2 33% CO_2 (light green triangles), 58% N_2 42% CO_2 (dark green diamonds), and 50 % N_2 50% CO_2 (red astricsk).

of the ion and neutral gas with the largest effect seen for low mass-to-charge ions.

5.5 Helium

Helium has the lowest mass and is the least polarizable of carrier gases employed in FAIMS separations. Clustering of helium with ions is highly unlikely at the temperatures typically employed in FAIMS separations and measured low field mobilities using He are a factor of four to five greater than mobilities under identical conditions using N_2[9]. The use of helium in concentrations between 30-75% has been shown to cause large shifts in compensation voltage relative to nitrogen and provides a substantial increase in resolving power, the highest measured resolving power for FAIMS was achieved using a 75% helium/nitrogen mix in a planar FAIMS analyzer[6, 14].

Unfortunately, the use of He in FAIMS analyzers is limited due to instrumental factors such as the reduced dielectric strength of He and decreased pumping speed of turbomolecular pumps. High concentrations of He also lead to an overall loss in sensitivity due to increased diffusion in the FAIMS device. The experiments discussed in the following sections are intended to determine the maximum useful percent blend of He/N_2 for the G3 device, and provide methods of improving separation performance while limiting the ion loss associated with high He concentrations.

5.5.1 Instrumental limitations

The maximum potential which can be applied between two parallel plates is a function of the pressure and distance between the plates, as well as the composition of the gas which separates the electrodes (section 4.4.4). Helium has a high ionization potential relative to other carrier gases (24.6 eV for He vs. 14.5 eV for N_2), which may lead one to believe that He would be able to withstand higher potentials without dielectric breakdown.

This is not the case because He lacks any modes of vibrational relaxation and can only release internal energy through electronic transitions. A plot of Paschen's curve[20] for N_2 and He (figure 5.4) indicates that the G3 device with a 100% He carrier gas would be limited to

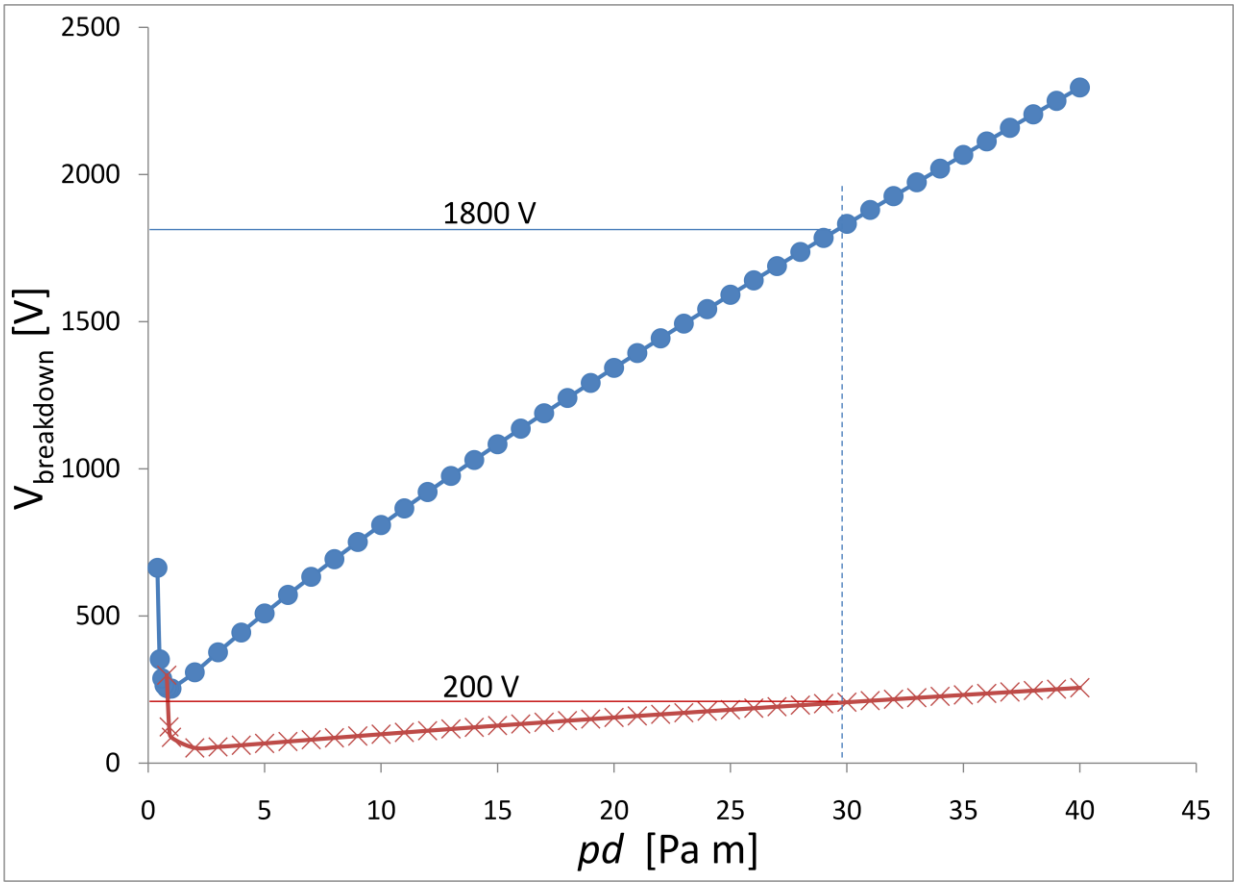

Figure 5.4 Breakdown potentials calculated using equation 4.3 for 100% nitrogen (blue circles) and 100% helium (red Xs) with dashed line drawn in for *Pd* of the G3 FAIMS device. The maximum calculated voltage which can be applied between the electrodes in 100% nitrogen and helium is 1800 V and 200 V respectively. This matches reasonable well to the observed maximum DV with pure N_2 of 1900-2000 V, as the analytical gap is slightly larger than 0.3 mm.

11 % of the maximum dispersion voltage achievable with N_2. However, in practice blends of helium and nitrogen typically do not exceed 70 % He, which limits dispersion voltage to 80% of the maximum for pure N_2 with arcing occurring at 1600 V for the G3 device. For the small gap size of the G3 the standard operating conditions are typically 25% below the dielectric breakdown threshold for nitrogen, which provides a reasonable compromise between

sensitivity and resolution because of the high electric field strength over a small gap (section 4.4.3). However, this is not true for planar and cylindrical FAIMS devices with larger analytical gaps, which often operate within 10% of their maximum dispersion voltage, and must be operated at reduced DV when using carrier gases exceeding 50% He.

Another problem which is universal for all FAIMS devices is that coupling of FAIMS with mass spectrometry relies on the vacuum system of the mass analyzer to pull gas through the FAIMS device. With N_2 used in FAIMS this arrangement works well because the source conductance limits are designed for N_2 from nebulizing gas and drying gas and the vacuum system is sized to maintain optimal pressures in the mass analyzer. Unfortunately He is not efficiently pumped by most turbomolecular pumps due to the high velocity of helium atoms which can decrease the effective pumping speed of the source region by up to 50%[21]. High percentages of helium in the carrier gas for FAIMS can exceed the pumping limits of the first vacuum region leading to a runaway process in which the pressure increases until vacuum system failure. The pumping speed of turbomolecular pumps is also dependent on the pressure of the gas being pumped, with optimal pressure for most turbomolecular pumps being below 10^{-2} Torr. As source pressure increases and pumping speed decreases one of two things will happen, either the electrical load of the turbomolecular pump will exceed manufactures recommendation or the pumps rotational speed will decrease below the minimum set point. In either event the turbo controller will shut down power to the pump, venting the mass analyzer. The maximum flow of He a vacuum system can pump varies from vacuum system to vacuum system being dependent on the conductance limits between vacuum regions, the specific turbomolecular pump used, and the pumping provided by backing pumps. In the case of the Bruker Esquire 3000, using an Edwards EXT255HI

turbomolecular pump backed by an Edwards e2m18 mechanical rough pump, the flow of helium into the system should not exceed 3.5 l/min, equal to 70% of the carrier gas composition.

5.5.2 Loss of signal due to increased diffusion

The diffusion coefficient (D) for an ion is a function of the gas it diffuses through because of the ion's mobility (K) in equation 5.6. K for ions in He is typically a factor of >3

$$D = K\frac{k_B T}{q} \qquad \text{Equation 5.6}$$

larger than in N_2 resulting in higher diffusion in gas mixtures containing He, while the temperature (T) charge (q) and Boltzmann's constant are unchanged between carrier gases.

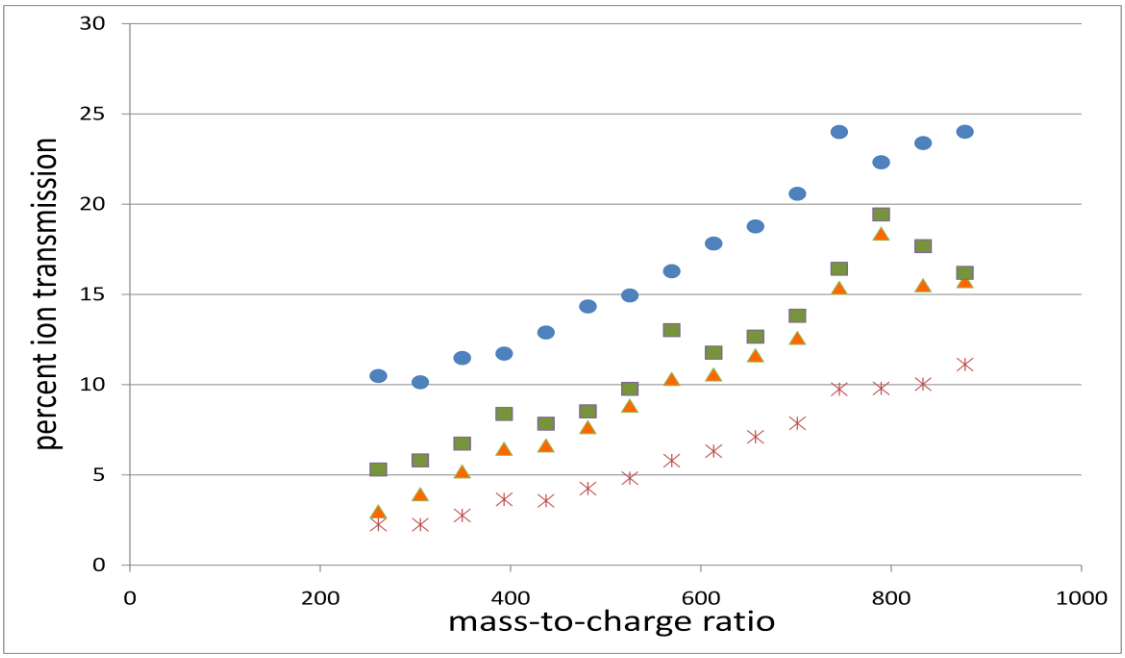

Figure 5.5 Ion transmission for singly charged PEG 600 ions in the G3 in pure N_2 (blue dots), and blends of N_2 with 29% He (green squares), 44% He (orange triangles), and 60% He (red asterisk). Ion loss due to diffusion increases for all ions due to increased mobility in He.

Because mobility is proportional to mass, diffusion losses are greatest for low mass-to-charge ratio ions (figure 5.5 and covered in more depth in chapter 6). The result of diffusion in FAIMS is that low mass-to-charge ions are preferentially eliminated (table 5.1).

Table 5.1 Ion signal relative to 100% N_2 carrier gas for +1 charge state PEG 600 ions

m/z	100% N_2 0% He	71% N_2 29% He	66% N_2 44% He	40% N_2 60% He
261	100%	51%	28%	21%
349	100%	58%	45%	24%
437	100%	60%	51%	28%
525	100%	65%	59%	32%
613	100%	66%	59%	35%
701	100%	67%	61%	38%
789	100%	87%	82%	43%

5.5.3 Increased resolving power

High He composition carrier gases adversely affect the sensitivity for low mass-to-charge ratio ions because of a proportionally large change in low field mobility leading to increased losses through diffusion. Resolving power follows the same trend as ion transmission with the compensation voltage (figure 5.6) for lower mass-to-charge ions increasing faster than for heavier ions. However, the loss of ions due to diffusion results in no signal being observed for the lowest mass-to-charge ratio ion tested (Hexakis (2,2-Difluoroethoxy) Phosphazene (622 m/z)) at gas mixtures with greater than 40% He. Current methods which use a fixed ratio gas blend across the entire CV scan range are limited to either analyzing high mass-to-charge ratio analytes, or limiting gains in resolving power by using gas blends which are optimized for the lowest mass-to-charge analyte of interest. Development of a scan method which links CV and carrier gas composition is necessary to maximize separation performance for complex mixtures as discussed in the following section.

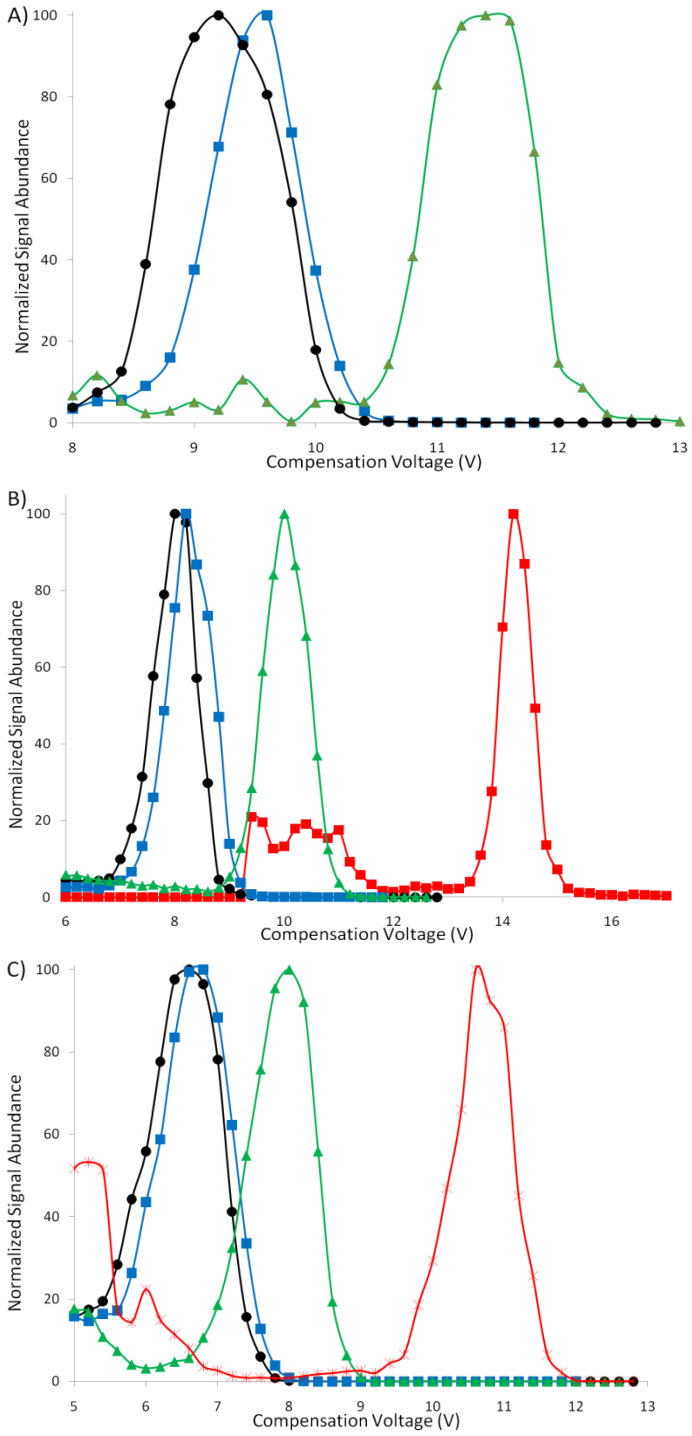

Figure 5.6 CV scan plot of A) Hexakis(2,2-Difluoroethoxy)Phosphazene (622 m/z) B) Hexakis(1H, 1H, 3H-tetrafluoropropoxy)Phosphazene (922 m/z) and C) hexakis(1H, 1H, 5-Octafluoropentoxy)Phosphazene (1522 m/z) in 100% N_2 (black circles), 80% N_2 20% He (blue squares), 60% N_2 40% He (green triangles), and 40 % N_2 60% He (red astricsk) not shown in figure A) because of the total loss of signal due to diffusion related losses.

5.5.4 The future of helium in FAIMS

In cases where the maximum possible separation of a wide range of mass-to-charge ratios is desired it may be advantageous to link scans of CV with He concentration to improve resolution for high mass-to-charge ions without adversely affecting detection of lower mass-to-charge ratio ions. At this time the software and hardware necessary to perform these scans is in development, but based on the data presented in **section 5.5.3** it appears possible to improve ion transmission for low mass-to-charge ratio ions while maintaining maximum resolving power for high mass-to-charge ratio ions, with the additional advantage of being able to choose where to place peaks in the CV spectrum. Theoretically it is possible to choose where a peak falls in a CV spectrum by varying gas composition. If gas composition can be varied rapidly peak position can be controlled by varying both gas composition and compensation voltage (Figure 5.7). By increasing the helium composition to 60% during the CV range immediately after the 1522 m/z peak, the 922 m/z component is not transmitted. When the CV value reaches 10 V the percentage of He can be reduced to 40% again to transmit the 622 m/z ion which is not observed above 40% He blend. After the elution of the 622 m/z ion the He content can again be increased to 60% in order to transmit the 922 m/z peak at maximum resolving power. Performing scans in this manner should allow for optimization of resolving power for each component, reduction in peak overlap, and an increase in the analytically useful CV range which increases peak capacity. However to be a viable option the gas composition must be able to be changed rapidly, on the same order as the CV, and requires modification from the current gas controller configuration to minimize the volume of gas between flow controller and FAIMS device.

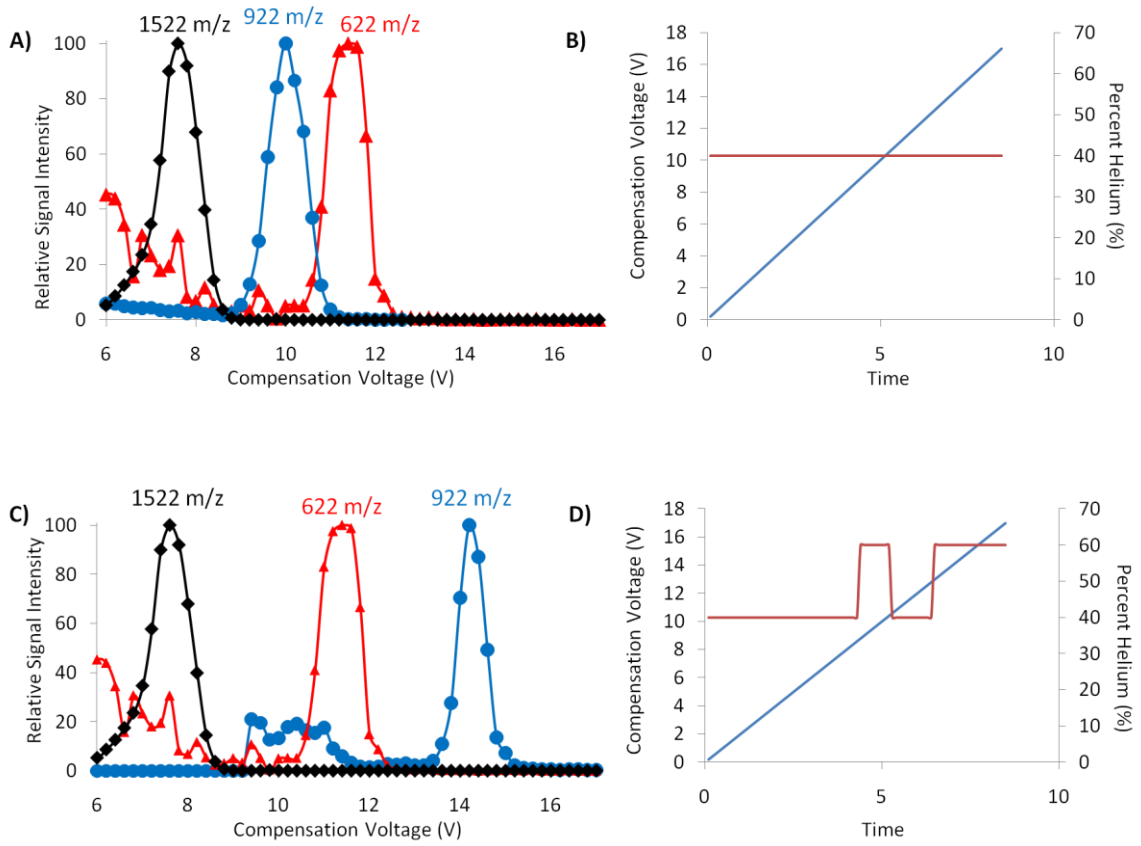

Figure 5.7 CV scan using fixed 40% He blend A) with a plot showing the He composition (red line) and CV (blue line) vs. time B). Plot C) is a theoretical spectrum produced by varying He concentration between 40 and 60 % as shown in plot D).

5.6 Summary

Mixtures of Ar, CO_2, and He with N_2 were evaluated on their ability to improve ion transmission in passive mode and to improve resolving power and ion transmission during active CV scans. No mixture of gases resulted in improved ion transmission for passive mode, while CO_2 improved ion transmission in active mode for low mass-to-charge ions but at the cost of resolving power. Increasing the mass of the neutral collision gas relative to N_2 decreased the CV of the ions tested while decreasing the mass of the neutral collision gas

leads to increases in CV. Contrary to published results no blend of gases tested allowed simultaneous improvements in sensitivity and resolution. While improvements in resolution always coincide with a decrease ion transmission, control of carrier gases composition offers alternative scan modes for FAIMS which offer the possibility of reduced peak overlap and improved peak capacity with minimal loss in sensitivity.

5.7 References

1. Shvartsburg, A. A., *Differential ion mobility spectrometry: nonlinear ion transport and fundamentals of FAIMS*. CRC Press: Boca Raton, 2009.

2. Tang, K. Q.; Li, F. M.; Shvartsburg, A. A.; Strittmatter, E. F.; Smith, R. D., Two-dimensional gas-phase separations coupled to mass Spectrometry for analysis of complex mixtures. *Analytical Chemistry* **2005,** 77, (19), 6381-6388.

3. Viehland, L. A.; Guevremont, R.; Purves, R. W.; Barnett, D. A., Comparison of high-field ion mobility obtained from drift tubes and a FAIMS apparatus. *International Journal of Mass Spectrometry* **2000,** 197, 123-130.

4. Barnett, D. A.; Ells, B.; Guevremont, R.; Purves, R. W.; Viehland, L. A., Evaluation of Carrier Gases for Use in High-Field Asymmetric Waveform Ion Mobility Spectrometry. *Journal of the American Society for Mass Spectrometry* **2000,** 11, 1125-1133.

5. Barnett, D. A.; Purves, R. W.; Ells, B.; Guevremont, R., Separation of o-, m- and p-phthalic acids by high-field asymmetric waveform ion mobility spectrometry (FAIMS) using mixed carrier gases. *Journal of Mass Spectrometry* **2000,** 35, (8), 976-980.

6. Shvartsburg, A. A.; Danielson, W. F.; Smith, R. D., High-Resolution Differential Ion Mobility Separations Using Helium-Rich Gases. *Analytical Chemistry* **2010,** 82, (6), 2456-2462.

7. Ells, B.; Barnett, D. A.; Purves, R. W.; Guevremont, R., Detection of nine chlorinated and brominated haloacetic acids at part-per-trillion levels using ESI-FAIMS-MS. *Analytical Chemistry* **2000,** 72, (19), 4555-4559.

8. Hoffmann, E. d.; Stroobant, V., *Mass Spectrometry: Principles and Applications*. 2 ed.; John Wiley & Sons: New York, 2002; p 407.

9. Eiceman, G. A.; Karpas, Z., *Ion Mobility Spectrometry*. Second ed.; CRC Press: 2005; Vol. 1, p 337.

10. Iinuma, K.; Imai, M.; Satoh, Y.; Takebe, M., Mobilities of Li+ Ions in HCl, HBr, and HI at Room-Temperature. *Journal of Chemical Physics* **1988,** 89, (11), 7035-7036.

11. Satoh, Y.; Takebe, M.; Iinuma, K., Mobilities of Cluster Ions of Li+ in Some Molecular Gases. *Journal of Chemical Physics* **1988,** 88, (5), 3253-3259.

12. Lozeille, J.; Winata, E.; Soldan, P.; Lee, E. P. F.; Viehland, L. A.; Wright, T. G., Spectroscopy of Li+center dot Rg and Li+-Rg transport coefficients (Rg = He-Rn). *Physical Chemistry Chemical Physics* **2002,** 4, (15), 3601-3610.

13. Hickling, H. L.; Viehland, L. A.; Shepherd, D. T.; Soldan, P.; Lee, E. P. F.; Wright, T. G., Spectroscopy of M+center dot Rg and transport coefficients of M+ in Rg (M = Rb-Fr; Rg = He-Rn). *Physical Chemistry Chemical Physics* **2004,** 6, (17), 4233-4239.

14. Shvartsburg, A. A.; Tang, K. Q.; Smith, R. D., Differential Ion Mobility Separations of Peptides with Resolving Power Exceeding 50. *Analytical Chemistry* **2010,** 82, (1), 32-35.

15. Matz, L. M.; Hill, H. H.; Beegle, L. W.; Kanik, I., Investigation of drift gas selectivity in high resolution ion mobility spectrometry with mass spectrometry detection. *Journal of the American Society for Mass Spectrometry* **2002,** 13, (4), 300-307.

16. Asbury, G. R.; Hill, H. H., Using different drift cases to change separation factors (alpha) in ion mobility spectrometry. *Analytical Chemistry* **2000,** 72, (3), 580-584.

17. Kanu, A. B.; Hill, H. H., Identity confirmation of drugs and explosives in ion mobility spectrometry using a secondary drift gas. *Talanta* **2007,** 73, (4), 692-699.

18. Vachet, R. W.; Glish, G. L., Effects of Heavy Gases on the Tandem Mass Spectra of Peptide Ions in the Quadrupole Ion Trap. *Journal of the American Society for Mass Spectrometry* **1996,** 7, 1194-1202.

19. Danell, R. M.; Danell, A. S.; Glish, G. L.; Vachet, R. W., The Use of Static Pressures of Heavy Gases within a Quadrupole Ion Trap. *Journal of the American Society for Mass Spectrometry* **2003,** 14, (10), 1099-1109.

20. Friedrich, P., Ueber die zum Funkenübergang in Luft, Wasserstoff und Kohlensäure bei verschiedenen Drucken erforderliche Potentialdifferenz. *Annalen der Physik* **1889,** 273, (5), 69-96.

21. *Product and Vacuum Technology Reference Book*. Leybold Vacuum Products Inc. and Leybold Inficon Inc.: Export, PA, 1991.

Chapter 6
Design and Development of an in-source FAIMS analyzer

6.1.1 Generation 4.0 (G4) goals

Goals for the G4 were to make a device invisible to users while maintaining the resolution and ion transmission achieved with the G3, if not surpassing the G3. The G4 should add no length to the transfer capillary, so that all components fit within the ion source enclosure. External dimensions could not be substantially larger than the standard capillary and ideally the G4 would retain use of the source door and electrospray emitter positioning, making the G4 set up identical to the standard electrospray transfer capillary.

The G4 would be sealed to the capillary, permanently becoming a single entity with the ESI transfer capillary. The sealing of the G4 to the capillary would need to be gas tight, as we had learned in previous designs (chapters 3 and 4). The design should also be rugged enough to allow the capillary to be installed and removed from the system for the life of the capillary without damaging the G4. The reduced size of the G4 relative to the G3 would require isolation between electrodes and the outer housings to be exceptional to withstand the high voltages (over 3000 $V_{peak\text{-}peak}$) applied to electrodes.

6.1.2 G4.0 Design

Figure 6.1 is a drawing of the first proposed G4.0 design. In this design the standard ESI transfer capillary is cut shorter and then one end is ground to a reduced diameter (figure 6.1a). Planar electrodes similar to those used in the G3, are held in a vespel outer housing and press fit onto the reduced diameter capillary (figure 6.1b). A Teflon sleeve between the

vespel outer housing and the ground capillary provides the gas tight seal and flush fitting counter sunk screws are used to secure and align the electrodes, as well as providing the electrical contacts for the asymmetric waveform and compensation voltages(figure 6.1b). The planar electrodes are half cylinders like the G3 design but with a small groove machined into the rear of the electrode, and the addition of polyamide coating triangles to the rear half of the electrodes (figure 6.1a).

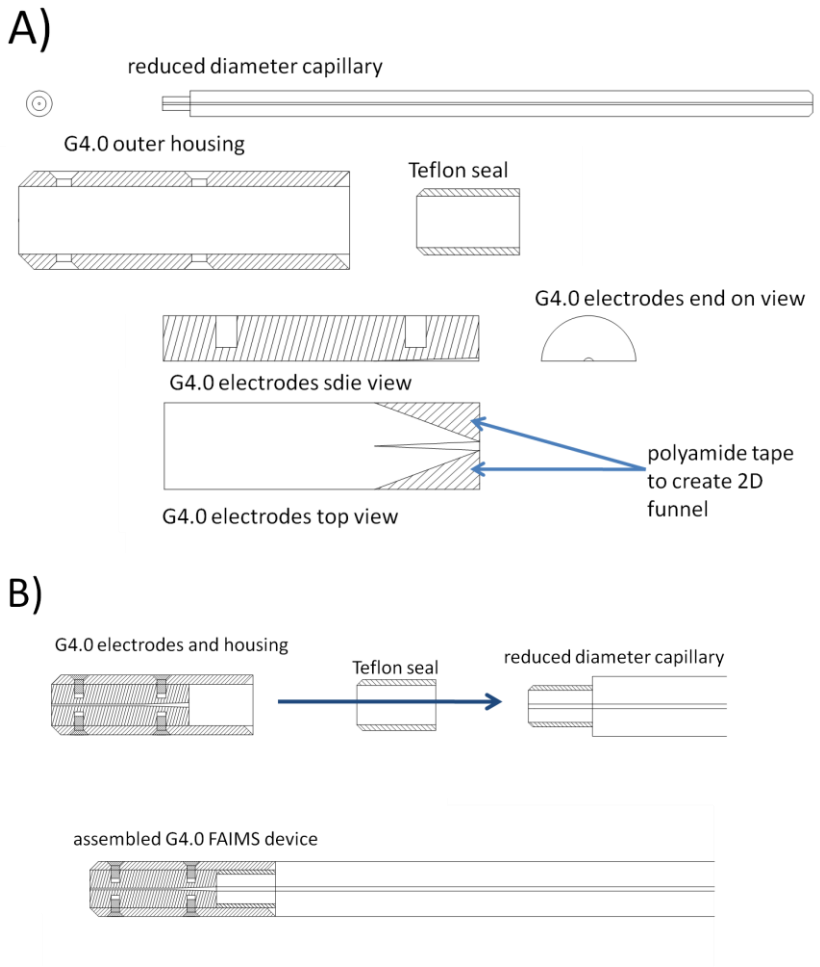

Figure 6.1 Mechanical drawings of the G4.0 with labeled components A) and the completed assemble B).

Preliminary testing of the G4 electrode design was carried out using a G3 analyzer with modified electrodes (results discussed in section 6.2.2). Test of the polyamide tape funnel

design revealed poor ion transmission (42% lower when tape was applied to electrodes); no separations were attempted with these electrodes. With the results indicating that polyamide

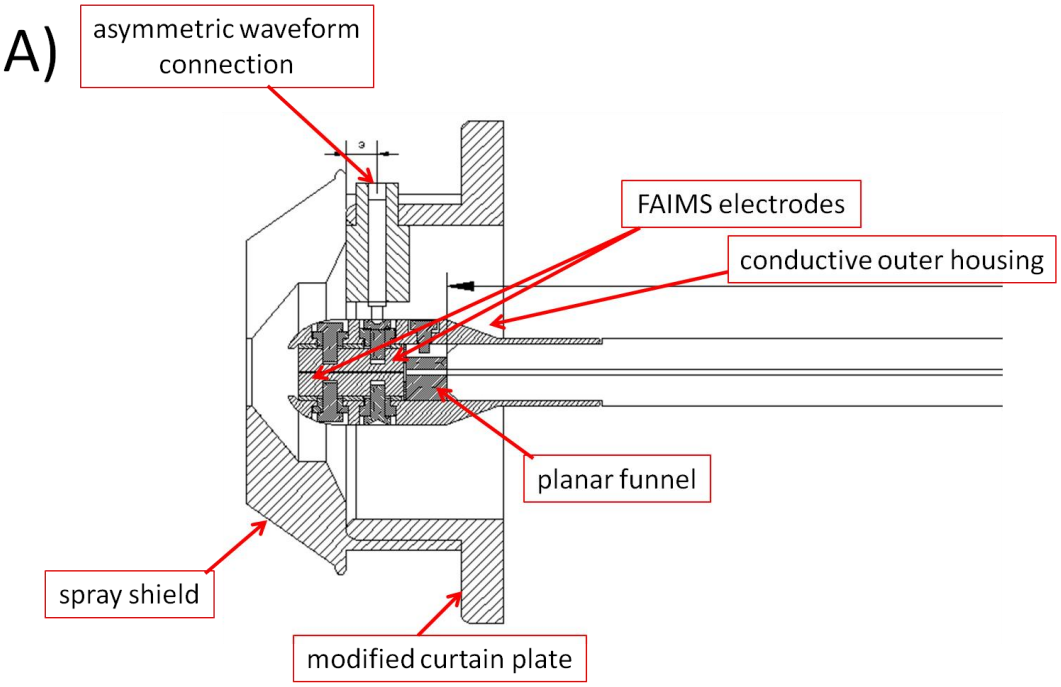

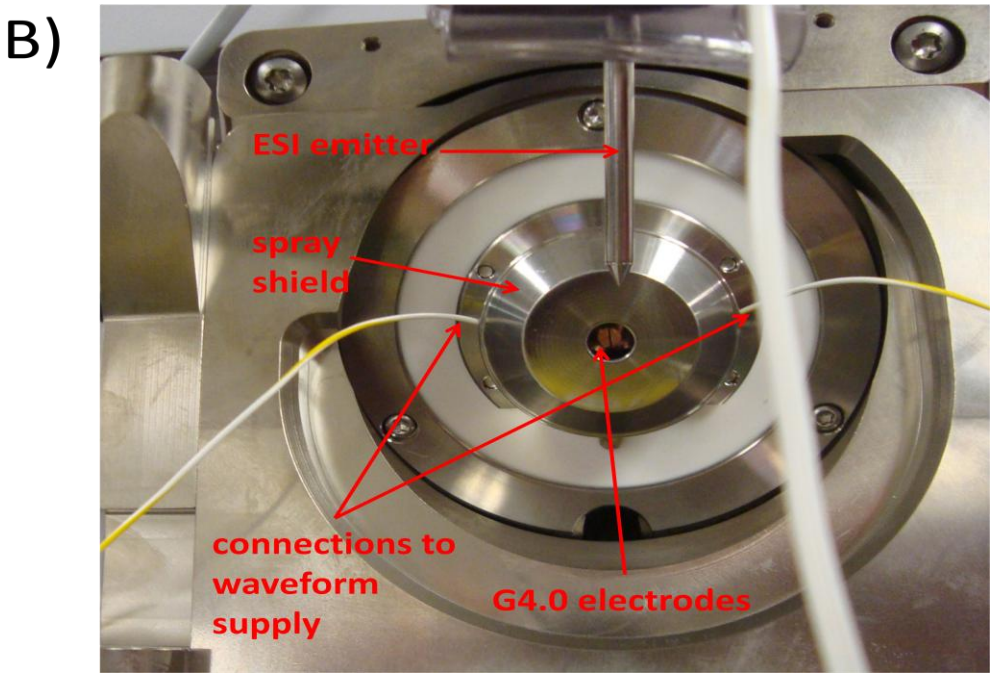

Figure 6.2 Drawing of G4.0 capillary FAIMS device with components labeled A). The device fits any current generation Bruker electrospray ion source, only the G4 capillary and modified curtain plate differ from the standard source B).

coatings would not be a viable replacement for the 3D funnel used in the G3, the initial G4.0 designs were modified. The final design of the G4.0 (figure 6.2) includes an additional conductive outer housing to prevent charging of the vespel housing, and a metal planar funnel between the electrodes and glass transfer capillary. The metal outer housing also serves as counter electrode to the ESI emitter for ion generation.

In commercial sources the source door is in electrical contact with the vacuum housing held at ground potential. In this configuration the ESI potential (~4000 V) is applied to the spray shield and transfer capillary. With the G4 design, the metal outer housing and electrodes of the FAIMS replaced the metalized coating of the transfer capillary. Prototype testing continues to use the UNC built waveform generator discussed in chapter 2, which has insufficient electrical isolation to allow the supply to float at the >4000 V dc needed to perform electrospray ionization using an ESI emitter held in the door. At the outset of G4 design, development of an asymmetric waveform power supply began which included high DC isolation between outputs and ground, computer control of waveform amplitude and new circuitry to provide low voltage output monitors but construction of this new supply, would take weeks due to the extensive design changes. In the intervening time testing of the G4 was conducted with the G4 metal outer housing held at ground potential, while 4000 V was applied to an electro spray emitter held in a ring stand and positioned as the emitter would be with the source door attached.

6.2 Ion transmission

High ion transmission in the passive mode remained a priority for the G4 device. With reduced electrode length ion transmission was only expected to increase relative to the G3 which had shown 100% ion transmission for some ions. Oddly transmission for the G3

sometimes exceed 100% relative to standard ESI conditions for highly charged ions, while for low mass-to-charge ratio ions transmission was reduced to < 10%. With the development of the G4, changes were made which would improve ion transmission independent of mass-to-charge ratio. To remove factors external to the FAIMS device the G4 was installed on a non-trapping mass analyzer and tested with low concentration samples to reduce the effects of space charge. Improvements in the FAIMS design where instituted as well which reduced ion losses due to the diffusion of ions within the FAIMS device.

6.2.1 Low mass-to-charge discrimination

Ion transmission through a narrow bore is inversely related to the mobility of an ion[1]. The mobility of an ion roughly correlates to the mass-to-charge ratio of the ion[2]. Plots of ion transmission with the G3 installed as a percentage of ion signal with the conventional source layout such as figure 6.3 have the appearance of a high pass filter. Ions above a specific mass-to-charge ratio have transmission near or at 100% while ions below a specified mass-to-charge ratio have a negative correlation between mass-to-charge and percent ion transmission. The profile of a transmission vs. mass-to-charge plot is a function of electrode length, electrode gap, the distance between electrodes and the ESI transfer capillary (dead volume) and residence time (t_{res}) in the device. Narrower gaps reduce t_{res} but also reduce the distance an ion can travel from the center of the analytical gap without being neutralized. Reducing electrode length likewise reduces t_{res}, increasing ion transmission for high mobility ions, but resolving power will decrease as a function of $\sqrt{t_{res}}$ as stated by equation 4.2. The optimal means of increasing ion transmission for high mobility ions is to minimize "dead volume" in the device. Dead volume is any volume in the device which does not affect the separation of ions, i.e. the volume of the capillary union, and distance from capillary

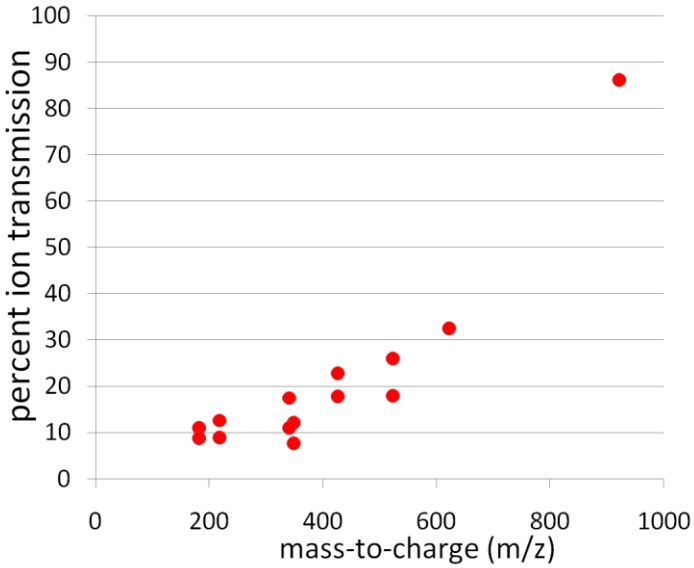

Figure 6.3 Ion transmission plot for G3 FAIMS as a function of mass to charge. Ions below 900 m/z have lower ion transmission due to diffusion in the device

to electrodes. Careful design of these components, and ultimately integration of the device into the capillary, result in improvement of transmission of low mass-to-charge ions as is discussed in section 6.2.2.

6.2.2 Improved capillary union

Flared capillaries had been used in the G3 design, but mass biasing had been observed and attributed to the dead volume resulting from the three dimensional flare (section 6.2.1). The initial G4 electrodes included polyamide coatings intended to replace the flared capillary from the G3, by directing gas flow into the 0.6 mm diameter conductance limit in the glass transfer capillary. To gain the improved ion transmission of the 3D flare, without the mass biasing induced by the dead volume in the capillary union, use of a two dimensional planar flare was proposed. A two dimensional planar flare would allow effective sampling of the analytical gap, which eliminated the unused volume of the flare which was shielded by the electrodes (figure 6.4).

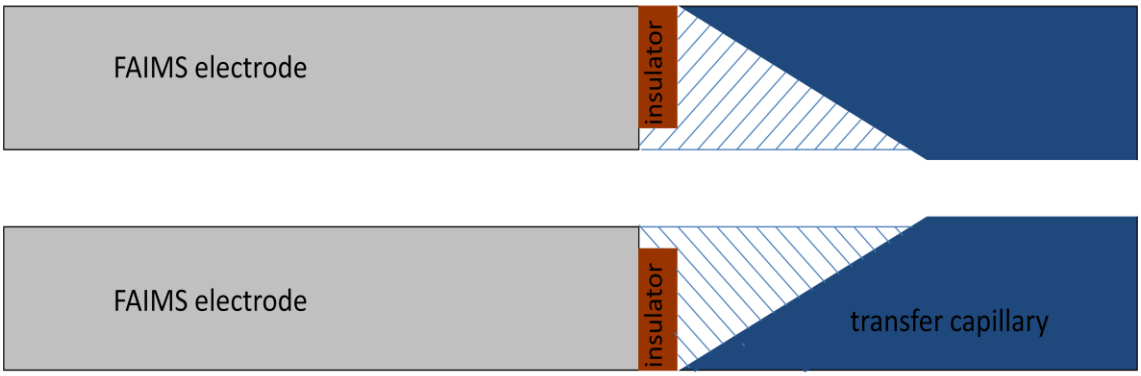

Figure 6.4 Cutaway side view drawing of the dead volume (space filled with diagonal lines) introduced by 3D flared capillaries. Dead volume in flare decreases gas velocity in the flare increasing t_{res} for all ions. Low mass-to-charge ratio ions are preferentially lost due to higher rates of diffusion causing ions to contact the metalized surface of the transfer capillary.

Integrating the flare into the FAIMS electrodes would be the ideal way to eliminate dead volume, but the flare would have to be designed so as not to limit resolution. The proposed planar flare was constructed using a G3 device and polyamide tap applied to the rear of the electrodes (figure 6.5a). Polyamide tap is an insulator with a high dielectric breakdown threshold of 12 kV/mm. An insulator of dielectric strength surpassing air was necessary to assure that the flare did not reduce the DV applied to the electrodes. As can be observed in figure 6.5b the introduction of polyamide tap to create a two dimensional funnel caused ion transmission to decrease by an average of 42% relative to the unmodified electrodes. In hind sight this should have been predicted, the G2 had already showed that non-conductive materials cannot be used near the ion beams path. The polyamide tape flare caused the gap dimensions to decrease to an aspect ratio of 6:1 at the exit. The failure of this design provided a reinforcement of the previously decided upon minimum aspect ratio of >

6:1 (**Chapter 4**). Due to this result the design for the G4 was revaluated.

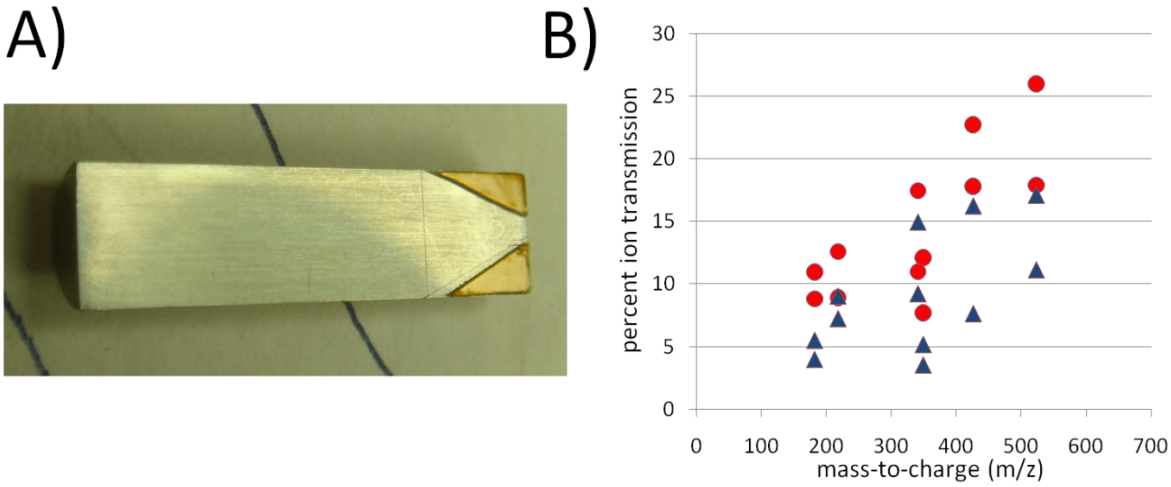

Figure 6.5 Photograph of G3 electrodes modified with polyamide tape funnel A) and a plot of percent ion transmission vs. mass to charge for the unmodified electrodes (red circles) and electrodes with tape funnel (blued triangles) B). While both data sets demonstrate the same trend of increasing transmission with higher mass the blue triangles are shifted to lower transmission by almost a factor of 2.

The G4 device went back to the drawing board in search of another solution to improved ion transmission while reducing mass discrimination. The dead volume of the 3D flare could be eliminated by filling in the flare above and below where the FAIMS electrodes blocked ions from entering the 3D flare, without reducing transmission. Filling in this dead volume produces a flared slot, which transitioned from a rectangular slot 0.3 mm X 6 mm to a circular outlet measuring 0.6 mm in diameter. To assure optimal ion transmission the planar flare must be conducting, which requires it to be well isolated from the FAIMS electrodes. Incorporating the planar flare into the G4 required increasing the overall length of the FAIMS analyzer section by 10 mm but, also simplified the G4 FAIMS electrode design, allowing use of electrodes similar to the G3 but 15 mm shorter.

6.2.3 Space charge in trapping instruments

As the name implies, ion trap analyzers accumulate and store ions prior to mass analysis. The accumulation of ions in a fixed volume is limited to a maximum charge density. When this maximum charge density is reached an equilibrium condition occurs where the addition of an ion requires the loss of another trapped ion. Accumulation of large numbers of ions (on the order of 1 X 10^6 ions per cm^3) causes loss of resolution in the mass spectrum, improper assignment of mass-to-charge ratio, and the preferential storage of low mass ions at the cost of high mass ions[3, 4]. Loss of mass analyzer performance due to high charge density is referred to as the "space charge effect" and has been an issue since the first trapping mass analyzers were developed[5]. Modern commercial instruments provide ion current controls (ICC) to limit the maximum number of ions which can be accumulated in the trap[6]. However, these ICC only limits the maximum amount of charge in the trap, and does not differentiate between unwanted background and analyte ions.

3D rf ion traps, such as the Bruker Esquire 3000, store ions in a pseudo potential well, the depth of which (D_z) can be calculated as a function of ion trap rf drive frequency (Ω), the internal radius of the trapping volume in the z-coordinate direction (z_0), mass of the ion (m_1), charge of the ion (e) and the stability parameter (q_z) for a particular ion. Equation 6.1 is valid only for ions of q_z <0.4 and with no dc applied to

$$\overline{D_z} = \frac{m_1 z_0^2 \Omega^2}{16e} q_z^2 = \frac{4eV^2 z_0^2}{m_1 \left(r_0^2 + 2z_0^2\right)^2 \Omega^2} \qquad \text{Equation 6.1}$$

$$q_z = \frac{8eV}{m_1 \left(r_0^2 + 2z_0^2\right) \Omega^2} \qquad \text{Equation 6.2}$$

the ring or end cap electrodes of the trap. The larger the value of D_z the more tightly ions are held in the center of the trapping volume. An ion's q_z is proportional to the charge (e), and

zero to peak amplitude of the rf tapping voltage (V), and inversely related to the mass of an ion (m),the internal dimensions of the trap ($r_0^2 + 2z_0^2$), and frequency of the rf trapping voltage (Ω). The pseudo potential well reaches a maximum value at a q_z of 0.8, prior to mass ejection at a q_z of 0.908. Because of the inverse dependence of D_z on mass-to-charge, low mass-to-charge ratio ions will be stored with the highest density at the center of the ion trap, while higher mass-to-charge ratio ions will have larger ion trajectories which spend less time near the center of the ion trap. As charge increases at the center of the ion trap, ions outside of the center are forced farther away. This phenomenon results in a pushing out of, and eventual loss of lower q_z ratio ions (higher relative mass-to-charge ratio) as an increasing number of low relative mass-to-charge ions accumulate in the center of the ion trap[4].

One of the results commonly observed on FAIMS equipped ion traps is >100% ion transmission for some ions (Figure 6.6). Because FAIMS preferentially discriminates against

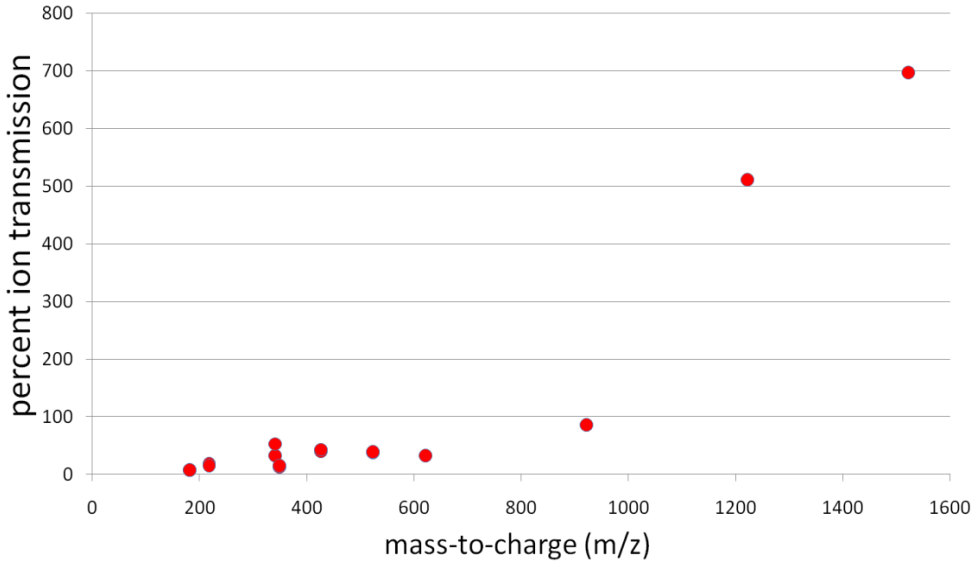

Figure 6.6 plot of percent ion transmission for G3 FAIMS vs. standard transfer capillary showing >100% ion transmission for high mass-to-charge ratio ions due to reduction in space charge effects.

low mass to charge ions, an increased number of higher mass-to-charge ratio ions are trapped, and the overall signal contribution of higher mass-to-charge ratio ions is increased. While this is sometimes advantageous, for the purposes of characterizing the ion transmission of a new analytical device it poses an issue. Determining whether observed signal is due to the ion transmission through FAIMS, or improvements in trapping conditions in the mass analyzer, requires testing of the FAIMS system with a non-trapping beam type mass analyzer. Therefore the G4.0 was installed on a Bruker Micro ToF-Q instrument. The use of an orthogonal quadrupole time of flight analyzer also improved the mass range over which the G4 could be evaluated.

6.2.4 Improved transmission

Elimination of variables in the measurement of ion transmission due to space charge and other effects unique to ion traps made the study of G4 ion transmission more straightforward. With the G4 installed in a Q-ToF instrument ion signal intensities for a complex mixture of differing charge and mass ions were determined, and then repeated with a standard ESI capillary installed. The percent ion transmission for the G4 with the 2D planar funnel union relative to a standard ESI transfer capillary is plotted in figure 6.7. Figure 6.7 demonstrates the high pass filter behavior of passive FAIMS. Ions which diffuse rapidly (low mass-to-charge ratio) are preferentially lost, while those below some maximum diffusion rate will have no attenuation. Ideally the roll off point for the high pass filter action of the G4 would be below the minimum mass to charge which the mass spectrometer is capable of analyzing. As is, the roll off point (~300 *m/z*) is well within the range of most mass analyzers.

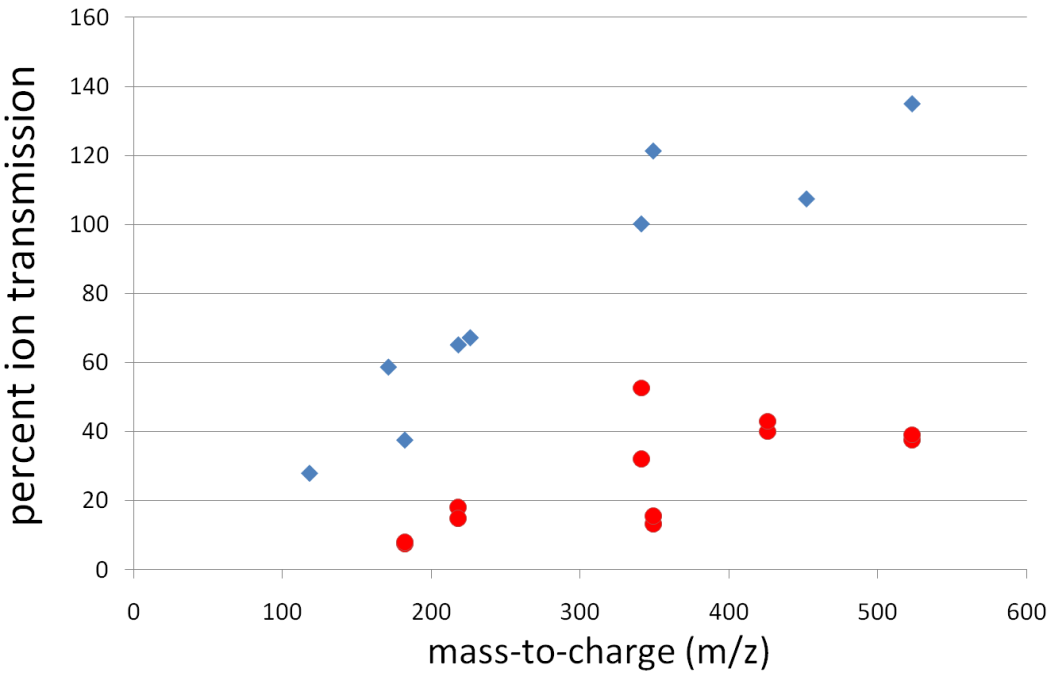

Figure 6.7 Percent ion transmission relative to the standard ESI transfer capillary for the G4.0 (blue diamonds) and G3.0 (red circles). Ion transmission for the G4 over the 100-600 m/z range is improved 2X compared to the G3.

6.3 Resolution

Due to the reduced length of the G4 compared to the G3 a decrease in resolution equal to approximately a factor of $\sqrt{t_{resG3} - t_{resG4}}$ was expected. Calculating residence time from pumping speed and the volume of the G3 and G4, the resolving power for the G4 would be approximately 66% of the G3. The G3 had shown resolving power of over 30 for several test compounds, and by extension the G4 should have been able to achieve a resolving power of approximately 20. Compared to the resolving power of 10-15 typical for cylindrical FAIMS devices[7-12], a resolving power of 20 seemed an acceptable trade-off for reduced size of the G4 device. As with most prototype designs the initial results where discouraging, resolving power for the 622 *m/z* component of Agilent ESI tune mix was 10 (figure 6.8), much lower than the initial expectation. Eventually the importance of careful electrode alignment, never

a serious issue in the G3 design, due to the additional length of the electrodes which placed screw holes farther apart and aided in alignment, became clear and resolution improved to within 66% of the G3.

6.3.1 Reduced resolution?

The resolving power of the G4 was evaluated using the Agilent ESI tune mix previously used to test the G3 device (figure 4.10). Updated asymmetric waveform electronics were installed to run the G4 which now operated at a frequency of 2.5 MHz, while the previous G3 had operated at 1.5 MHz. The increase in waveform frequency increases the calculated effective gap (equation 4.1) by reducing t_h. The method of generating CV scans had also been modified due to the change in instruments. Previous CV scans had been triggered off the gating of ions into the ion trap. The use of a Q-ToF mass

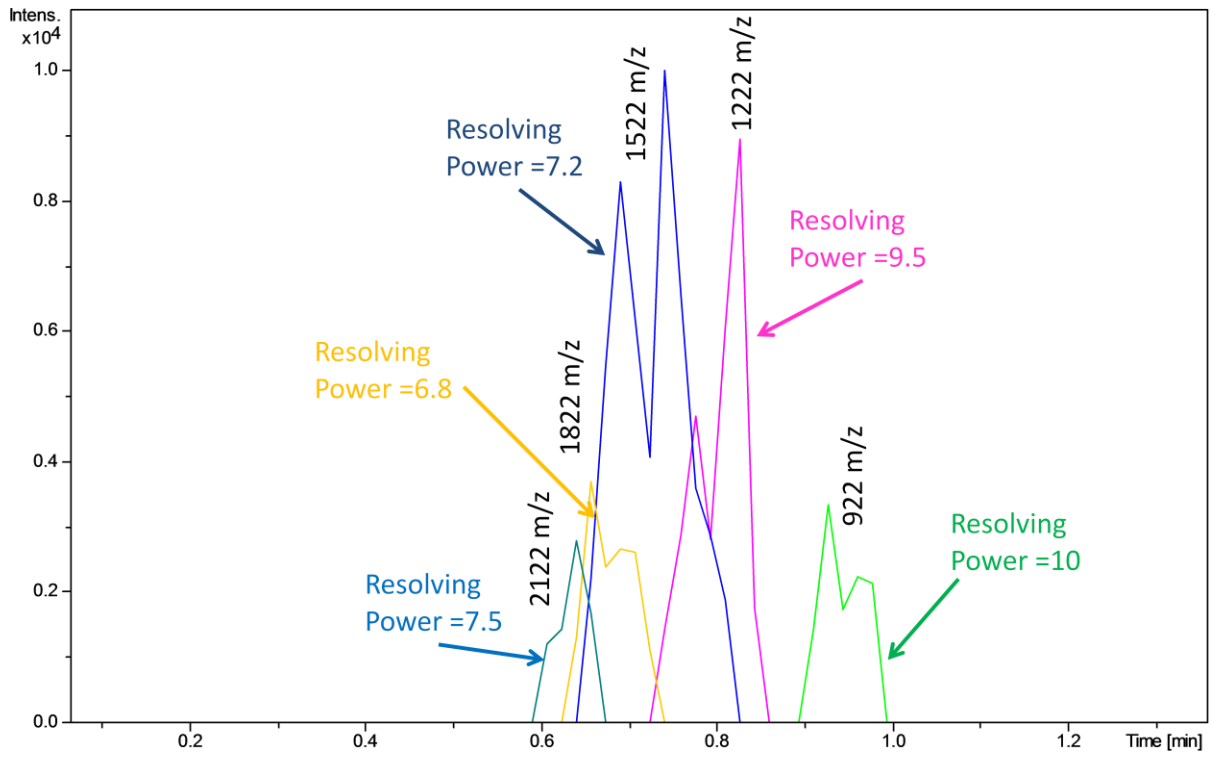

Figure 6.8 The first CV spectrum acquired by the G4.0. Dispersion voltage for the scan is 1.4 kV, CV scan rate is 12 V/min.

analyzer eliminated the previous trigger source and required the use of a fixed duration clock. The first spectra acquired (figure 6.8) shows poor resolving power with a maximum resolving power of 10 for 922 *m/z*. Attempts to improve the resolution by increasing the dispersion voltage meet with disastrous results as discharges within the FAIMS device damaged the interior vespel FAIMS holder. Disassembly and replacement of the vespel housing resulted in slightly improved performance. The G4 was disassembled, cleaned, and reinstalled to find that resolution was again slightly improved. Hypothesizing that the solution to resolution had been found the G4 was again disassembled and thoroughly cleaned. The device was then reassembled and reinstalled only to find that resolving power had decreased back to the level of figure 6.8.

It was determined that how the device was reassembled, not the cleaning of the electrodes, influenced separation performance. With every cleaning, gap alignment changed. Electrode gap alignment had been assured in the G3 by the long electrodes and the distance between screw holes. With the shorter G4 design locating of the electrodes can only be reliably accomplished with the use of a precision gauge inserted into the analytical gap. However, using a gauge of 0.3 mm +/- 0.001 mm, gaps vary as much as +/- 3%. While variation in analytical gap across the width of the device should always be minimized, a <5 % relative error in gap width across the gap has proven acceptable and provides spectra such as figure 6.9.

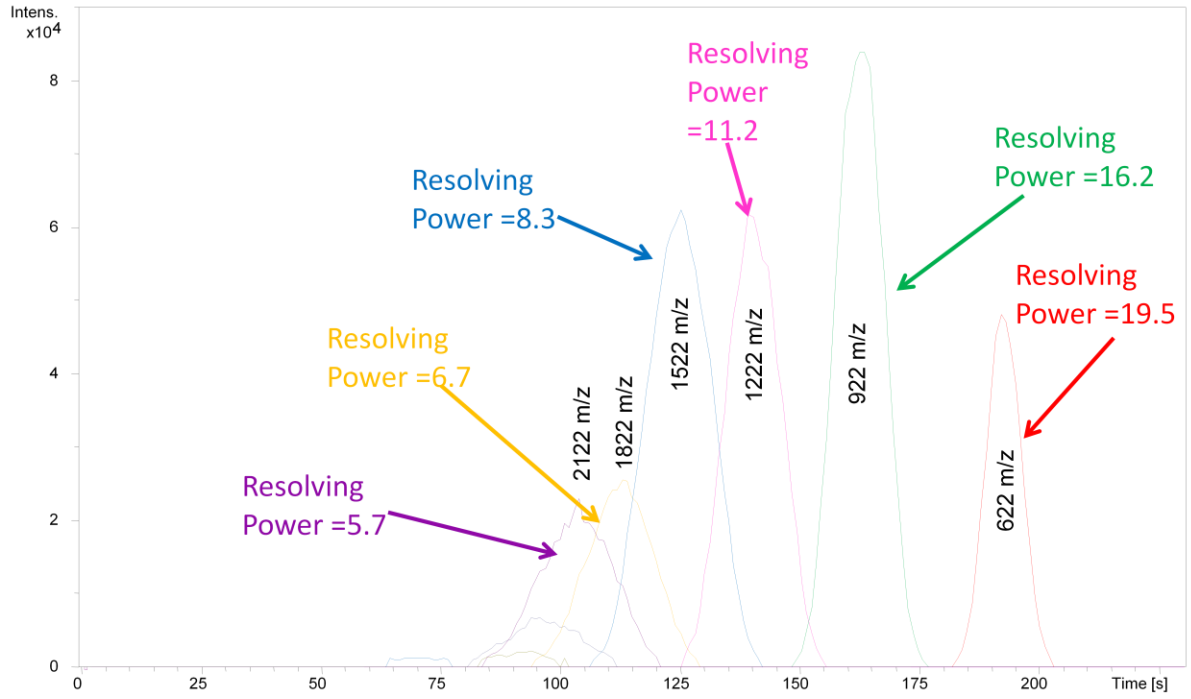

Figure 6.9 G4.0 CV spectra after careful alignment of electrodes. A resolving power of 19.5 matches well to the predicted resolution of the G4. Dispersion voltage is 1.8 kV, CV scan speed is 0.1 V/s.

6.3.2 Generation 4.1 (G4.1) design

With an increased understanding of how critical alignment is, and the difficulty of aligning the short half cylinder electrodes, design of a G4.1 with improved electrode alignment began (figure 6.10). The device could be assembled using a high precision jig and the alignment pins pressed in place. This design would not allow cleaning or disassembly of any kind. While a simple solution, permanent alignment through the use of press fit pins is not ideal because the ability to assemble and disassemble the device is necessary in a prototype device. In order to maintain the ability to assemble the G4.1 using screws, while improving alignment a new FAIMS outer housing was designed. The FAIMS electrodes are no longer cylindrical, but rectangular. Rectangular slots cut into ceramic electrode holders provide alignment regardless of the torque applied to mounting screws. The G4.1 also

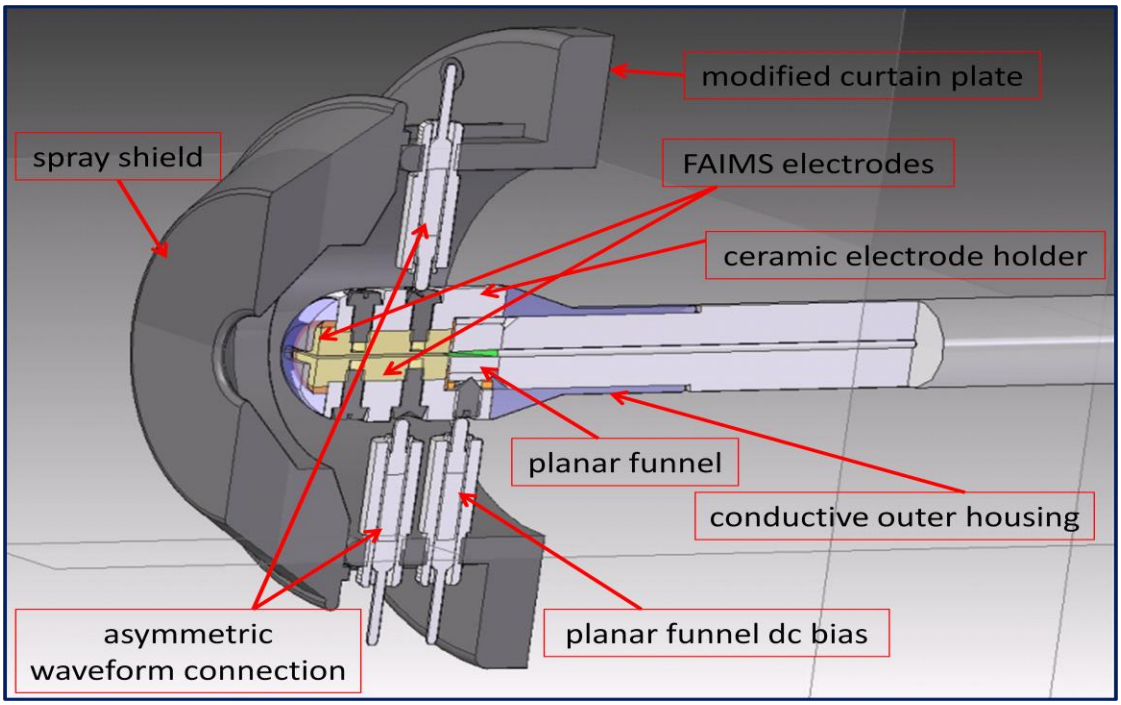

Figure 6.10 side on cutaway drawing of G4.1 with major components labeled. Dimensionally identical to the G4.0, the 4.1 has the addition of a planar funnel dc bias and machined ceramic holders for improved alignment of the FAIMS electrodes.

has improved electrical isolation between the planar funnel and the outer housing. Isolation of the planar funnel allows a potential gradient to be applied along the length of the device, which should improve ion transmission for lower mass-to-charge ratio ions. The components for G4.1 are in the process of being machined, and will not ready for installation until late October.

6.4 Applications

The G4 has been used to analyze a number of samples and demonstrates the ability to perform many of the same functions as the G3 such as filtering of complex mixtures to reduce spectra complexity and improving limits of detection. The G4 also is capable of separations of isobaric (same mass within the accuracy of the mass spectrometer but different composition) and isomeric (same composition differing structure) mixtures. These

applications highlight the complementary nature of FAIMS to mass spectrometry, as a high speed gas phase ion separation technique, and a tool for structural selection.

Mature technologies such as gas chromatography and liquid chromatography can in many cases perform separations of much higher resolution than FAIMS on identical samples. However, the G4 device provides three advantages over more mature separation techniques: 1) The G4 compared to bench top chromatography systems takes up no additional space, requires no additional setup, and uses no additional consumables. The design of the G4 device has no real cost to the user other than the initial purchase of the device and electronics. 2) Separations in the G4 occur on the order of milliseconds and full (from 0 to 40V CV) high resolution scans are acquired in less than ten minutes. 3) The G4 can produce CV scans similar to chromatograms, or isolate a single analyte in a static filtering mode. Once the conditions to transmit an analyte of interest have been determined the G4 has the ability to operate at 100% duty cycle when selecting for a single analyte.

In the following sections data is presented demonstrating the capabilities of the G4 device. Work to this point has been focused on optimization of the device design rather than the identification of unique applications in which to show the analytical strength of the G4, and these spectra are simple test systems. Dynamic range and resolution over a range of analytes for the G4 has yet to be fully evaluated, but from the preliminary data presented here the G4 should prove a higher performance analyzer than any currently commercially available FAIMS analyzer.

6.4.1 Atmospheric pressure ion filter

The most common application for FAIMS is high speed atmospheric pressure ion separation of complex multi component mixtures[8, 10, 12-15]. To demonstrate the ability of FAIMS to

rapidly separate complex mixtures, and improve the limits of detection for mass analyzers, a sample of 1 picomolar brain natriuretic peptide (BNP) in fetal bovine serum was analyzed. BNP is a hormone biomarker associated with heart failure. Concentrations in the human blood above 35 picomolar are considered to be a sign of heart failure[16]. Typically the analysis of BNP is carried out using LC-MS, which has detection limits of picomolar levels and moderate speed, the instruments performing this analysis are limited to about 50 samples per day[17]. Figure 6.11a shows the CV scan of the sample, the high intensity black solid line is the total ion signal, the red line of low intensity which peaks at a compensation voltage of 4.8 V is an extracted ion chromatogram for BNP+5. Comparison of the total ion intensity to that for BNP shows that 99.6% of the ion signal is of background ions while only 0.4% of ion signal is from BNP. In the absence of the FAIMS the signal for BNP is not observed (figure 6.11b), due to the elevated background, making BNP undetectable. With the selection of BNP by application of the optimal DV and CV the background signal is decreased to only 81% of the total spectrum while BNP represents 19% of total ion signal. The increase is BNP signal relative to back ground is even more impressive than the 40X increase in relative abundance might first indicate. Because the background signal is spread across all mass-to-charge ratios while the BNP is at one mass-to-charge ratio, the increase relative abundance leads to an increase in signal-to-noise ratio on the order of 500X with the G4 present compared to without FAIMS. The increase in BNP signal relative to background produces the mass spectrum seen in figure 6.11c, demonstrating clear detection of 1 picomolar BNP. The time required for this analysis, including sample preparation was less than 15 minutes.

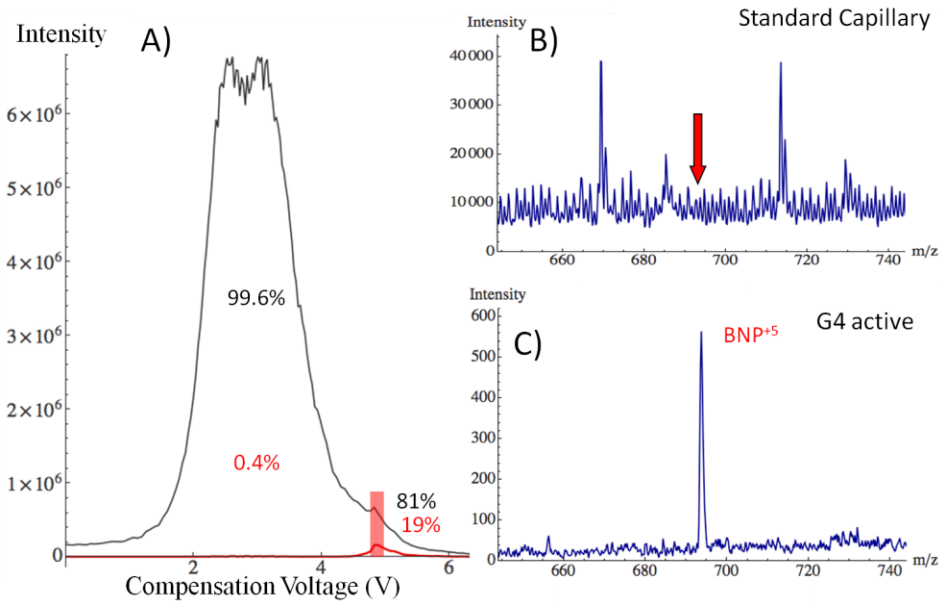

Figure 6.11 CV spectra for mixture of 1 picomolar BNP in fetal bovine serum sample at a DV of 1.09 kV A) Spectra of sample acquired using the standard ESI capillary with arrow marking the position of the +5 peak of BNP B) and a mass spectra taken at optimal CV for BNP C).

6.4.2 Separation of isobars

Isobars are compounds which have nominally identical mass but different composition. In some cases isobaric peaks can be separated with high resolving power mass analyzers but such high resolution instruments are expensive to own and operate[18]. Alternatively isobars can be detected in tandem mass spectrometry experiments due to unique fragmentation patterns for each isobar[19, 20], however this requires instruments which are capable of tandem mass analysis. FAIMS has the ability to separate isobars prior to mass analysis, allowing analysis of isobaric mixtures by low resolution instruments. Figure 6.12 shows a series of CV scans for the compounds mianserine (264.365 *m/z*) (figure 6.12a) tetracain (264.363 *m/z*) (figure 6.12b) and a mixture of the two compounds of approximately equal concentration (figure 6.12c&d). Although the two compounds are nearly identical in mass ($\Delta m = 0.002$ da), the center of the peaks differ in the G4 CV scan by three volts. In the case of the G4 a relatively modest resolving power of 10 is adequate to separate these two

peaks. In comparison to separate the peak of these two isobars in a single stage mass analyzer would require a resolving power of over 100,000.

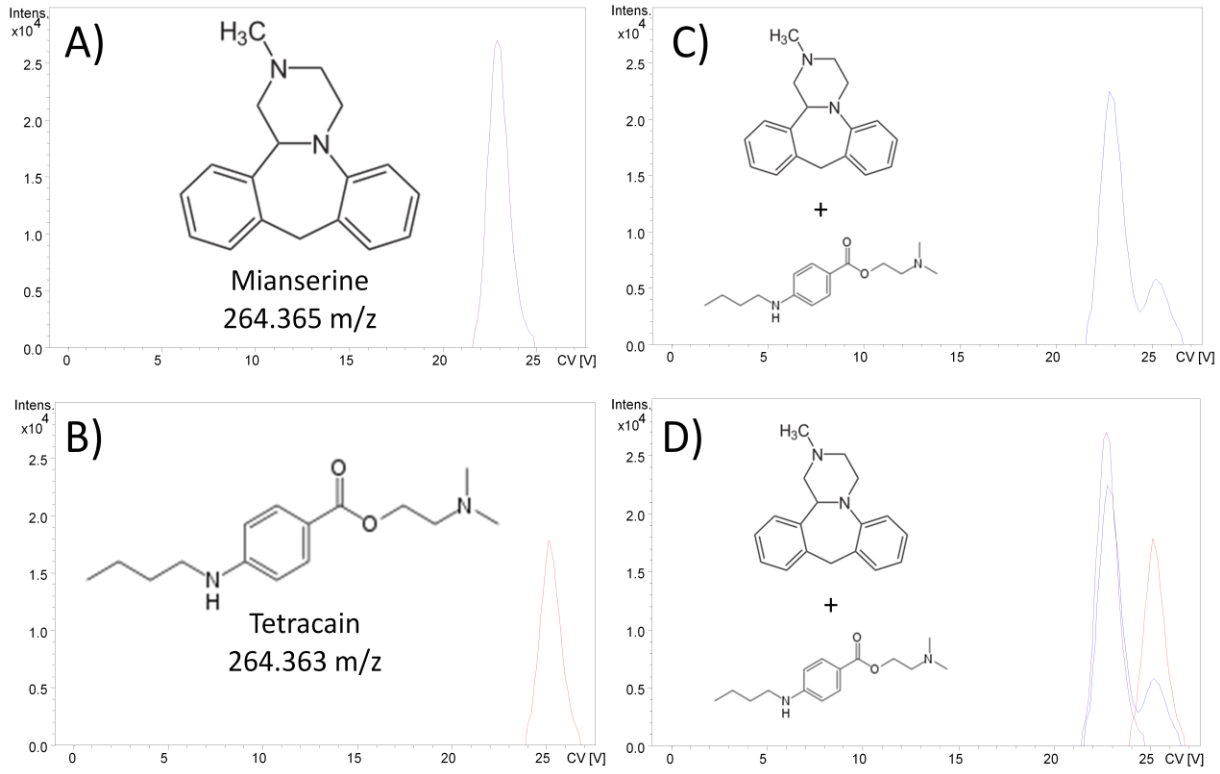

Figure 6.12 CV scans of a 2µM solution of mianserine A) 2µM tetracain B) and a mixture of 2µM mianserine and tetracain C&D. Plot C contains the CV scan of the mixture, while D contains the mixture with CV scans of the pure compounds overlaid for comparison. Separations where carried out at 1.8 kV DV, with 0.1 V/s scan rate.

6.4.3 Separation of protein conformations

Protein conformations have traditionally been analyzed through nuclear magnetic resonance[21-24] and x-ray crystallography[25]. However the speed and sensitivity of mass analysis has provided strong motivation to develop means of studying protein conformations in the gas phase[26]. Unfortunately the ability of mass spectrometers to isolate and interpret three dimensional structure is limited. Ion mobility spectrometry (IMS)[27, 28], and FAIMS[9] have provided tools for the isolation of structure prior to mass analysis.

The performance of the G4 in separation of protein conformations was evaluated by separation of the conformations for the +13, +12, and +11 charge states of bovine ubiquitin figure 6.13. Previous studies using IMS[29-34], H/D exchange[35], and FAIMS[36-38] have focused

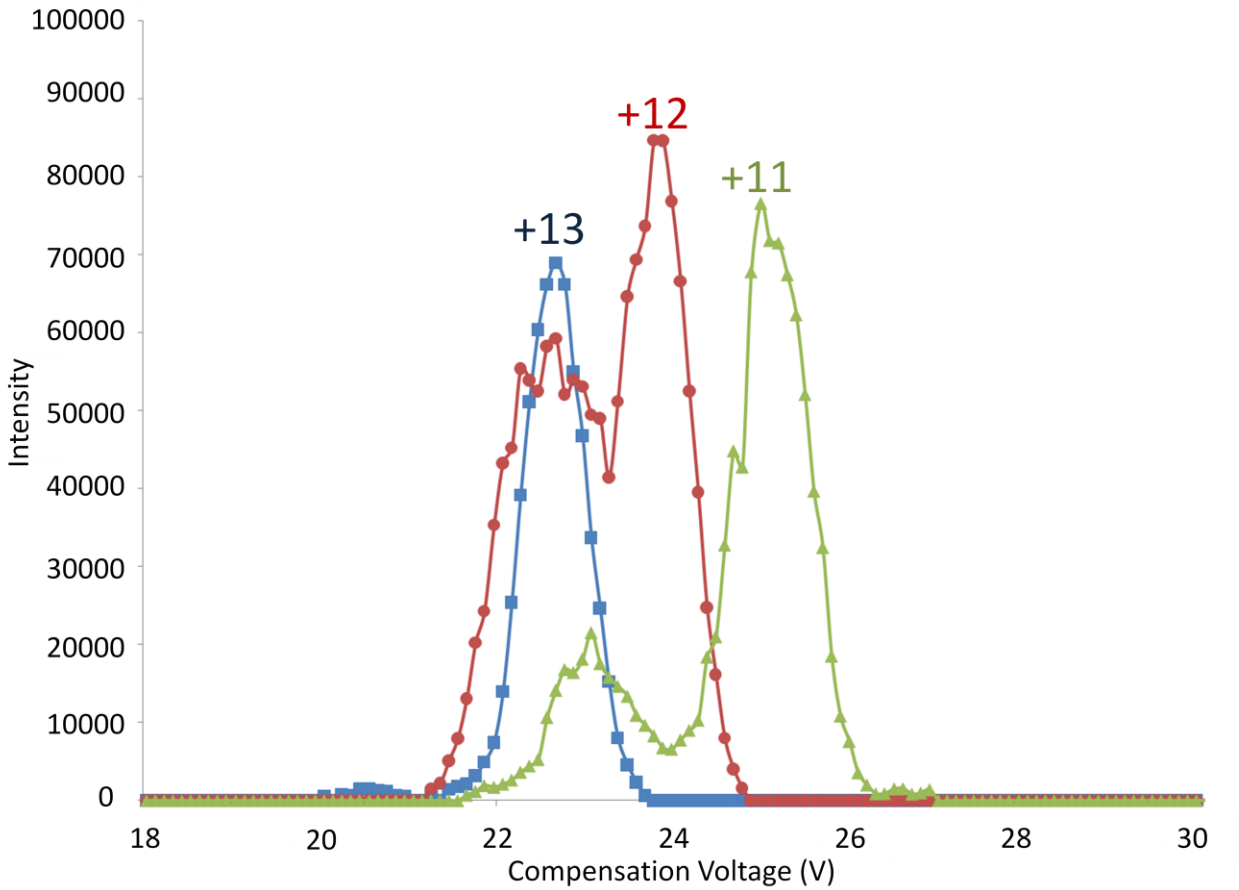

Figure 6.13 CV spectra for the +11 (780 m/z), +12 (715 m/z), +13 (660 m/z) charge state of ubiquitin. Of interest is the overlap of the maxima are for the +13 peak, with the lower CV component of the +12 and +11 indicating structural similarity, an observation supported by H/D exchange experiments[35].

on the elongated structures for these higher charge states due to the presence of multiple conformations for each charge state. Analysis of the +11 through +13 charge states of bovine ubiquitin are in excellent agreement with H/D exchange data[35]. In both cases two structures are clearly present for the +11 and +12 charge state. Also matching is that as charge state increases from +11 deuterium incorporation decreases, implying a structure which is less open. Similarly in the CV scans shown increasing charge states decrease in

CV, an atypical trait for proteins of increasing charge. These results indicate that the G4 can be used as a tool for the separation of protein conformations prior to further structural investigation.

6.5 Summary

The G4.0 device is the first successful in capillary FAIMS device constructed to date. The G4.0 device is capable of 100% ion transmission for ions above 300 *m/z* due to reduced length and an improved planar flare between the FAIMS electrodes and ESI transfer capillary. Resolving power of ~20 is achievable with the G4 device, with CV scan rates on the order of 0.1 V/s. The G4.0 device has shown value in improving limits of detection through eliminating background noise, the separation of isobaric compounds, and the separation of conformations for gas phase protein ions. Future development of the G4.0 is aimed at further reductions in dead volume to improve the useful mass range of the device, and to improve resolution through improved control of electrode alignment.

6.6 References

1. Page, J. S.; Marginean, I.; Baker, E. S.; Kelly, R. T.; Tang, K. Q.; Smith, R. D., Biases in Ion Transmission Through an Electrospray Ionization-Mass Spectrometry Capillary Inlet. *Journal of the American Society for Mass Spectrometry* **2009,** 20, (12), 2265-2272.

2. Valentine, S. J.; Counterman, A. E.; Clemmer, D. E., A Database of 660 Peptide Ion Cross Sections: Use of Intrinsic Size Parameters for Bona Fide Predictions of Cross Sections. *Journal of the American Society for Mass Spectrometry* **1999,** 10, 1188-1211.

3. March, R. E.; Todd, J. F. J., *Quadrupole Ion Trap Mass Spectrometry*. 2nd ed.; John Wiley & Sons, Inc.: Hoboken, NJ, 2005; Vol. 165, p 346.

4. Tolmachev, A. V.; Udseth, H. R.; Smith, R. D., Radial stratification of ions as a function of mass to charge ratio in collisional cooling radio frequency multipoles used as ion guides or ion traps. *Rapid Communications in Mass Spectrometry* **2000,** 14, (20), 1907-1913.

5. Fischer, E., Die dreidimensionale Stabilisierung von Landungsträgern in einem Vierpolfeld. *Z. Phys.* **1959,** 156, 1-26.

6. Belov, M. E.; Rakov, V. S.; Nikolaev, E. N.; Goshe, M. B.; Anderson, G. A.; Smith, R. D., Initial implementation, of external accumulation liquid chromatography/electrospray ionization Fourier transform ion cyclotron resonance with automated gain control. *Rapid Communications in Mass Spectrometry* **2003,** 17, (7), 627-636.

7. Barnett, D. A.; Belford, M.; Dunyach, J. J.; Purves, R. W., Characterization of a Temperature-Controlled FAIMS System. *J Am Soc Mass Spectrom* **2007,** 18, 1653-1663.

8. Barnett, D. A.; Ells, B.; Guevremont, R.; Purves, R. W., Application of ESI-FAIMS-MS to the analysis of tryptic peptides. *Journal of the American Society for Mass Spectrometry* **2002,** 13, (11), 1282-1291.

9. Guevremont, R., High-field asymmetric waveform ion mobility spectrometry: A new tool for mass spectrometry. *Journal of Chromatography A* **2004,** 1058, (1-2), 3-19.

10. Guevremont, R.; Barnett, D. A.; Purves, R. W.; Vandermey, J., Analysis of a tryptic digest of pig hemoglobin using ESI-FAIMS-MS. *Analytical Chemistry* **2000,** 72, (19), 4577-4584.

11. Shvartsburg, A. A., *Differential ion mobility spectrometry : nonlinear ion transport and fundamentals of FAIMS*. CRC Press: Boca Raton, 2009.

12. Tang, K. Q.; Li, F. M.; Shvartsburg, A. A.; Strittmatter, E. F.; Smith, R. D., Two-dimensional gas-phase separations coupled to mass Spectrometry for analysis of complex mixtures. *Analytical Chemistry* **2005,** 77, (19), 6381-6388.

13. Guevremont, R.; Purves, R. W., High field asymmetric waveform ion mobility spectrometry-mass spectrometry: An investigation of leucine enkephalin ions produced by electrospray ionization. *Journal of the American Society for Mass Spectrometry* **1999,** 10, (6), 492-501.

14. Cui, M.; Ding, L. Y.; Mester, Z., Separation of cisplatin and its hydrolysis products using electrospray ionization high-field asymmetric waveform ion mobility spectrometry coupled with ion trap mass spectrometry. *Analytical Chemistry* **2003,** 75, (21), 5847-5853.

15. Venne, K. B., Eric; Eng, Kevin; Thibault, P., Improvement in Peptide Detection for Proteomics Analyses Using Nano LC-MS and High-Field Asymmetry Waveform Ion Mobility Mass Spectrometry. *Analytical Chemistry* **2005,** 77, (7), 2176-2186.

16. Bolger, A. P.; Sharma, R.; Li, W.; Leenarts, M.; Kalra, P. R.; Kemp, M.; Coats, A. J. S.; Anker, S. D.; Gatzoulis, M. A., Neurohormonal activation and the chronic heart failure syndrome in adults with congenital heart disease. *Circulation* **2002,** 106, (1), 92-99.

17. Vatansever, B.; Lahrichi, S. L.; Thiocone, A.; Salluce, N.; Mathieu, M.; Grouzmann, E.; Rochat, B., Comparison between a linear ion trap and a triple quadruple MS in the sensitive detection of large peptides at femtomole amounts on column. *Journal of Separation Science* 33, (16), 2478-2488.

18. He, F.; Hendrickson, C. L.; Marshall, A. G., Baseline mass resolution of peptide isobars: A record for molecular mass resolution. *Analytical Chemistry* **2001,** 73, (3), 647-650.

19. Prazeller, P.; Palmer, P.; Boscaini, E.; Jobson, T.; Alexander, M., Proton Transfer Reaction Ion Trap Mass Spectrometer. *Rapid Communications in Mass Spectrometry* **2003,** 17, 1593-1599.

20. Jublot, L.; Linforth, R. S. T.; Taylor, A. J., Direct Atmospheric Pressure Chemical Ionization Ion Trap Mass Spectrometry for Aroma Analysis: Speed, Sensitivity and Resolution of Isobaric Compounds. *International Journal of Mass Spectrometry* **2005,** 243, 269-277.

21. Wand, A. J.; Roder, H.; Englander, S. W., Two-Dimensional Proton NMR Studies of Cytochrome c: Hydrogen Exchange in the N-Terminal Helix. *Biochemistry* **1986,** 25, (5), 1107-1114.

22. Moy, F. J.; Haraki, K.; Mobilio, D.; Walker, G.; Powers, R.; Tabei, K.; Tong, H.; Siegel, M. M., MS/NMR: A Structure-Based Approach for Discovering Protein Ligands and for Drug Design by Coupling Size Exclusion Chromatography, Mass Spectrometry, and Nuclear Magnetic Resonance Spectroscopy. *Analytical Chemistry* **2001,** 73, 571-581.

23. Takeuchi, K.; Ng, E.; Malia, T. J.; Wagner, G., 1-13C amino acid selective labeling in a 2H15N background for NMR studies of large proteins. *Journal of Biomolecular NMR* **2007,** 38, (1), 89-98.

24. Brunner, K.; Gronwald, W.; Trenner, J. M.; Neidig, K.-P.; Kalbitzer, H. R., A general method for the unbiased improvement of solution NMR structures by the use of related x-ray data, the AUREMOL-ISIC algorithm. *BMC Structural Biology* **2006,** 6, No pp. given.

25. Kendrew, J. C.; Dickerson, R. E.; Strandberg, B. E.; Hart, R. G.; Davies, D. R.; Phillips, D. C.; Shore, V. C., Structure of Myoglobin - 3-Dimensional Fourier Synthesis at 2 a Resolution. *Nature* **1960,** 185, (4711), 422-427.

26. Bakhtiar, R.; Tse, F. L. S., Biological mass spectrometry: a primer. *Mutagenesis* **2000,** 15, (5), 415-430.

27. von Helden, G.; Wyttenbach, T.; Bowers, M. T., Conformation of Macromolecules in the Gas Phase: Use of Matrix-Assisted Laser Desorption Methods in Ion Chromatography. *Science* **1995,** 267, (5203), 1483-1485.

28. Wyttenbach, T.; Helden, G. v.; Bowers, M. T., Gas-Phase Conformation of Biological Molecules: Bradykinin. *Journal of the American Chemical Society* **1996,** 118, 8355-8364.

29. Valentine, S. J.; Counterman, A. E.; Clemmer, D. E., Conformer-Dependent Proton-Transfer Reactions of Ubiquitin Ions. *Journal of the American Society for Mass Spectrometry* **1997,** 8, 954-961.

30. Li, J.; Taraszka, J. A.; Counterman, A. E.; Clemmer, D. E., Influence of solvent composition and capillary temperature on the conformations of electrosprayed ions: unfolding of compact ubiquitin conformers from pseudonative and denatured solutions. *International Journal of Mass Spectrometry* **1999,** 185/186/187, 37-47.

31. Myung, S.; Badman, E.; Lee, Y.; Clemmer, D., Structural transitions of electrosprayed ubiquitin ions stored in an ion trap over similar to 10 ms to 30 s. *Journal of Physical Chemistry A* **2002,** 106, 9976-9982.

32. Badman, E. R.; Hoaglund-Hyzer, C. S.; Clemmer, D. E., Dissociation of Different Conformations of Ubiquitin Ions. *J Am Soc Mass Spectrom* **2002,** 13, (6), 719 - 723.

33. Koeniger, S. L.; Clemmer, D. E., Resolution and Structural Transitions of Elongated States of Ubiquitin. *Journal of the American Society for Mass Spectrometry* **2007,** 18, 322-331.

34. Koeniger, S. L.; Merenbloom, S. I.; Clemmer, D. E., Evidence for Many Resolvable Structures within Conformation Types of Electrosprayed Ubiquitin Ions. *Journal of Physical Chemistry B* **2006,** 110, 7017-7021.

35. Freitas, M. A.; Hendrickson, C. L.; Emmett, M. R.; Marshall, A. G., Gas-phase bovine ubiquitin cation conformations resolved by gas-phase hydrogen/deuterium exchange rate and extent. *International Journal of Mass Spectrometry* **1999,** 185/186/187, 565-575.

36. Purves, R. W.; Barnett, D. A.; Ells, B.; Guevremont, R., Elongated Conformers of Charge States +11 to +15 of Bovine Ubiquitin Studied Using ESI-FAIMS-MS. *Journal of the American Society for Mass Spectrometry* **2001,** 12, 894-901.

37. Shvartsburg, A. A.; Li, F. M.; Tang, K. Q.; Smith, R. D., High-resolution field asymmetric waveform ion mobility spectrometry using new planar geometry analyzers. *Analytical Chemistry* **2006,** 78, (11), 3706-3714.

38. Purves, R. W.; Ells, B.; Barnett, D. A.; Guevremont, R., Combining H-D exchange and ESI-FAIMS-MS for detecting gas-phase conformers of equine cytochrome c. *Canadian Journal of Chemistry-Revue Canadienne De Chimie* **2005,** 83, (11), 1961-1968.

Chapter 7
Summary and Future Directions

7.1 General Summary

The previous chapters have described the development of a complete high field asymmetric ion mobility system from design and construction of the power supply used to produce high amplitude asymmetric waveforms (**Chapter 2**) to the latest planar FAIMS device which can be installed on any mass analyzer using an ion transfer capillary (**Chapter 6**). Results from the third generation (G3) (**Chapter 4**) FAIMS device show performance equal to or exceeding any FAIMS device published to date when operating with a 100% nitrogen carrier gas composition. Results presented in **Chapter 6** show potential applications for the fourth generation (G4) FAIMS device, including improving limits of detection for ions in complex matrixes, and the separation of isobaric and isomeric compounds. This chapter is intended to summarize the results from each of the preceding chapters and suggest directions for future work.

7.2 FAIMS waveform generators

A power supply was designed and developed in the UNC Department of Chemistry for the production of high amplitude asymmetric waveforms through the sum of sinusoidal waves (**Chapter 2**). This power supply differs from all other asymmetric waveform supplies currently used with FAIMS due to the use of two separate tunable LC resonant circuits to produce sinusoidal waves, which can then be summed across the analytical gap of a FAIMS device to produce the desired asymmetric waveform. There are several advantages

to this design, such as the capability to produce high amplitude asymmetric waveforms (dispersion voltage may exceed 8 kV as compared to the 5 kV max for most other designs), increased flexibility via the ability to tune the LC resonant circuits independently, low power consumption, and low cost of construction. The UNC-developed waveform supply has shown < 2% RSD drift over days of operations without retuning. It has also proven to be versatile enough to power four different FAIMS analyzer designs over a range of frequencies from 750 kHz to 2.5 MHz. All FAIMS separations presented in this dissertation have been achieved using this asymmetric waveform power supply design.

Work continues on the development of these power supplies through the collaboration between the Glish lab and Bruker Daltonics. New versions of the high amplitude asymmetric waveform power supply incorporate computer controlled amplitude and phase, the combination of electrospray ionization potential with the asymmetric waveform, and modifications to allow low voltage waveform monitoring. The result is a more user-friendly supply that retains the major features of the original design. Future development of this supply will need to focus on built in auto tune and feedback control of the waveform, as the current design requires some knowledge of how to build the asymmetric waveform from properly scaled and phased sinusoidal waves.

7.3 Modifications to conventional planar FAIMS devices and the use of carrier gas blends

Chapter 3 focused on the use of the UNC-developed high amplitude asymmetric waveform generator to power a FAIMS analyzer designed by the Pacific Northwest National Labs (PNNL). The PNNL-designed FAIMS device demonstrated the ability to separate conformations of proteins in single charge states, but proved to lack sensitivity and was frustrating to use due to an inability to transmit ions in a "passive mode". Modifications to

the PNNL device to improve ion transmission resulted in a 2X improvement in ion signal. Further attempts to improve resolution by cooling the PNNL FAIMS device proved more difficult, and the lowest temperature achieved was 0 °C. Reducing the temperature in the PNNL FAIMS device by 20°C led to a shift in the population of conformations present in the +6 charge state of ubiquitin, favoring ion structures which transmitted at higher compensation voltage. However, overall resolution did not improve, and temperatures will need to be significantly reduced to shift the entire population of ions in the +6 charge state to a single ion structure.

In addition to cooling FAIMS devices, the compensation voltage at which an ion is transmitted at may be changed through the use of different carrier gas compositions. The use of argon, carbon dioxide, and helium in various mixtures with nitrogen was investigated in using the G3 analyzer in **Chapter 5**. Argon and carbon dioxide showed only slight increases in compensation voltage when used in low percentage blends. Addition of helium lead to increases in compensation voltage and corresponding improvement in resolving power for the compounds tested in all blends evaluated. However, high percentage blends of helium with nitrogen result in increased diffusion losses for low mass-to-charge ratio ions. To maximize sensitivity and resolution a method of scanning gas composition in conjunction with compensation voltage is proposed. This would not only reduce ion losses for low mass-to-charge ratio ions, but also allow improved use of the compensation voltage range, and provide enhanced resolving power.

7.4 Development of planar FAIMS devices for high ion transmission, resolution, and speed

Four generations of planar FAIMS devices were designed and developed through the collaboration between the Glish Lab and Bruker Daltonics. While the first two generations,

designed to replace the electrospray transfer capillary, proved unsuccessful the G3 (**Chapter 4**) and G4 (**Chapter 6**) have shown the ability to perform a number of applications with ion transmission, resolution, and speed of analysis matching or exceeding all commercially available FAIMS designs. Most FAIMS analyzers designs to date have sought to increase resolution at the cost of analysis speed. Increasing residence time of ions in the FAIMS device also increases losses due to diffusion. In contrast the G3 and G4 designs have improved resolution through the use of reduced analytical gap dimensions (0.3 mm for both the G3 and G4) which allow increased electric fields relative to larger devices due to Paschen's Law (**Chapter 4**). Higher electric fields provide a means of improving resolving power, while decreasing residence time, analysis speed, and ion losses due to diffusion.

FAIMS designs continue to evolve. Generation 4.1 (G4.1 **Chapter 6**) will include the ability to create low amplitude axial electric fields to change the residence time of ions in the FAIMS device. Future electrodes may be made of resistive material to allow potential gradients along the length or width of the analytical gap to improve ion focusing. In addition the analysis speed of the current generation will be retained, allowing for future applications in which FAIMS devices are placed between chromatography and mass spectrometry to provide an added dimension of separation.

7.5 Future direction

This dissertation has focused on the development of FAIMS instrumentation for high-speed gas phase separations and the study of biological molecular ion structure. A few simple examples demonstrate the usefulness of FAIMS-based ion selection coupled to mass spectrometry, but the work described here only begins to demonstrate the versatility and unique capabilities of this technique. Further, an interesting challenge is to develop

experiments that can improve the understanding of the fundamentals of FAIMS, as there is a lack of theoretical tools that model and predict ion behavior in FAIMS systems. Hopefully the instruments developed during the course of this work will prove useful tools in the future research of the Glish Lab.

Appendix

In this section I will just paste the front panel to the CV scan VI, provide the schematics for triggering the CV scan, and include the mechanical drawings for FAIMS analyzers.

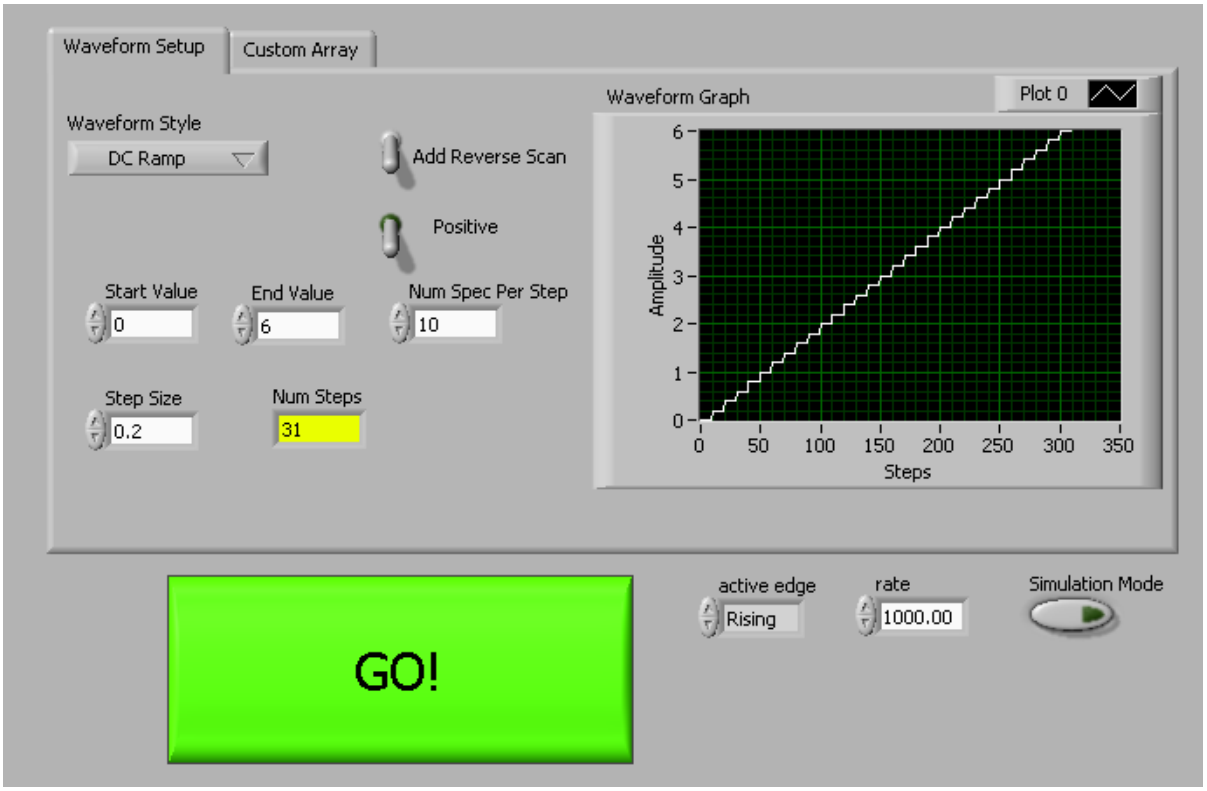

This is the front panel of the CV scan software. Start value is the initial CV value, end is the last CV, number of spec per step is the number of scans you average in the Esquire acquisition software. Add reverse scan scans the CV back to the start value after reaching the end value.

CV Trigger Interface for Esquire 3000

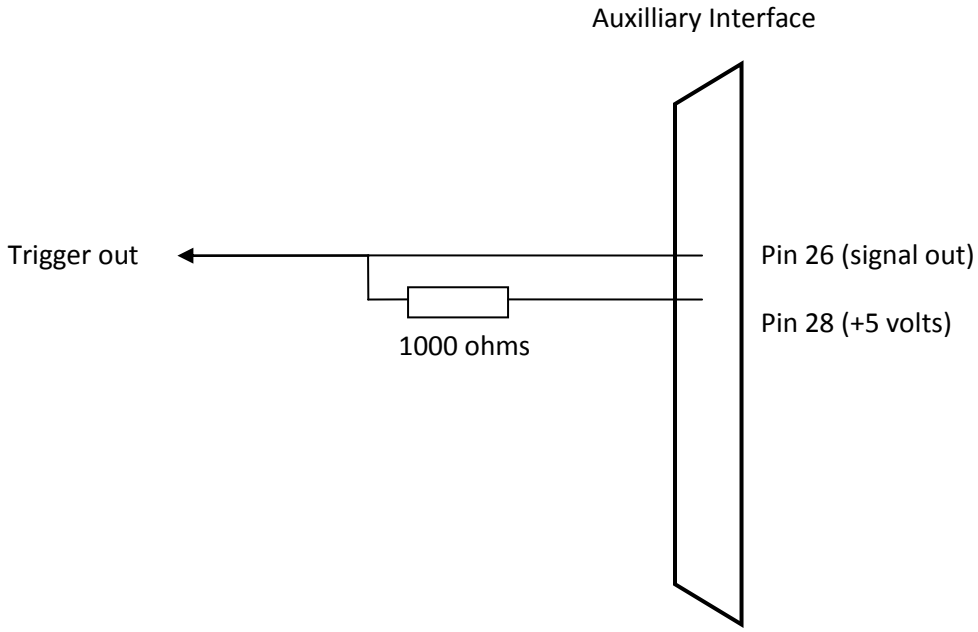

Desciption: Pin 26 is connected to an open collector.

The states can only be: ground or open.

To get a TTL signal a pull-up resistor is needed (1000 ohms)

The trigger out goes to the NI 6211 card and serves as the trigger for changes in CV to control the timing of this trigger.

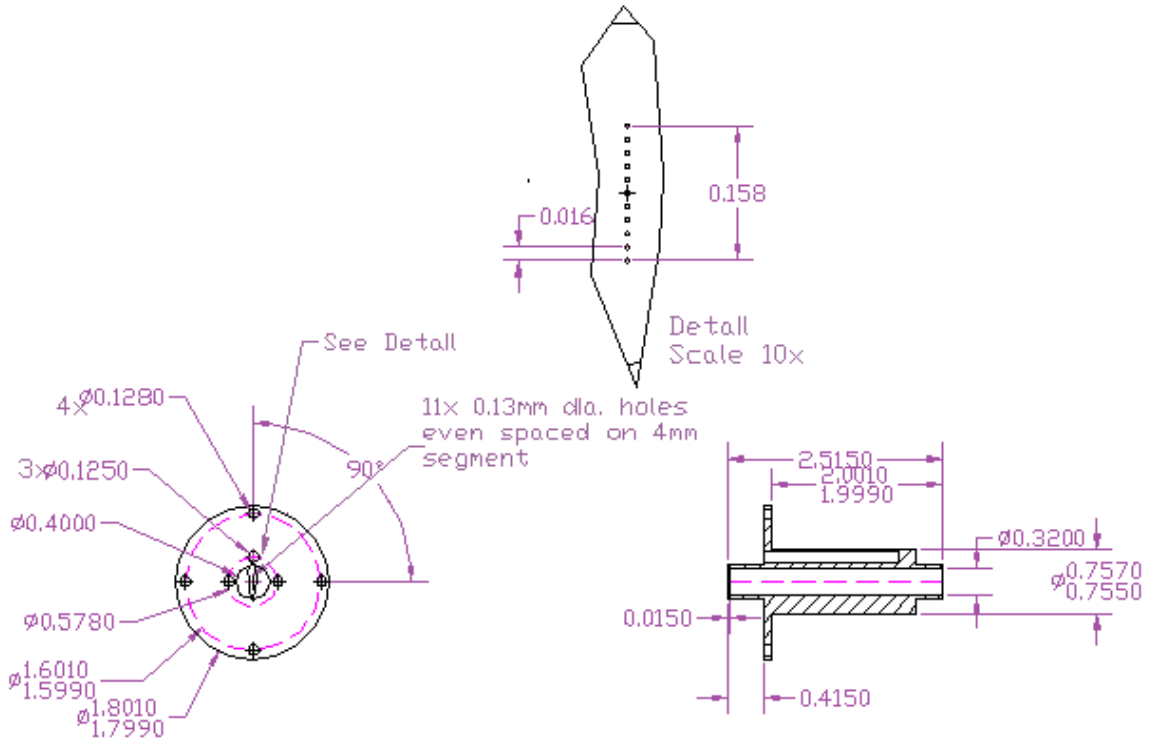

Conductance limit apertures for PNNL FAIMS

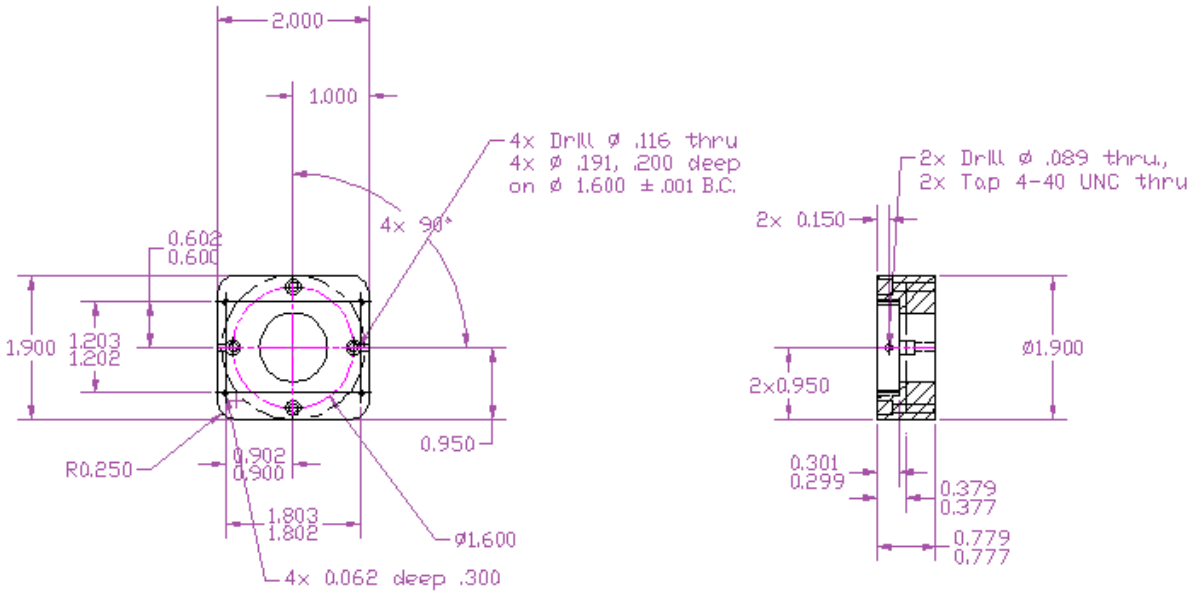

Holder which mounted to mass analyzer source and PNNL FAIMS press fit into, this design lacks any vacuum tight seals

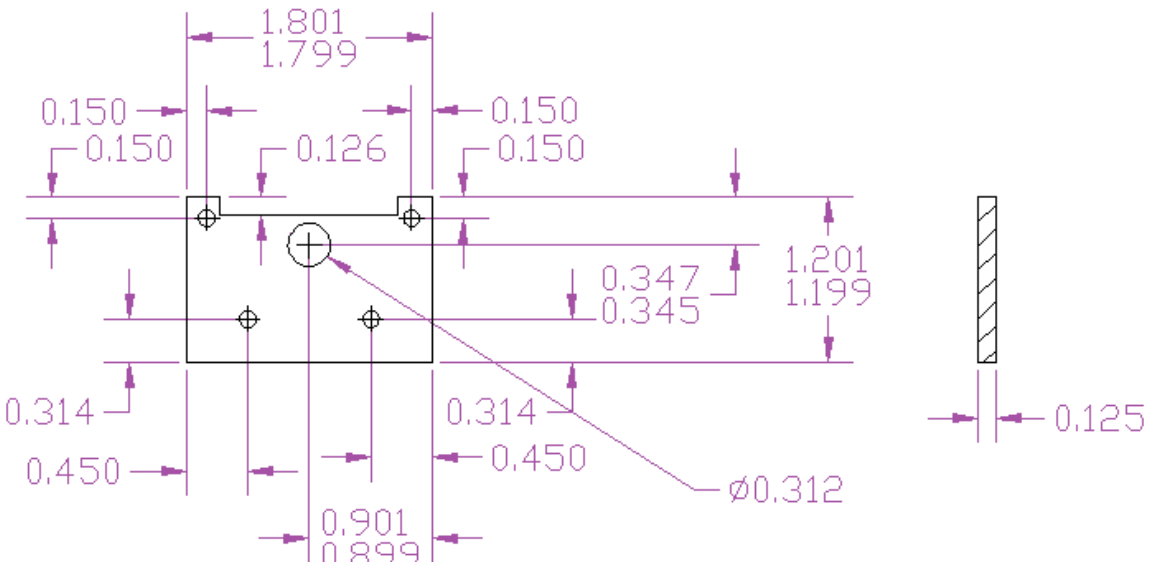

Rear cover plate for PNNL FAIMS, again no seals

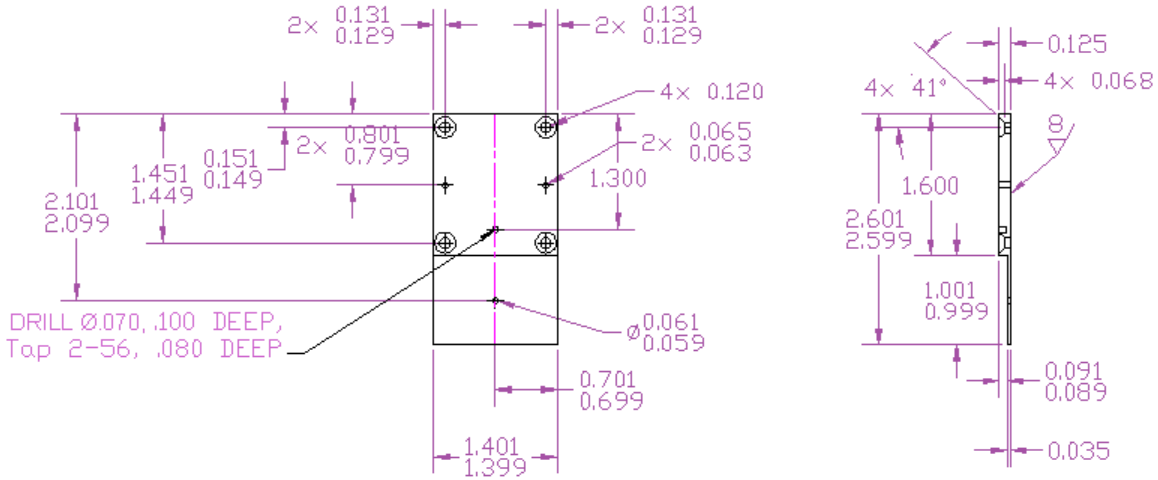

FAIMS electrode on the ion source side of the PNNL analyzer

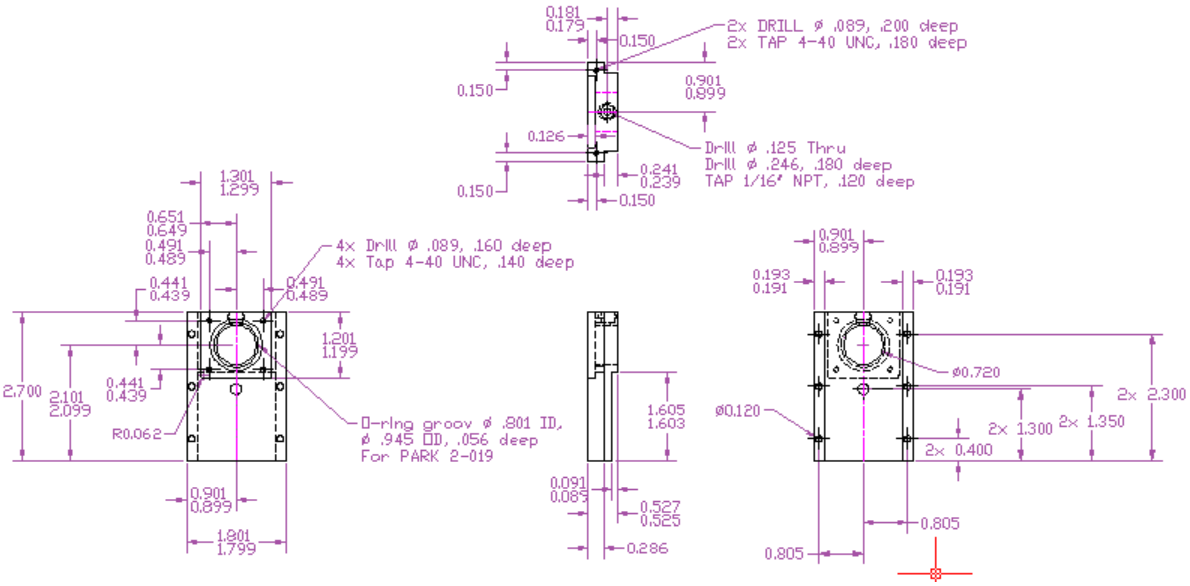

PEEK outer housing for the ESI source side of the PNNL analyzer

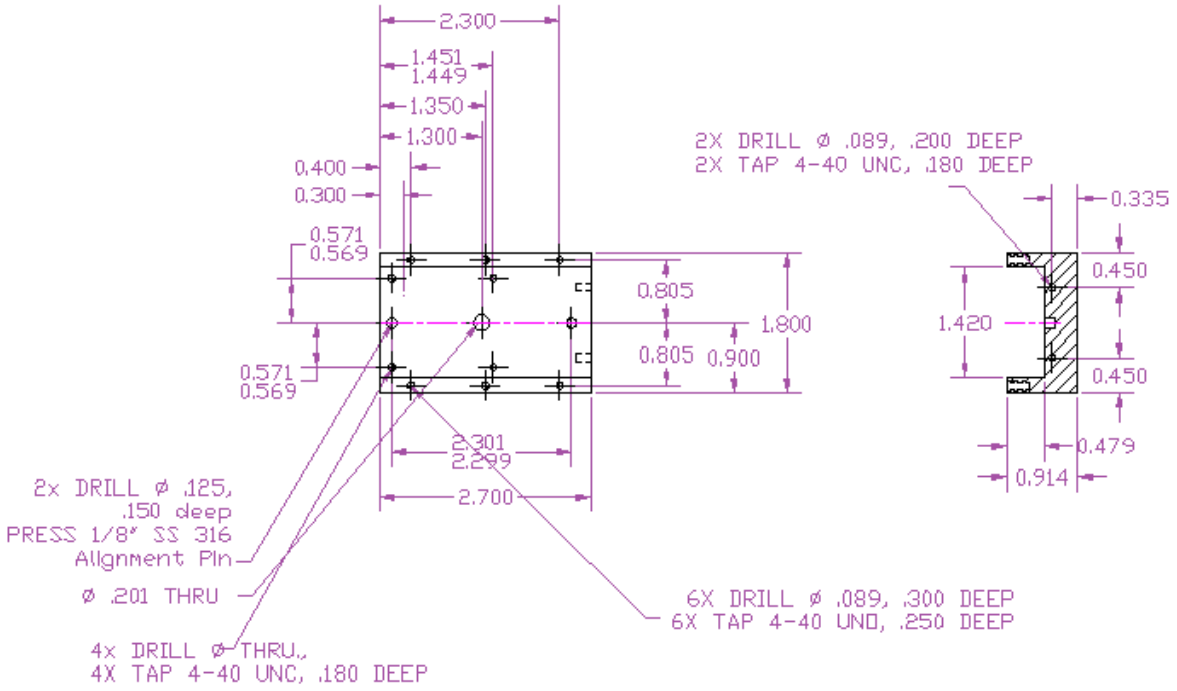

PEEK holder for side of PNNL FAIMS opposite the ion source

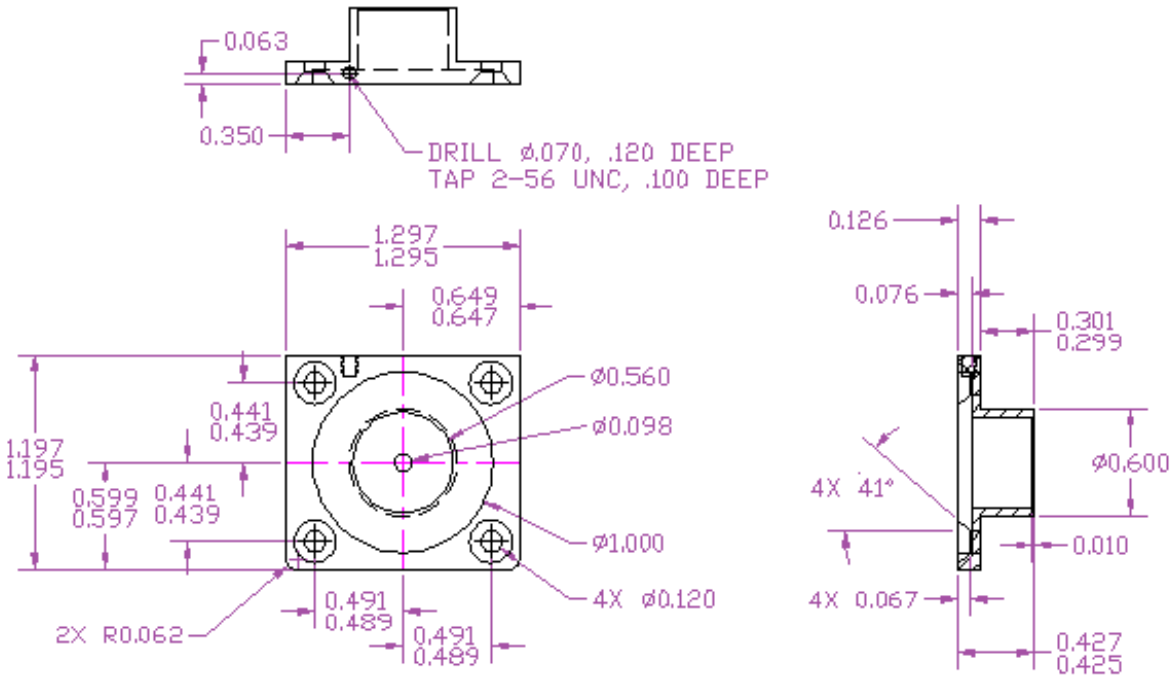

ESI source curtain plate for PNNL FAIMS analyzer

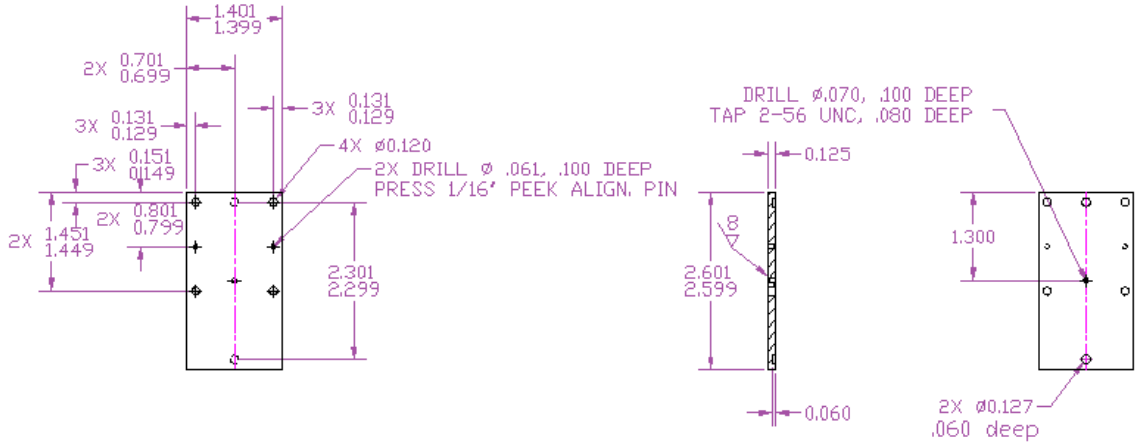

FAIMS Electrode opposite ESI source in PNNL analyzer

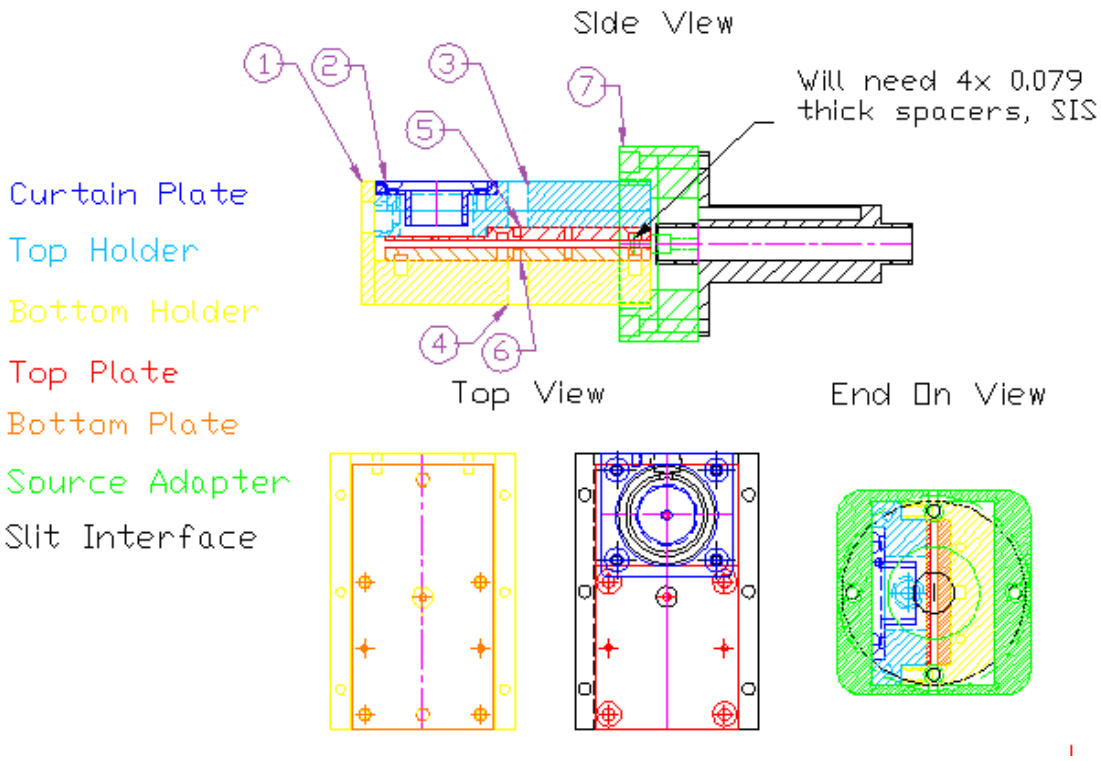

The PNNL FAIMS assemble prior to modification with collinear ion source or peliter cooling

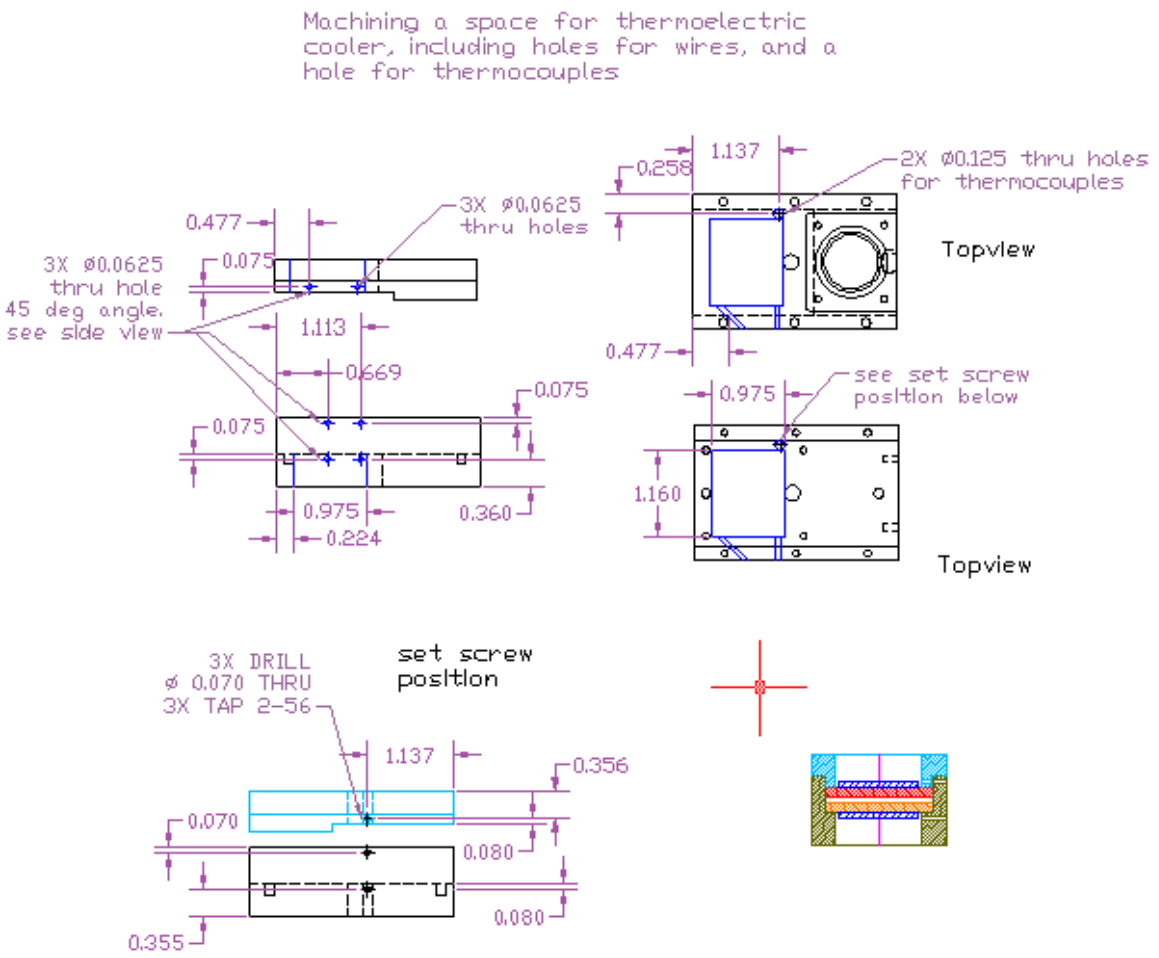

Modification to outer housing of PNNL designed FAIMS to allow installation of Peltier thermoelectric coolers

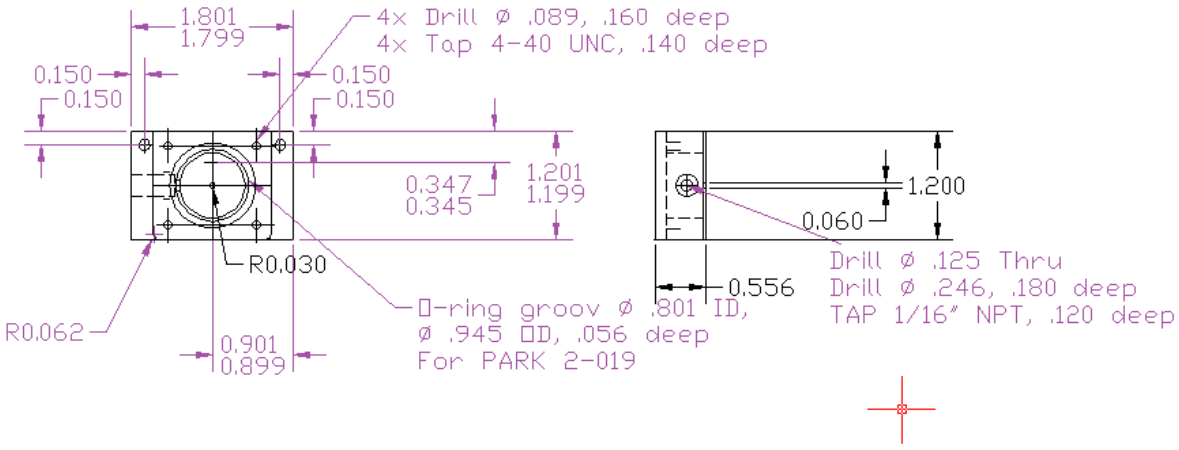

Colinear ESI curtain plate holder for PNNL FAIMS analyzer

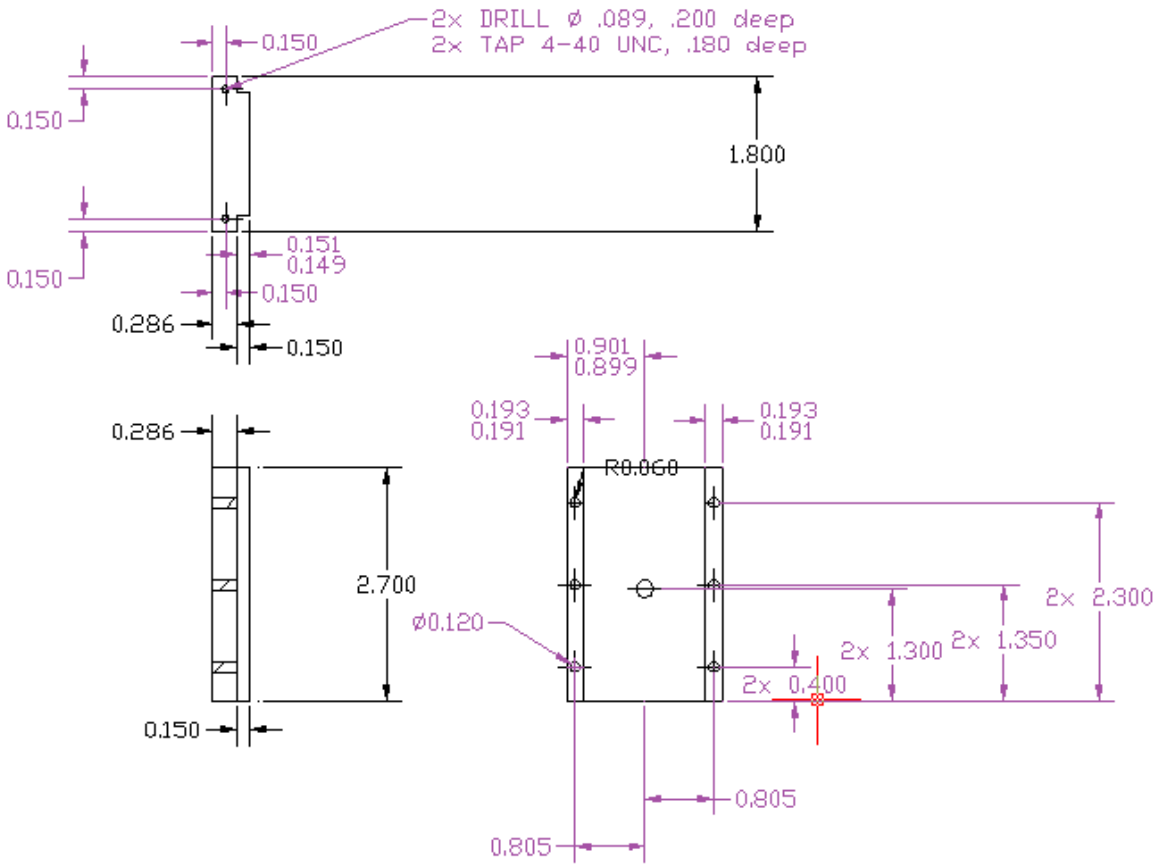

Modification to the PNNL FAIMS outer housing on the side which previous held the ESI source, to eliminate the source and attempt to improve gas tight sealing

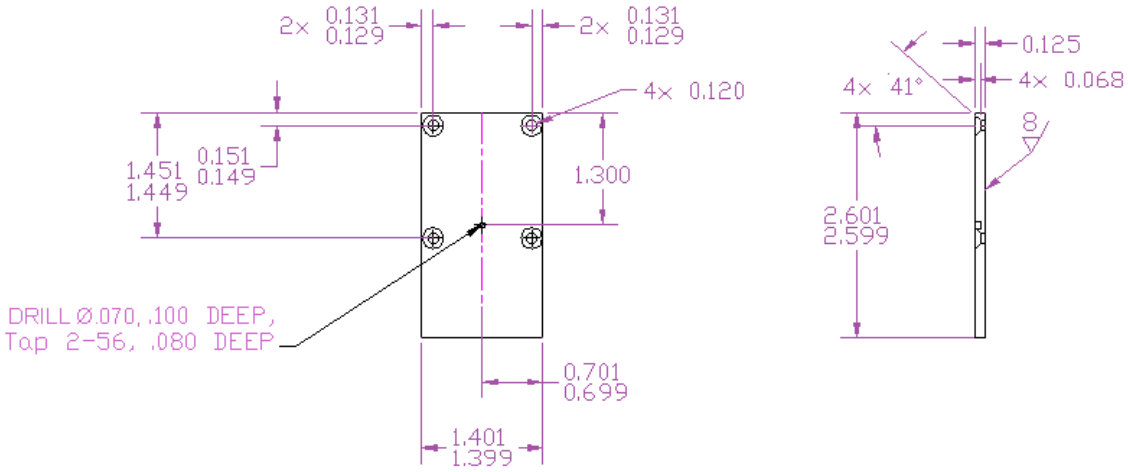

Replacement electrode for the ESI side of the PNNL FAIMS to eliminate the hole previously used for orthogonal ion injection

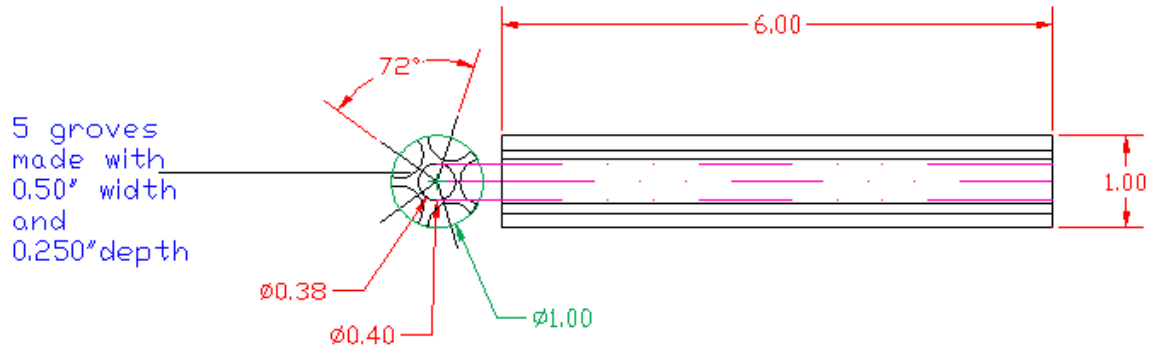

Heatsink for transformers used in the UNC high amplitude asymmetric waveform power supply

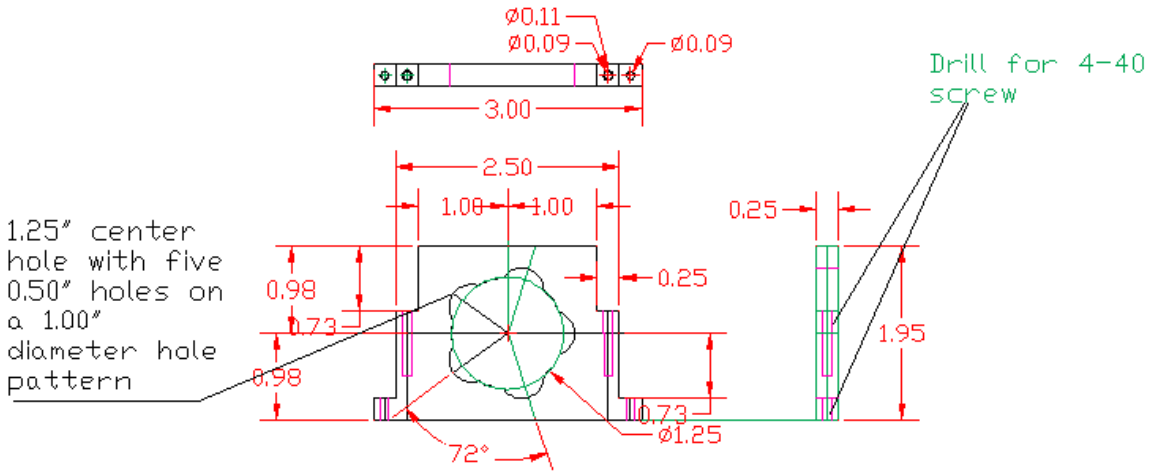

Transformer mount for the UNC high amplitude asymmetric waveform power supply

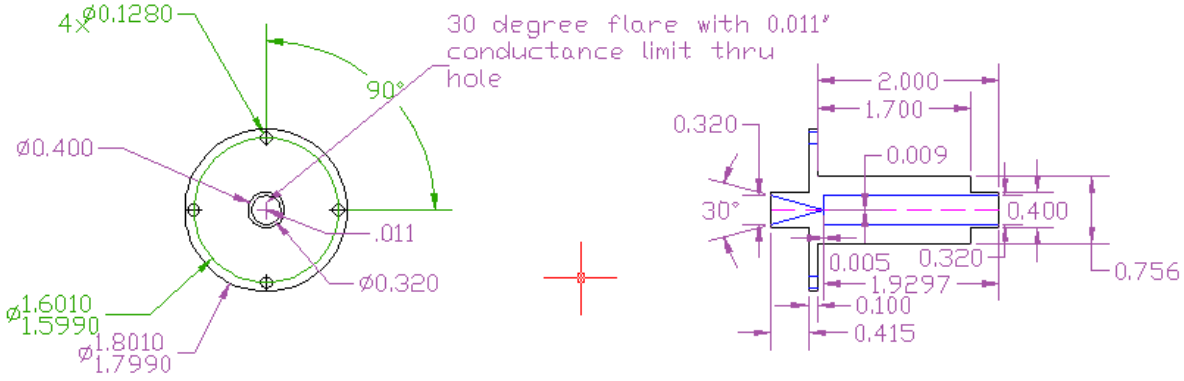

Alternative to the multiholed inlet used with the PNNL FAIMS. This inlet uses a single aperture but has a flare to increase the effective sampling area

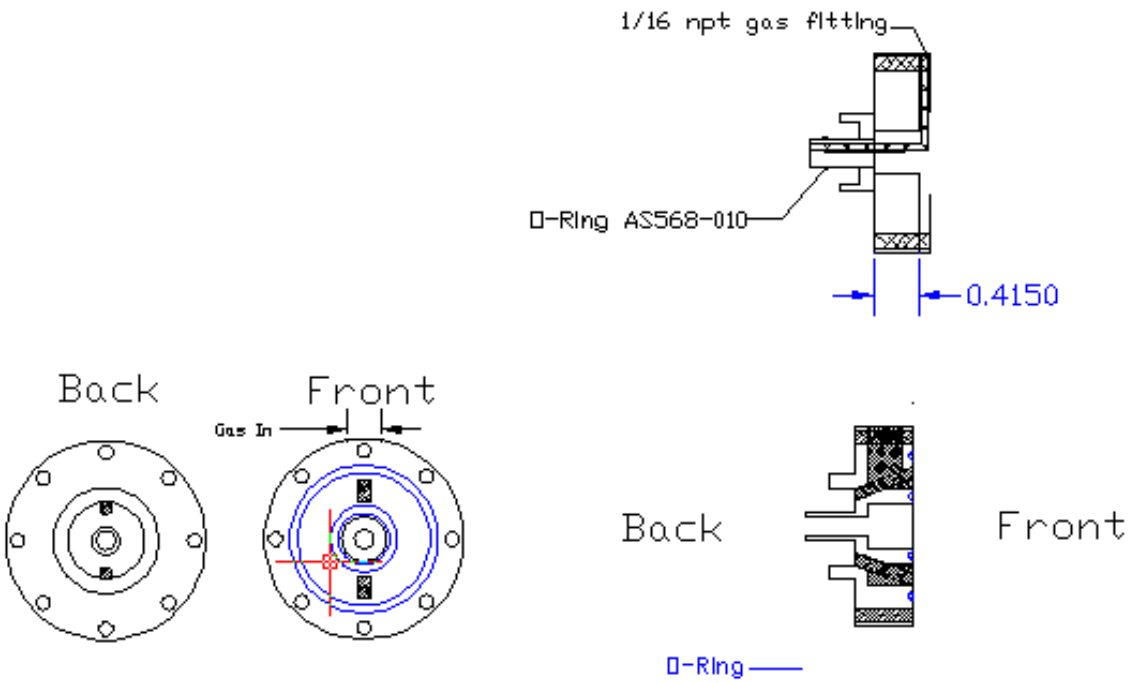

Adaptor to use the G3 device on the FAIMS-QEB instrument

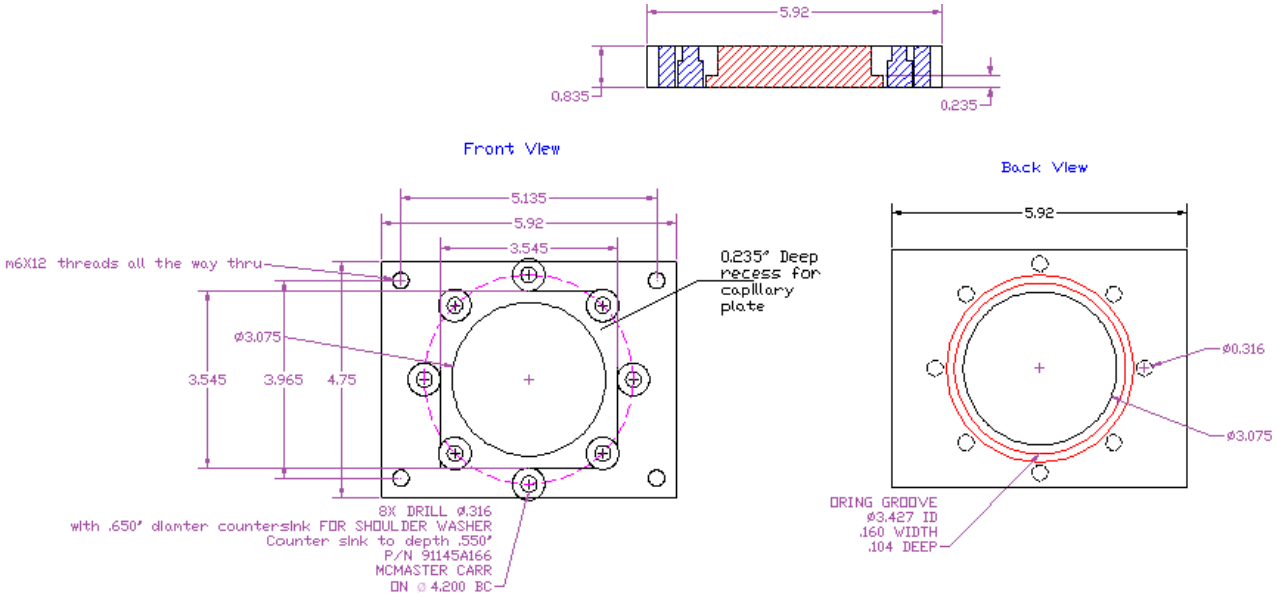

Adaptor to allow the use of the G4 FAIMS on the FAIMS-Q-EB instrument

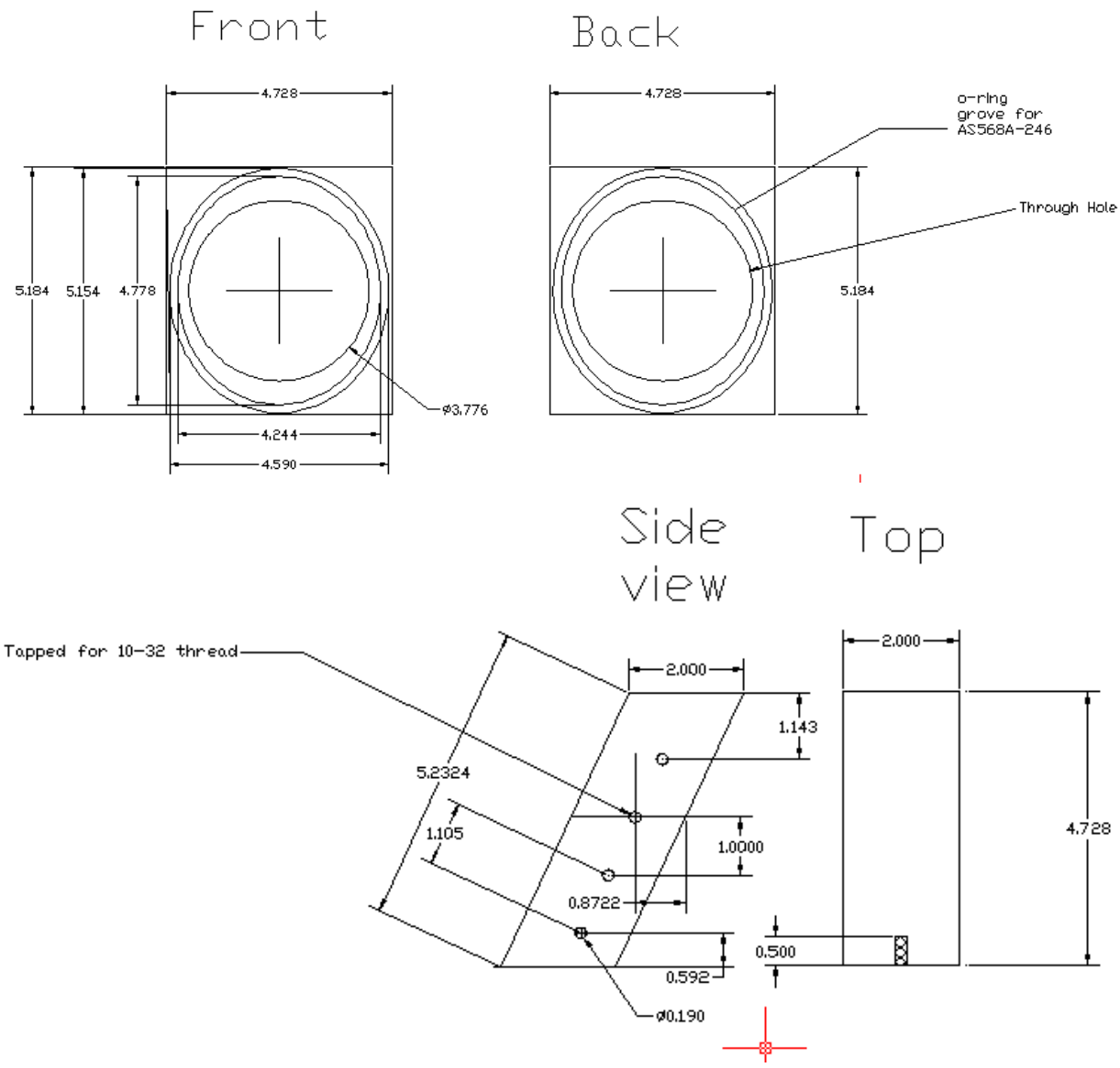

Spacer to allow use of source door on Bruker Esquire 3000 when using the G3 FAIMS